Utrecht University
Faculty of Geosciences

Estimating land subsidence based on hydrogeological and lithological data from 1991-2016 in the Mekong Delta, Vietnam

Author:
Coen van den Nouweland
c.vandennouweland@students.uu.nl

Supervisor:
Dr. Esther Stouthamer

Utrecht, the Netherlands
September, 2018

Cover: photos of the effect of land subsidence in the Mekong Delta. Top: A farmer in the Ca Mau provinces inspects its failed rice crop due to salinized water. The Ca Mau province is the lowest laying province in the Mekong Delta. Bottom left: An improvised river embankment in the Ca Mau province to prevent seawater from entering the rice fields. Bottom right: Cracks caused by land subsidence in the Cai Rang Bridge in Can Tho.

Table of contents

I. Abstract

Many deltas in the world are experiencing an increasing vulnerability to geohazards such as flooding, salinization and land subsidence. Land subsidence in the Mekong Delta is a relatively new hazard caused by the extensive groundwater extraction in the delta. Since the exact effect of groundwater on land subsidence is unknown, feasible groundwater policies and proper water management are difficult to achieve in the Mekong Delta. This study provides land subsidence estimates of the Mekong Delta for the years 1991-2016 based on detailed characterization of the subsurface, geotechnical parameterization of the different hydrogeological layers and groundwater extraction data. By integrating lithological & hydrogeological data a detailed database of the subsurface is created. This database is equipped with geotechnical parameters for all the different boreholes in the Mekong Delta. Accompanied with groundwater extraction rates of each aquifer land subsidence rates are estimated for each aquifer and aquitard for each borehole. The result shows an average land subsidence rate of 43.3 cm in 25 years in the Mekong Delta. The hotspots are located in the urban areas of Ca Mau (70 cm) and Soc Trang (50-60 cm) Over time the average land subsidence equals 17,33 cm in 5 years, 26,45 cm in 10 years, 32,87 cm in 15 years and 38,14 cm in 20 years. Primary subsidence causes 30% of the total land subsidence while secondary subsidence causes 70% of the total land subsidence. The results are exceeding previous research due to the high clay fractions in the hydrogeological layers which cause relatively a high amount of creep. Spreadsheet models are developed to estimate land subsidence in different years over 25 years. The spreadsheet model and results in this study contribute to a more thorough understanding of the different parameters and the quantification of the effect of these parameters on land subsidence.

II. List of abbreviations

DGMS = Division of Geology and Minerals of the South of Viet Nam

DWRPIS = Division for Water Resources Planning and Investigation for the South of Vietnam

ESLR = Effective sea-level rise

GSO = General Statistics Office of Vietnam

InSAR = Interferometric Synthetic Aperture Radar

LECZ = Low elevation Coastal Zone

LMG = Last Glacial Maximum

MKD = Mekong Delta

msl = mean sea level

III. List of Figures

IV. List of tables

1. Introduction

Deltas are an area of interest in many studies due to the increasing amount of challenges these areas have to cope with (Millman et al., 1989; Nicholls, 1995; Nicholls & Cazenave, 2010). Salinization (Gkiougkis et al. 2015), the increasing storm frequency (Neumann et al., 2015), flooding events (Nicholls, 2004), droughts (Dettinger & Cayan, 2014) and land subsidence (Syvitski et al., 2009) are all water-related threats that deltas have to face in coming decades. These challenges emerge globally and affect enormous deltas such as the Ganges Delta (Karim & Mimura, 2008), the Mississippi Delta (Blum & Roberts; 2009) and the Mekong Delta (Erban et al., 2014).

While the vulnerability and exposure of deltas increased over the past decades, the population and economic activities in deltas continue to grow (Syvitski et al., 2009). Mcgranahan et al. (2007) concludes that low elevation coastal zones (LECZ), which are defined as areas less than 10 meters above sea level, covers 2% of the world's land area but contains 10 % of the total world population, often centralized in large urban areas with a high population density. These urban areas affect the coastal environment heavily due to the high urbanization rate and the high consumption rate of food, water, space and energy of the residents (Sekovski et al., 2012). The high demand for food, water, space and energy causes a degradation of the coastal environment along with the social and ecological resilience rate of delta's (Adger et al., 2005).

The amount of people prone to coastal hazards due to both high urbanization rates and coastal-environmental degradation requires governmental institutions in those deltas to be actively involved in flood-risk management, city planning and environmental conservation to decrease the risks and impacts of coastal hazards such as flooding (Chan et al. 2012; Zhang et al. 2008).

The Mekong Delta (MKD) (Figure 1) is one of the deltas experiencing an increase in the amount of challenges. The delta is affected by sea-level rise and faces an increase in vulnerability to hazards such as salinization (Wassmann et al., 2004), flooding (Dinh et al., 2012) and more intense and frequent storms (Nguyen et al., 2007).

An underlying and relatively new hazard of the MKD is land subsidence. Land subsidence is caused by the withdrawal of fluids from the subsurface and was first described in 1969 (Poland & Davis, 1969). However, it is only recently related to the situation in the MKD (Erban et al., 2014; Minderhoud et al. 2017). The delta suffers from a decreased resilience rate and is more vulnerable to flooding, salinization and other water-related natural hazards. A main factor which quantifies the risk on water-related natural hazards is effective sea level rise (ESLR) (Ericson et al. 2006). ESLR is the sum of absolute sea-level rise, natural deposition of fluvial sediments and accelerated subsidence of human-induced activities such as groundwater pumping, loading and drainage. Land subsidence increases the ESLR which increases the vulnerability of the delta.

Land subsidence in the MKD started only recently, but the land is expected to remain subsiding in the future (figure 2). Minderhoud et al. (2017) developed a delta-wide hydrogeological 3D-model of the Mekong delta with an integrated subsidence model and proved that groundwater withdrawal caused the land to subside ~18 cm over the past 25 years. Currently, the subsidence rate is on average 1.1 cm yr^{-1} and this rate is most likely to increase in the future since the groundwater extraction rate is expected to increase as well. These estimates are in line with the results from Erban et al. (2014). This study estimated land subsidence rates

between 1-4 cm yr^{-1} based on interferometric synthetic aperture radar-data (InSAR) and monitoring the hydraulic head drop.

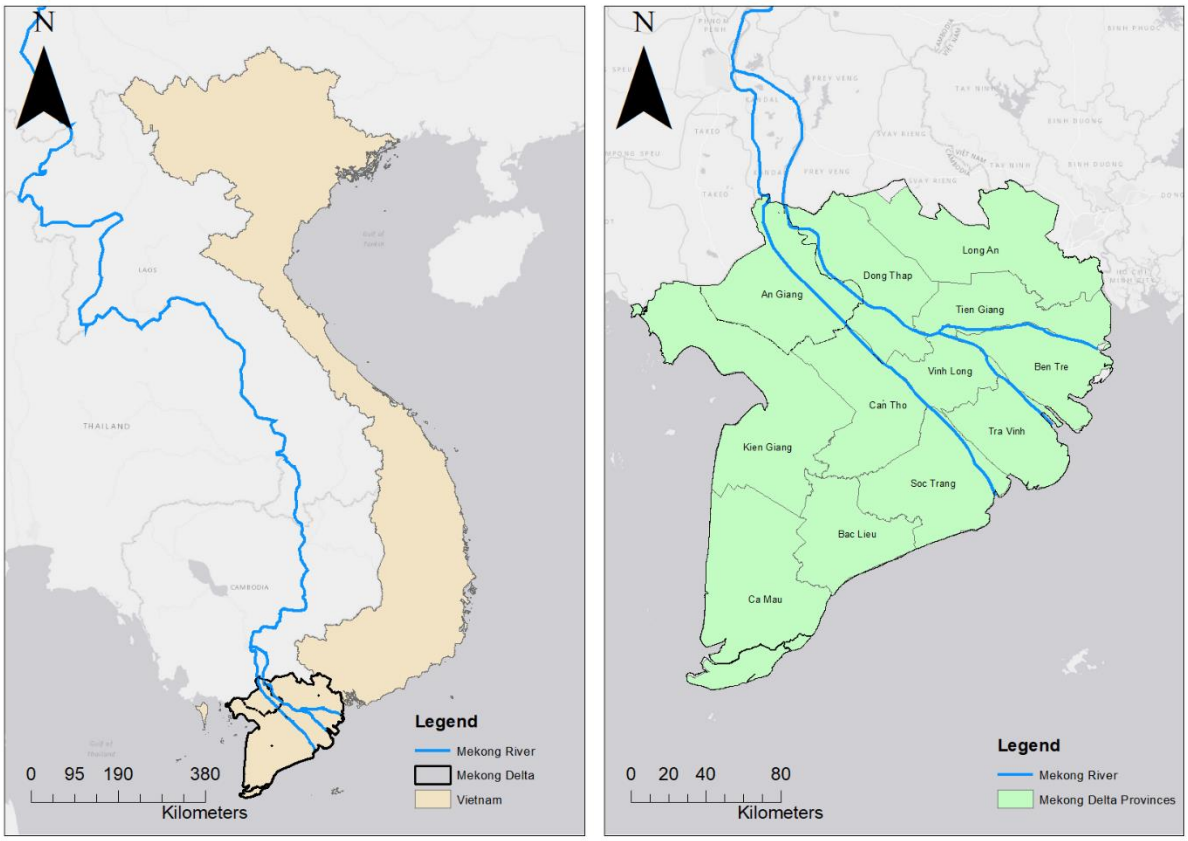

Figure 1: left: the location of the Mekong Delta in Vietnam. Right: the Mekong Delta and its provinces.

Land subsidence varies spatially within the MKD due to differences in the composition of the subsurface and differences in hydrostatic pressure declines generated by groundwater withdrawal. The composition of the subsurface influences the vertical permeability of a layer which is relevant for the amount of groundwater withdrawal. Gaining insight into the subsurface of the MKD is therefore relevant for both land subsidence estimates and groundwater extraction estimates.

The lithological composition of underground layers is determined by geomorphological processes. The geomorphology of the MKD is complex with influences of marine, glacial and tectonic processes resulting in many different forms of deposits and heterogenous strata. The delta experienced periods of progradation and retrogradation, which influenced the type of deposits and the shape of the MKD (Wagner et al. 2012).

Minderhoud et al. (2017) attempted to model land subsidence based on geological interpretations of the subsurface of the Mekong Delta. Seven aquifers, seven aquitards and a phreatic top-layer were identified including the depth of each layer, but this was done by partly taking local heterogeneity into account. Geotechnical parameters were determined assuming aquifers were consisting purely out of sand and aquitards

were consisting for 1/3rd out of sand. By assuming fixed fractions sand, clay and silt lithological variety is simplified and this causes land subsidence estimates to be less accurate.

Currently, the effect of groundwater extraction on land subsidence in the Mekong delta is partly known (Minderhoud et al., 2017). Previous research (Wagner et al. 2012; Minderhoud et al. 2017) identified geological units and assigned them with fixed geotechnical parameters, neglecting local varieties and the lithological differences within an aquifer or aquitard. The subsidence rate estimated by Minderhoud et al. (2017) does not match with InSAR-measured subsidence rates on certain locations. One of the possible explanations for the difference in subsidence rate is the local differences in subsurface conditions over relatively short distances. Local differences in subsurface conditions have been observed other deltas such as the the Rhine-Meuse delta (Asselen et al. 2009; Koster et al. 2016), the Mississippi delta (Tornqvist et al. 2008) and the Ganges-Brahmaputra delta (Higgins et al. 2014). A complete understanding of the sensitivity of the subsurface to the extraction of groundwater and land subsidence is not reached yet due to simplifying local heterogeneity. Due to this knowledge gap, appropriate groundwater extraction policies are developed without taking the exact consequences of land subsidence into account. Currently, groundwater extraction thus happens without taking the exact consequences regarding land subsidence properly into account.

Therefore, the objectives of this study are: (1) improve the schematization of the Late Tertiary and Pleistocene subsurface of the MKD in South Vietnam by integrating datasets of both lithological and geological subsurface information and exploring trends regarding grain-size distribution. (2) Assigning each aquifer and aquitard with geotechnical parameters relevant for land subsidence estimates by using in field measurements of the Division for Water Resources Planning and Investigation for the South of Vietnam (DWRPIS). (3) Determine the effect of hydraulic head drop by groundwater extraction on the amount of land subsidence by analyzing the hydraulic head drop of each aquifer and relate this to geotechnical parameters to estimate land subsidence.

The study contributes to gaining a more precise and complete knowledge of the process of land subsidence in the MKD by taking into account a schematization of the subsurface, geotechnical parameters and groundwater withdrawal data. By improving the understanding of land subsidence, regional governmental institutions are better able to develop proper groundwater withdrawal policies to relocate groundwater withdrawal and protect fast-subsiding areas.

The geomorphology of the study area is introduced in section 2. Section 3 explains the methodology on how each objective is reached. First, the process of creating an integrated database is explained in section 3.1. Subsequently, the process of developing delta-wide subsurface maps is illustrated. The apex-to-coast analysis is described in section 3.3. The assignment of geotechnical parameters is explained in section 3.4. Section 3.5 and 3.6 explain how hydraulic head drop rates are integrated and how the subsidence potential is calculated respectively. The results are presented in section 4 where section 4.1 presents the results of the integrated database. Section 4.2 presents the subsurface maps. Section 4.3 shows the results of the apex-to-coast analysis. Section 4.4 displays the geotechnical parameterization. Section 4.5 offers the results of the hydraulic head drop and section 4.6 presents the subsidence rates for different parts of the Mekong Delta. Section 5 gives an interpretation of the estimated subsidence rates, discusses the limitations of the study and offers improvements. Finally, in section 6 a conclusion is provided.

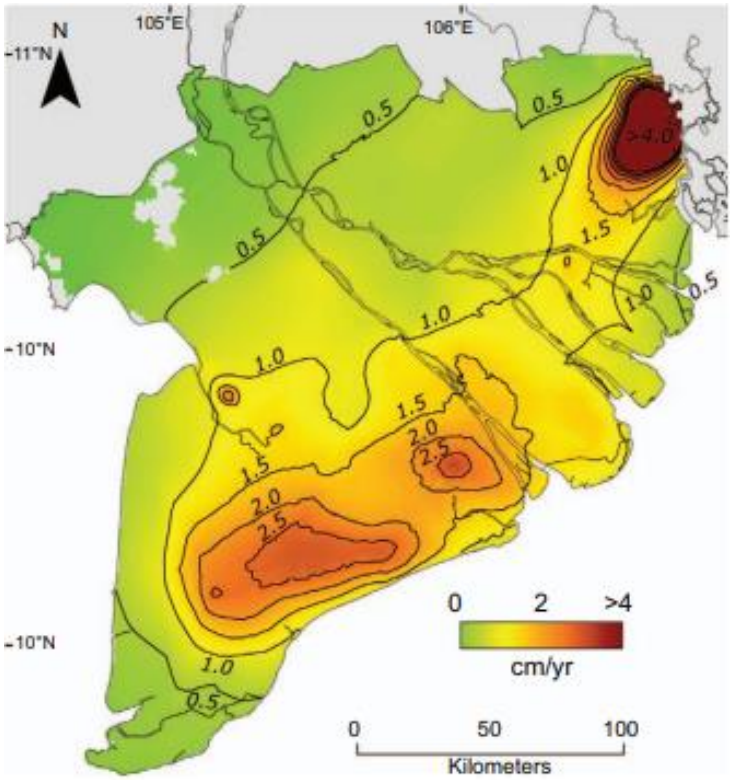

Figure 2: Modelled subsidence rate of the Mekong Delta (Minderhoud et al. 2017)

2. Study area

2.1 Geological setting and geomorphology

The Mekong Delta is located in the south of Vietnam. The delta is named after the Mekong River which is the 12th longest river globally. The river descends from the Tibetan plateau in China and runs through Myanmar, Laos, Thailand, Cambodia & Vietnam. In Vietnam the river splits into a western tributary channel (Mekong River) and an eastern tributary channel (Bassac River). Finally the river flows into the South China Sea. (Liu et al. 2009). The Mekong River catchment is divided in an upper basin located in China, and a lower basin located in Myanmar, Laos, Thailand, Cambodia & Vietnam. The catchment area of the Mekong River has a size of 800.000 km^2. The Vietnamese Mekong Delta is only 65.000 km^2 which is around 8% of the total catchment area (MRC, 2005) (Figure 3).

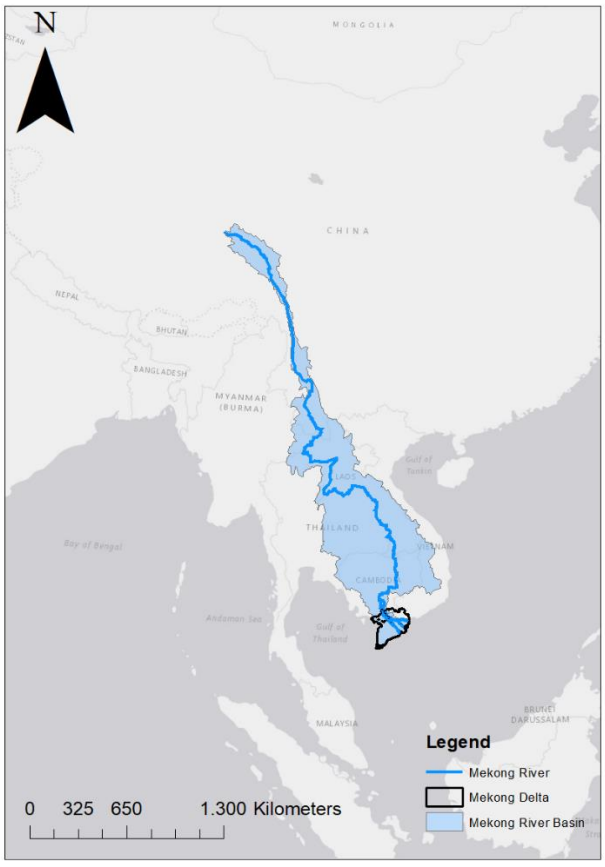

Figure 3: the Mekong River (blue), the Mekong River Catchment (light blue) and the Mekong Delta (black).

Accumulation of sediment from the Himalayan mountain ranges at the Mekong Rivers mouth in combination with ongoing subsidence of the basin resulted in the development of the former MKD (Xue et al., 2010). The present MKD started forming 15 ka ago when the sea level rise after the last glacial maximum

(LGM). The sea level rose for more than 120 meter during the last 16 – 6 ka. After the sea reached its maximum height around 5.5 ka BP, the sea level has been decreasing (Ta et al. 2002).

During the LGM 16 ka BP (Late-Pleistocene) the south china sea was significantly reduced in size and the Sunda Shelf was exposed. This shelf is the largest non-polar shelf and studied by Hanebuth et al. (2000) to reconstruct Pleistocene sea level rise based of radiocarbon dating of the sediment. This was used to determine the depositional environment during the LGM. The depositional environments found were mangrove swamps and mud flats.

During the last 6 ka BP (Late-Holocene) the delta changed from tide-dominated to tide-wave dominated. Deltaic sediments were found overlaying the late Pleistocene sediments (Ta et al. 2002). Three boreholes were analyzed in Ta et al. (2002) showing the Postglacial transgression by a decreasing marine influence. This means a 13.5m thick clay deposit was found with abundant marine planktonic diatoms with the age of 5.3 ka BP in borehole log BT2 (Ta et al. 2001; figure 4). Subsequently, the regression period decreases the influence of marine sediments and is visible by tidal beach ridges in borehole cores (Ta et al. 2001). The change from marine transgression to regression changed the depositional environment from a marine environment to a deltaic environment. (Xue et al. 2010; Tanabe et al. 2003)(Figure 4).

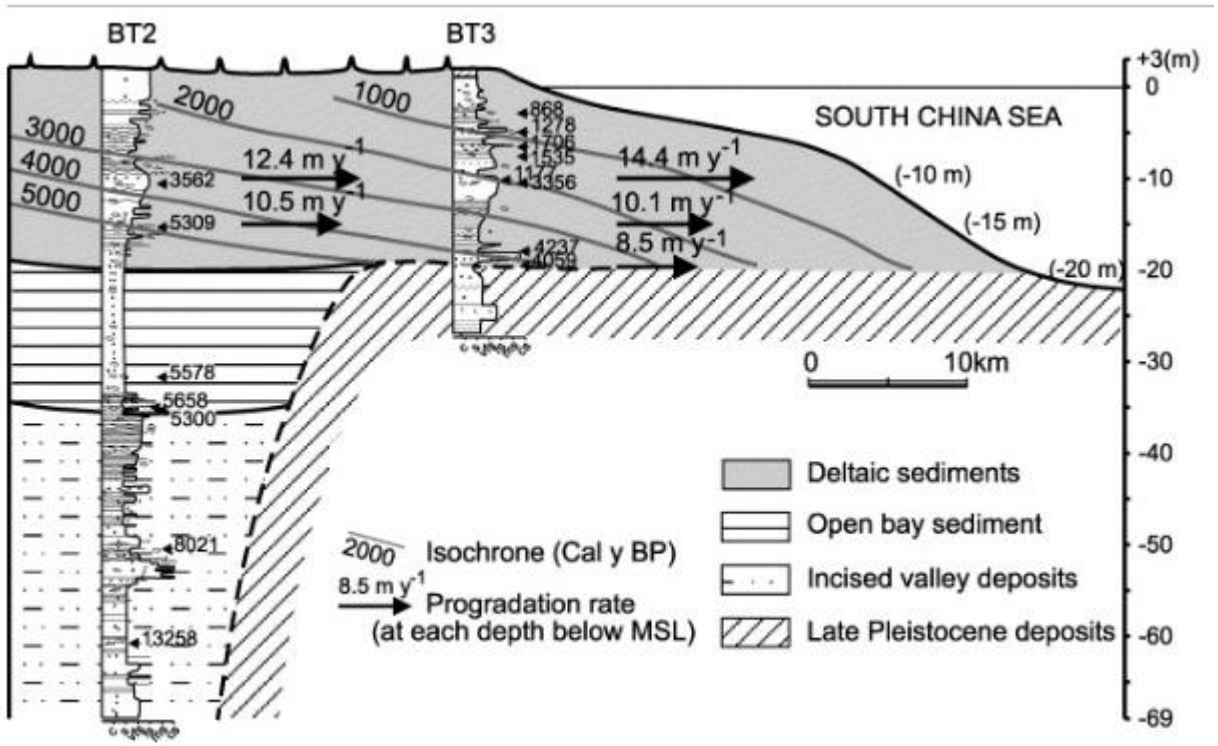

Figure 4: Depositional environments in the MKD and the borehole core BT2. For location BT2 see figure 6 (Ta et al., 2001; Ta et al. 2002).

The geological setting of the MKD is described in Nguyen et al. (2000) based on deep boreholes, seismic and aeromagnetic data. These geological surveys allowed for the identification of uplifting areas, depression areas and faults (Figure 5). The geological setting is interpreted as a depressed block bordered by parallel-

orientated faults known as a graben. A number of blocks sunk to different depths and are bounded by faults in the direction NW-SE, NE-SW or N-S. Some of these blocks are uplifting such as the Cantho, Long Xuyen & Baclieu-Soctrang and some blocks are depressing such as the Plain of Reeds and Phunghiep. These blocks are bordered by faults such as the Bassac river & Mekong River (Tran, 1986).

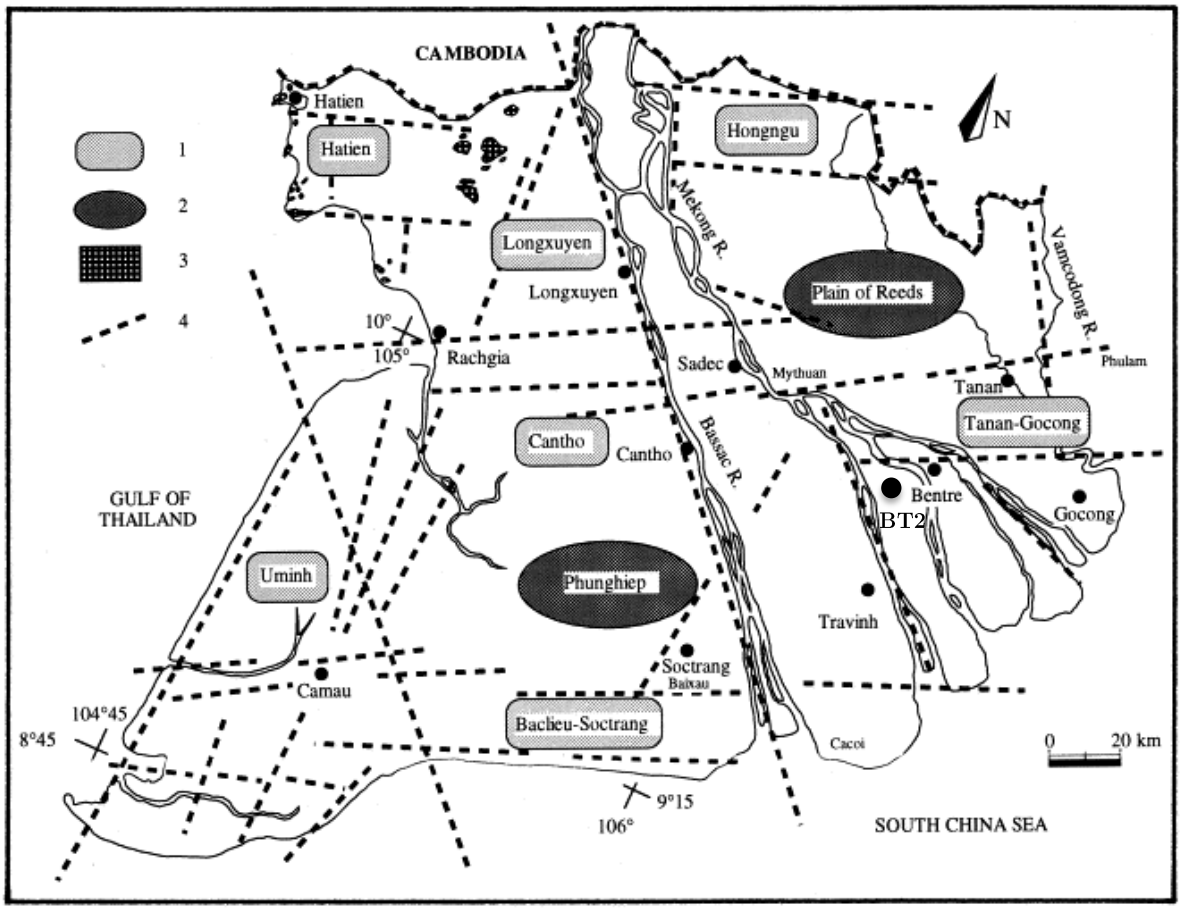

Figure 5: The geological setting of the Mekong Delta. 1. uplifting areas. 2. depression areas. 3. Basement rock. 4. Faults. (Nguyen et al. 2000)

The geohydrological setting in the MKD was formed by the final cycle of a interglacial period to a glacial period. During the last glacial high erosion rates creating incised valleys in the MKD. These valleys filled up with marine, sandy sediment during transgression periods more recently (20 ka BP) (figure 6). During the late-Holocene, peat beds and other sediment accumulated on top of these valleys, protecting them from salinization. This process created sandy, fresh water aquifers that are suitable for groundwater extraction (Wagner et al., 2012) and are the aquifers where groundwater is currently extracted from. However, the pollution and salinization of these Pleistocene aquifers have led to the development of wells to deeper located aquifers. These Neogene (Pliocene & Miocene) aquifers are used for groundwater extraction as well.

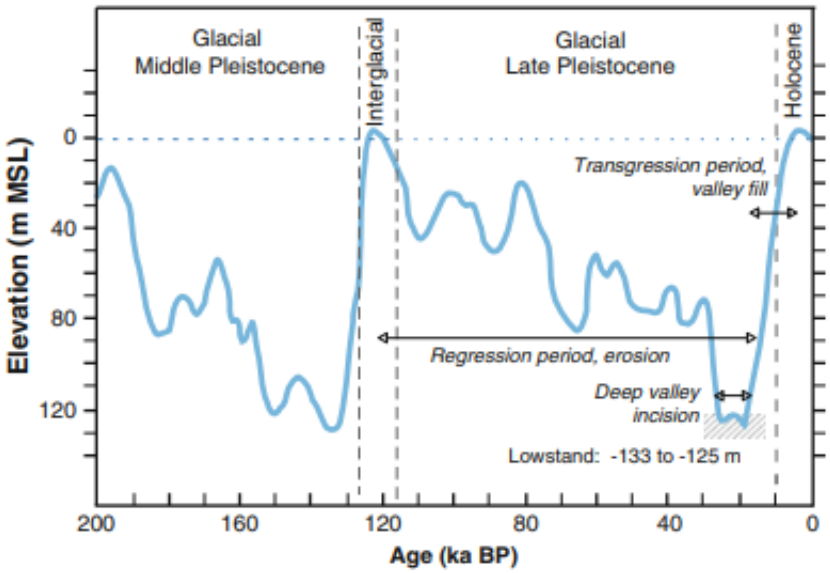

Figure 6: Mean sea level fluctuation since the Middle-Pleistocene (Wagner et al. 2012)

3. Data & Methodology

3.1 Integrated database

A valuable dataset for this research is a dataset containing 846 lithological borehole descriptions in the Mekong Delta from the DWRPIS (2017). Due to data limitations and inaccuracies 719 of the 846 descriptions are suitable for further data-processing and analyses. The spatial location, date, total depth and elevation of each borehole are recorded. Additionally, lithological units, the lower limit and the thickness of each layer were identified.

Subsequently, a similar dataset of the Mekong Delta is available containing 719 geological borehole logs. The geological information of the same boreholes as the lithological dataset is included in this dataset. In addition to the same variables as the lithological dataset, the sequence of geological units is recorded as well. This means the exact depth and thickness of hydrogeological aquifers and aquitards is recorded in this dataset. The dataset is provided by the DWRPIS (2018) and constructed with the help of field observations and in field borehole logs. The hydrogeological unit is recorded by determining the age of sediment samples. The lithology of the samples were analysed to relate each sample to a geological time period and thus a hydrogeological unit.

The improved dataset is provided by Minderhoud et al. (2017). This dataset holds the same information as the dataset by the DWRPIS, but is improved by using geological cross-sections. Four geological cross-sections were used to adjust the hydrogeological boundaries between aquifers and aquitards in 70 boreholes (Minderhoud et al. 2017).

To provide insight in the subsurface of the MKD, the lithological dataset is combined with both the geological datasets of the DWPRIS (2018) and of Minderhoud et al. (2017). This results in two integrated databases.

DATASET										
Lithologica	1		2		3		4		5	
Geological	1		2		3		4		5	
X	518274		532053,5		542003,7		523406,4		551364,5	
Y	1186733		1156189		1154761		1172853		1143944	
Geo Depth	161		285		263		50		50	
Litho Dept	161		285		263		50		50	
Litho Z	2		2,95		3,424		3,3		2,539	
Depth	**Lithology**	**Reclassifie**	**Lithology**	**Reclassifie**	**Lithology**	**Reclassifie**	**Lithology**	**Reclassifie**	**Lithology**	**Reclassifie**
1	0	0	BS	CLAY	BS	CLAY	B	SILT	0	0
2	0	0	BS	CLAY	M	CLAY	B	SILT	0	0
3	0	0	BS	CLAY	M	CLAY	BC	SILT	0	0
4	0	0	BS	CLAY	M	CLAY	BC	SILT	0	0
5	0	0	BS	CLAY	M	CLAY	BC	SILT	0	0

Figure 7: The lithology of the first five meters of depth for the Q2 aquitard for 5 boreholes.

Both datasets are combined with the lithological datasets to create two different integrated databases that combine the lithological and geological information of 719 borehole logs. This means that for each individual borehole log, for each meter of depth, the lithology and the hydrogeological unit is known and two excel-databases are created. The elevation of each borehole is documented as well, and a correction for this is executed. The depth of each borehole is relative to mean sea level. To illustrate the contents of the integrated databases a segment of the database is included in figure 7. The complete description of each parameter is given in the supplementary material (Integrated_Database).

The integrated databases describe the lithology of each meter depth using 16 different lithological units. The 16 classes are narrowed down to three lithological classes: clay, sand & silt, according to table 1. The simplification is done to create three coherent lithological fractions maps (see section 3.2) for each hydrogeological unit. Clay, sand & silt are the three lithological chosen due to their significant difference in void ratio, compressibility index and other geotechnical parameters regarding land subsidence sensitivity.

Table 1: The reclassification of 16 lithological classes into clay, sand & silt according to the classification of the database of the DWPRIS (2017).

Clay	**Sand**	**Silt**
Sét	Cát bột,	bột
Sét bột,	cát sạn sỏi	bột cát
bột sét	Cát	
Bùn		
bùn sét		

The integrated databases describe the geology of each meter depth by assigning it to a hydrogeological unit. The different hydrogeological units of the MKD are identified and defined by the Division of Geology and Minerals of the South of Viet Nam (DGMS, 2004) and used in studies by Wagner et al. (2012) and Minderhoud et al. (2017). Based on differences in lithology in the subsurface 15 different hydrogeological units were determined. The hydrogeological units are summarized in table 2.

Table 2: The geological division of the subsurface of the MKD according to DGMS (2004), Wagner et al. (2012) and Minderhoud et al. (2017).

Hydrogeological unit	**Abbreviation**
Phreatic Top Layer	PT
Holocene aquitard	Q_2
Holocene aquifer	qh
Upper Pleistocene aquitard	Q_1^3
Upper Pleistocene aquifer	qp_3
Upper-Middle Pleistocene aquitard	$Q_1^{2\text{-}3}$
Upper-Middle Pleistocene aquifer	$qp_{2\text{-}3}$
Lower Pleistocene aquitard	Q11
Lower Pleistocene aquifer	qp_1
Middle Pliocene aquitard	N_2^2
Middle Pliocene aquifer	n_2^2
Lower Pliocene aquitard	N_2^1
Lower Pliocene aquifer	n_2^1
Upper Miocene aquitard	N_1^3
Upper Miocene aquifer	n_1^3

The combination of the lithological classes and the hydrogeological units of the subsurface allows for a precise identification of the lithology of each aquifer and aquitard of the MKD. Each hydrogeological unit is extracted from the integrated database to examine the exact depth, thickness and lithology of this hydrogeological unit. Subsequently, the lithology of each hydrogeological unit is calculated in fractions. This results in the fraction clay, sand and silt for 719 different locations for each hydrogeological unit. The results are summarized in a spreadsheet.

The fractions of both databases are compared and the database that associates the correct lithology with the correct hydrogeological unit (i.e. clay at aquitards and sand at aquifers) is the database that characterizes the subsurface more accurate and is used in the further analysis.

3.2 Subsurface lithology of the Mekong Delta

Next, the fractions clay, sand and silt of each borehole for each aquifer are visualized using ArcGIS. The fraction clay, sand and silt of each borehole are plotted as vector data. The data is interpolated to a continuous delta-wide map using ordinary kriging.

To achieve the most accurate kriging result spatial autocorrelation is examined by using a semivariogram (figure 8). The semivariogram depicts spatial autocorrelation by plotting the variance (y-axis) of two sets of sample points with a certain distance between them (x-axis). The distance plotted on the x-axis is grouped in lags. This size and the number of these lags should be determined manually. Generally, the lag size should be equal to the average nearest neighbour distance. The number of lags should be determined in a way when multiplying the number of lags and lag distance, this should cover approximately half of the largest distance between two sampling points (ESRI, 2017).

After that a model is fitted through the sampling points. This model shows the nugget, sill and range of the variogram quantifying to what extent autocorrelation exists within the sample points. The sill is the variance value where the model flattens out and no correlation exists anymore. The range defines the distance at which no correlation exists anymore. The nugget describes the error within the model. In theory, two sample points with the same location should have the same value so the nugget should be 0. If this is not the case, the nugget equals the difference between these points on the same location (Heege, 2013).

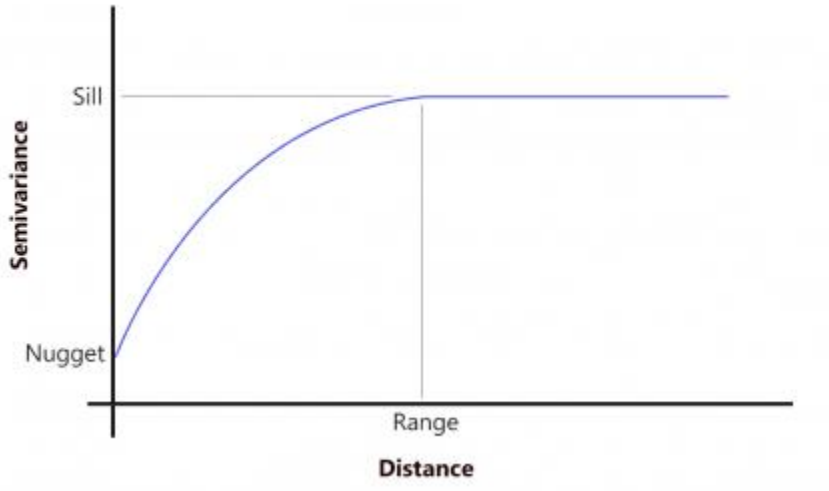

Figure 8: The nugget, sill and range from a semivariogram (GisGeography, 2018).

A semivariogram is constructed for each of the fractions (clay, sand & silt) for each of the aquifers and aquitards. The major range of all the semivariograms is 25 km. This means beyond this distance spatial correlation does not exist anymore. The reason 25 km is chosen as a correlation distance is that this distance results in a delta-wide covering map and does not neglect local variety. A distance smaller than 25 km results in an uncomplete map while a distance above 25 km reduces the local variety present in the subsurface. The lag size is based on the average nearest neighbour distance between sample points (2.2 km). The number of

lags is set to 59. When the lag size is multiplied by the number of lags this results in approximately half of the largest distance between two points (130 km)(ESRI, 2017).

When the semivariogram is constructed the kriging process starts. The kriging is done with a smooth searching parameter which means each location is influenced by a different number of sample points. A relatively low smoothing factor of 0.2 is used to reduce smoothing and maintain local variety. The search area is the same as the major range (25 km).

3.3 Apex-to-coast analysis

To determine apex-to-coast trends in the MKD a selection of sample points is made along the main tributary channels in the Mekong Delta: the Bassac river to the west, the Cổ Chiên River and the Mekong River in the east (figure 9). The distance from coast for each point is calculated. Subsequently, a scatterplot is created where the fractions clay, sand and silt of each aquifer and aquitard are plotted against the distance from the coast. A trendline is added to the scatterplot to determine if any trends exist.

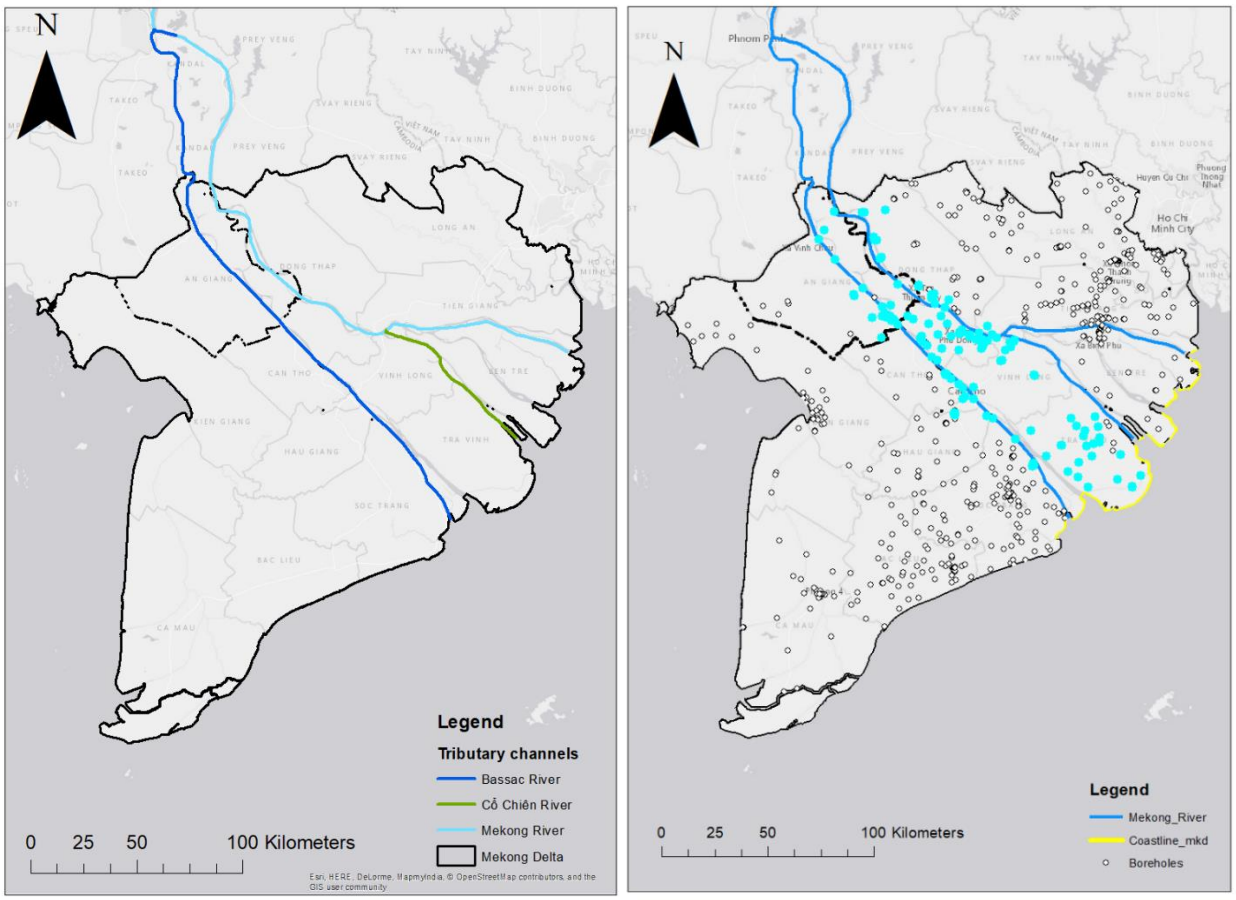

Figure 9: left: the Mekong River and its tributary channels. Right: The selection of boreholes used for the apex-to-coast analysis

3.4 Assigning Geotechnical parameters

To calculate the subsidence potential for the different hydrogeological units relevant geotechnical parameters are determined and calculated based on van Laarhoven (2017). A relevant parameter regarding land subsidence is the compressibility index (Cc). This index indicates how much a deposit can be compressed and is used to determine the amount of land subsidence. To calculate the compressibility index specific gravity (Gs), initial void ratio (e_0), liquid limit (LL) and bulk density (ρb) are taken into account. The specific gravity is the ratio of the density of the soil to the density of water (ρ_{soil}/ρ_{water}). Initial void ratio describes the ratio of the volume of the voids to the volume of solid soil particles in a soil (V_{voids}/V_{solids}). The liquid limit (%) describes the state of a soil regarding behaviour from a plastic soil to a liquid. Bulk density is the weight of the solids of a soil in a given volume (M_{solids}/V_{soil}). The deeper the soil, the greater the compaction and the higher the bulk density.

Many empirical equations exist to calculate the compressibility index (Park & Lee, 2011; Tiwari & Ajmera, 2011; Akayuli & Ofusu, 2013). In this study the equation of Moayed et al. (2017) is used (Equation 1 & 2). This equation is developed using neural network modelling which is a method to identify complex relationships between variables without using knowledge of the exact geological processes. The result showed that for the prediction of the compressibility index the combination of initial void ratio, liquid limit and specific gravity gave the best correlation (Moayed et al., 2017).

$$C_c = -13.59 + 1.503Y_c + 10.434G_s + 0.045Y_c^2 - 2.0014G_s^2 - 0.197G_s \cdot Y_c \quad \text{(Eq 1)}$$

where Gs is the specific gravity and Yc is calculated by:

$$Y_c = -0.152 + 0.472Ye_0 + 0.00095LL - 0.163e_0^2 - 0.000035LL^2 - 0.00446e_o \cdot LL \quad \text{(Eq 2)}$$

where e_0 is the initial void ratio and LL is the liquid limit.

The liquid limit, initial void ratio and specific gravity were extracted from geotechnical summary tables from the DWRPIS (2010). By using both equations the compressibility index is calculated for clay. The DWRPIS (2010) provided a geotechnical dataset based on in field measurements of the specific gravity, void ratio and liquid limit for clay and sandy soils in 12 different regions. The 12 different regions are shown in figure 11. Equation 1 and 2 are used to calculate an unique compressibility index for clay soils in each of the 12 regions. Sandy soils are less compressible compared to clay soils and no liquid limit was provided, the compressibility index for sand was assumed to be 0.01 (Widodo & Ibrahim, 2012).

Considering no measurements are made by the DWRPIS regarding silty soils and silt fractions are relatively low in the hydrogeological layers (see section 4.1; table 5), the compressibility index and initial void ratio of silt are estimated as the mean of the clay and sandy soils. This assumption is done based on various sources dedicated to the void ratio of sand-silt mixtures (Xenaki & Athanasopoulos, 2003) and the compressibility index of silty soils (Usaborisut & Ampanmanee, 2015).

To add vertical variability within the compressibility index the data of Gambolati et al. (1991) is used. In this study the relationship between the compressibility index and depth is found by performing analysis on core samples. The compressibility index of cohesive soils (clay) and granular soils (sand) is

determined by oedometer tests. The compressibility index is plotted against the depth for both soils in figure 10.

The same relationship is assumed to be true in the MKD as well. This means the geotechnical parameters differ for each region in the top 100 meters of the soil based on measurements of the DWRPIS (2010) and beyond these first 100 meters of depth the values of Gambolati et al. (1991) are assumed to be true. This data is shown in table 3 and 4. This results in 12 new logarithmic regression lines – 1 for each region - that can estimate the compressibility index at any given depth for any given location. The regression lines are reported in the spreadsheet model and explained in the supplementary material.

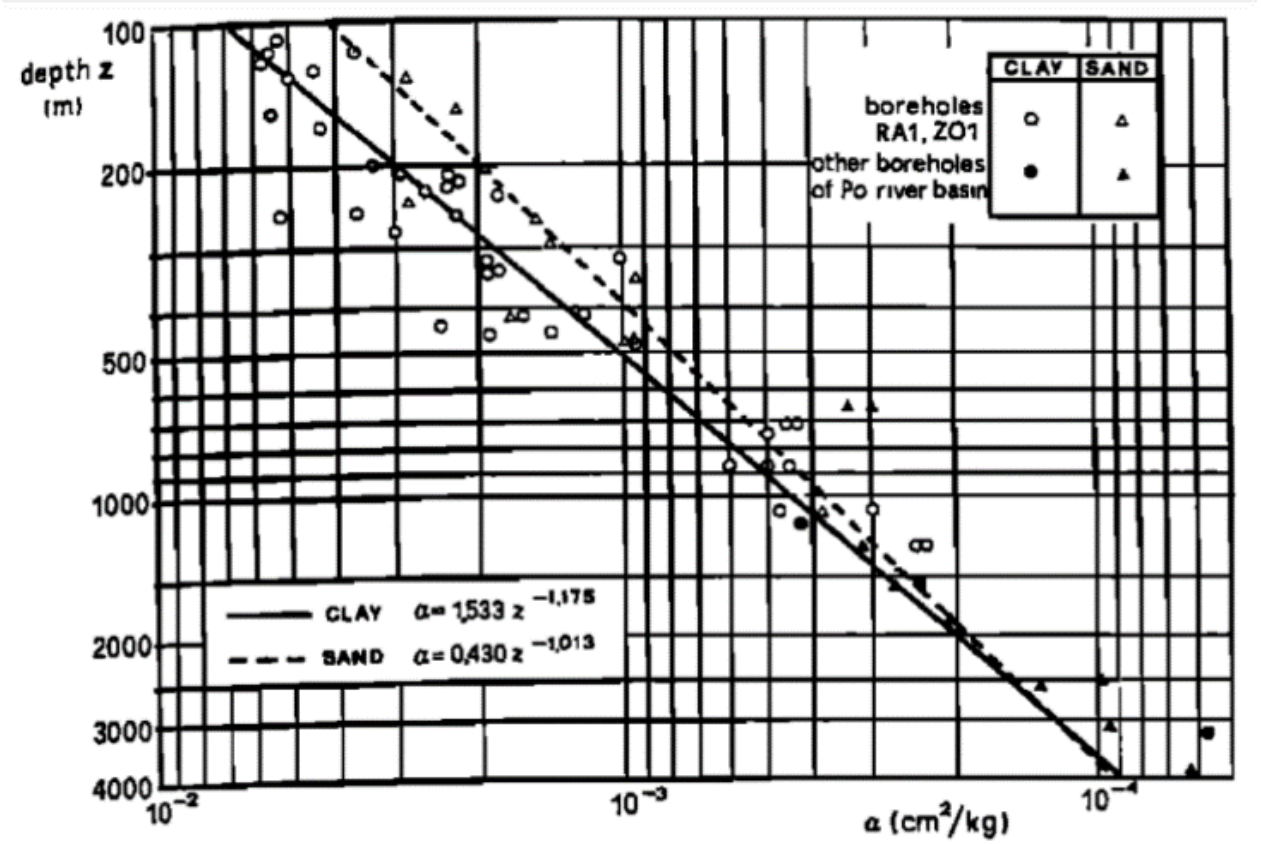

Figure 10: The relationship between compressibility index of sand and clay and depth (Gambolati et al., 1991)

Summarized, each borehole is first assigned with a region based on the location of the borehole and the spatial location of the region based on Thiessen Polygons (Figure 11). Next, the regression line is rewritten since the depth is known and the compressibility index is not. Finally, this results in 12 different regression equations for 12 different regions where depth is the independent variable and compressibility index can be calculated.

Table 3: The compressibility index of clay for different depths used to construct twelve different regression lines. Constructed based on data of the DWRPIS (2010) & Gambolati et al. (1991)

Coordinates & Region			Compressibility index for different depths (m)								
			DWRPIS (2010)	Gambolati et al. (1991)							
X	Y	Region	1	100	200	300	400	500	600	700	800
650572	1135108	Ben Tre	0,157708506	0,007	0,003	0,002	0,0015	0,001	0,0009	0,0007	0,0006
516452	1013930	Ca Mau	0,469018075	0,007	0,003	0,002	0,0015	0,001	0,0009	0,0007	0,0006
581128	1109637	Can Tho	0,427027155	0,007	0,003	0,002	0,0015	0,001	0,0009	0,0007	0,0006
569435	1156940	Cao Lanh	0,391873117	0,007	0,003	0,002	0,0015	0,001	0,0009	0,0007	0,0006
443809	1148459	Ha Tien	0,202083854	0,007	0,003	0,002	0,0015	0,001	0,0009	0,0007	0,0006
541838	1147935	Long Xuyen	0,373074207	0,007	0,003	0,002	0,0015	0,001	0,0009	0,0007	0,0006
649249	1146948	My Tho	0,346204881	0,007	0,003	0,002	0,0015	0,001	0,0009	0,0007	0,0006
512276	1105228	Rach Gia	0,385525869	0,007	0,003	0,002	0,0015	0,001	0,0009	0,0007	0,0006
532252	1113827	Rach Gia-Thon Not	0,425068743	0,007	0,003	0,002	0,0015	0,001	0,0009	0,0007	0,0006
585181	1136175	Sa Dec	0,390257583	0,007	0,003	0,002	0,0015	0,001	0,0009	0,0007	0,0006
607874	1062985	Soc Trang	0,412649212	0,007	0,003	0,002	0,0015	0,001	0,0009	0,0007	0,0006
657714	1172166	Tan An	0,319160731	0,007	0,003	0,002	0,0015	0,001	0,0009	0,0007	0,0006

Table 4: The compressibility index of sand for different depths used to construct a regression line. Constructed based on data of Widodo & Ibrahim (2012) & Gambolati et al. (1991)

Coordinates & Regions			Compressibilty index for different depths (m)								
			Widado & Ibrahim (2012)	Gambolati et al. (1991)							
X	Y	Region	1	100	200	300	400	500	600	700	800
650572	1135108	Ben Tre	0,01	0,004	0,002	0,0015	0,001	0,0008	0,00065	0,00055	0,0005
516452	1013930	Ca Mau	0,01	0,004	0,002	0,0015	0,001	0,0008	0,00065	0,00055	0,0005
581128	1109637	Can Tho	0,01	0,004	0,002	0,0015	0,001	0,0008	0,00065	0,00055	0,0005
569435	1156940	Cao Lanh	0,01	0,004	0,002	0,0015	0,001	0,0008	0,00065	0,00055	0,0005
443809	1148459	Ha Tien	0,01	0,004	0,002	0,0015	0,001	0,0008	0,00065	0,00055	0,0005
541838	1147935	Long Xuyen	0,01	0,004	0,002	0,0015	0,001	0,0008	0,00065	0,00055	0,0005
649249	1146948	My Tho	0,01	0,004	0,002	0,0015	0,001	0,0008	0,00065	0,00055	0,0005
512276	1105228	Rach Gia	0,01	0,004	0,002	0,0015	0,001	0,0008	0,00065	0,00055	0,0005
532252	1113827	Rach Gia-Thon Not	0,01	0,004	0,002	0,0015	0,001	0,0008	0,00065	0,00055	0,0005
585181	1136175	Sa Dec	0,01	0,004	0,002	0,0015	0,001	0,0008	0,00065	0,00055	0,0005
607874	1062985	Soc Trang	0,01	0,004	0,002	0,0015	0,001	0,0008	0,00065	0,00055	0,0005
657714	1172166	Tan An	0,01	0,004	0,002	0,0015	0,001	0,0008	0,00065	0,00055	0,0005

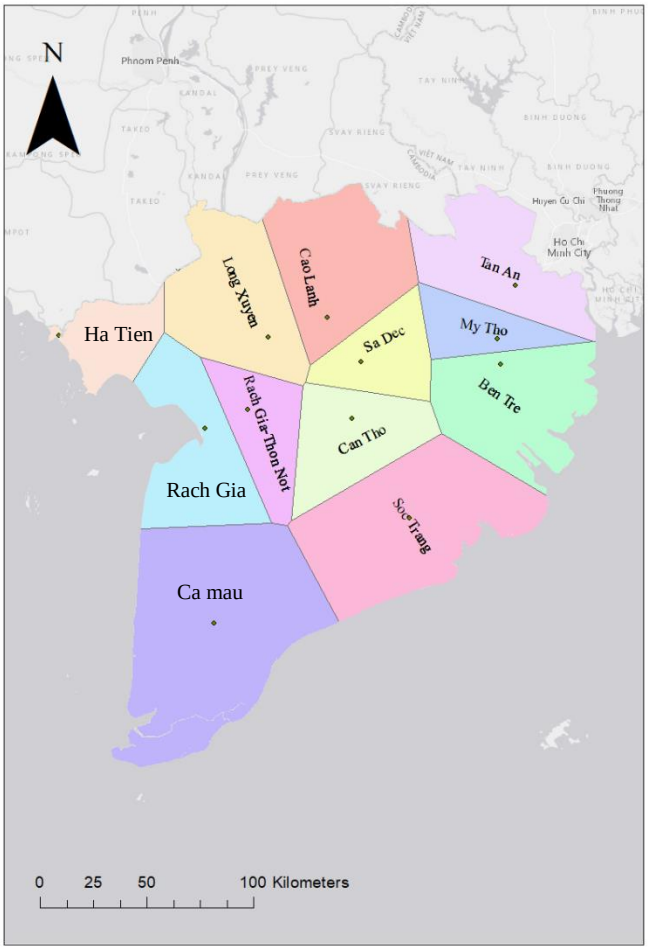

Figure 11: The twelve regions of the Mekong delta determined with Thiessen Polygons based on measurement data of the DWRPIS (2010)

Next, initial void ratio and bulk density are relevant geotechnical parameters regarding land subsidence. Initial void ratio is a relevant parameter to calculate land subsidence (section 3.6) and bulk density is used to calculate grain stress and changes in grain stress due to loading or groundwater extraction (section 3.5). Data regarding initial void ratio and bulk density originates from the DWRPIS geotechnical summary tables. Both parameters were measured during geological surveys in the MKD for both clay and sandy soils. The initial void ratio of silt is assumed to be the average of clay and sand since the grain size of silt is between the grain size of sand and the grain size of clay. For bulk density, the assumption is made that silt has the same bulk density as clay.

To create a delta-wide map of both parameters ordinary kriging is used. Kriging is a geostatistical interpolation tool to predict the value at any location based on a weighted average based on surrounding known values on different locations. Ordinary kriging is used since this method takes both the spatial distance and degree of variation among known points into consideration when calculating unknown values (Elbasiouny et al., 2014). The vector data is converted to raster data resulting in delta-wide maps of the initial void ratio and bulk density of both clay and sand. Subsequently, by using the extract values-to-point tool each borehole

was assigned with an unique initial void ratio for sandy soils, initial void ratio for clay soils, bulk density for sandy soils & bulk density for clay soils.

Vertical variability within the initial void ratio and bulk density is neglected. However, the bulk density is used to calculate the change of grain stress (equation 3). The depth of a soil is incorporated into the grain stress equation (See section 3.5).

Another geotechnical parameter determined is the secondary compressibility index (Ca). This index indicates the creep that occurs when an increase of grain stress is experienced in a soil. Due to an increase of stress the soil deforms and becomes more compacted. No field measurements were made so secondary compressibility index is estimated by using a Cc/Ca ratio of 0.04 (Mesri & Godlewski, 1977; Ladd et al., 1977). The assumption is made that creep only occurs in clay and silty soils, the secondary compressibility index for sand soils is assumed to be zero.

The compressibility index, initial void ratio and bulk density are determined for clay, sand and silt in each borehole. This means each borehole is assigned with a compressibility index, initial void ratio, and bulk density for sandy soils and clay soils. Since the fractions clay, sand and silt are known (Section 4.1) the value of the geotechnical parameters is multiplied by the fraction clay, sand and silt present in the borehole which results in unique geotechnical parameters for each borehole. An segment of the spreadsheet is shown in figure 12 to illustrate the description of geotechnical parameters. The complete database is added in the supplementary material (Subsidence.xlsx).

Geotechnical parameters									
Compressibility index (C_c)				ıry compressibility in		Initial void ratio (E_o)			
cc_clay	cc_sand	cc_silt	cc_final	ca_clay	ca_final	Iv_clay	iv_sand	iv_silt	iv_final
0,047542	0,006302	0,026922	0,047542	0,001902	0,001902	0,945209	0,748084	0,846647	0,945209
0,046487	0,006229	0,026358	0,015701	0,001859	0,000438	0,943193	0,74941	0,846302	0,795006
0,046661	0,006241	0,026451	0,028977	0,001866	0,001866	0,942306	0,749356	0,845831	0,85789
0,046836	0,006253	0,026545	0,034661	0,001873	0,001873	0,933563	0,749654	0,841609	0,87839
0,046313	0,006217	0,026265	0,046313	0,001853	0,001853	0,963784	0,748173	0,855979	0,963784
0,047542	0,006302	0,026922	0,047542	0,001902	0,001902	0,947117	0,748489	0,847803	0,947117

Figure 12: The compressibility index, secondary compressibility index and initial void ratio for clay, sand and silt soils for six boreholes in the Q2 aquitard.

3.5 Groundwater extraction rates

Land subsidence is increased by an increase in grain-stress. Groundwater extraction is a process that increases grain-stress in the subsurface due to the disappearing hydrostatic pressure. When the grain-stress increases due to the extraction of groundwater compaction will occur and this results in land subsidence (Gambolati & Teatini, 2015).

To implement groundwater extraction rates into the land subsidence potential estimation, the change in grain-stress due to groundwater extraction is relevant. First, the initial grain stress is calculated by equation 3 (Verruijt & Van Baars, 2007).

$$\sigma_v = (n \cdot \rho_w + (1-n) \cdot \rho_s) * H - \rho_w \cdot H = \rho_b \cdot H - \rho_w \cdot H \qquad \text{(Eq 3)}$$

Where σ_v is the grain stress, n the porosity, ρ_w the density of water, ρ_s the density of the sediment, ρ_b the bulk density, and H the thickness of the complete layer above. The bulk density is calculated in section 3.4 and the density of water is set at 10 kilonewton/m^3. Since the thickness in the spreadsheet (Subsidence_MKD) is referring to the thickness of just the segment of a borehole in the same hydrogeological unit and not the complete thickness of the overlaying section, the depth relative from mean sea level is taken instead of the thickness in equation 3. See Supplementary for a more detailed description of the spreadsheet.

Furthermore, the change in grain-stress is calculated by using measurements of the drop of the hydraulic head (DWRPIS, 2010; Minderhoud et al., 2017). The hydraulic head drop is described by Minderhoud et al. (2017) as aquifer drawdown. The aquifer drawdown is modelled from 1991-2016. The paper states that the modelled value of the hydraulic head is not exactly the same as the observed value, but this should not have any consequences for the land subsidence potential since the hydraulic head *change* is the relevant value regarding land subsidence potential. The hydraulic head change is modelled by Minderhoud et al. (2017) and these results are used as input data in this study (figure 13). The aquifer drawdown for each aquifer is extracted and converted to an increase in grain stress ($\Delta\sigma_v$) in kilo pascal (kpa). To calculate the increase in grain stress for each hydrogeological unit, the grain stress due to extractions in the aquifers above the specific hydrogeological unit is summed and added to the increase in grain stress in that specific hydrogeological unit. This means the increase in grain stress is the largest in the deepest aquitard (N13) and aquifer (n13).

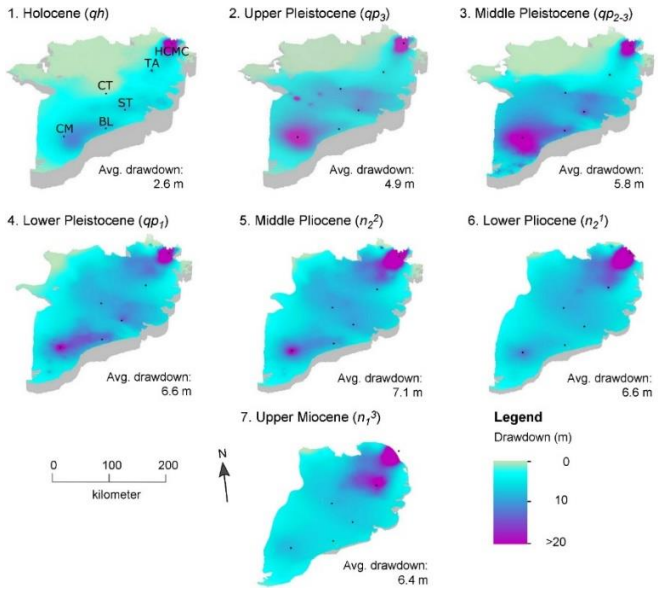

Figure 13: The drop of the hydraulic head of the seven aquifers in the MKD. (Minderhoud et al., 2017).

3.6 Subsidence Potential

The subsidence potential is estimated based on the characteristics of the subsurface, the selected geotechnical parameters and the change in stress due to groundwater extraction. To calculate the exact land subsidence potential the NEN-Bjerrum Method is used (equation 4). This method is often used to calculate the subsidence potential. The method is based on a linear correlation of subsidence to the logarithm of an increase in grain stress and a linear correlation of subsidence to the logarithm of time. The method is used in

this study because it calculates subsidence based on an increase in grain stress which in this case is caused by groundwater extraction, and a secondary compressibility index which is used to calculate subsidence based on creep (Ammerlaan, 2011).

$$\frac{-\Delta H}{H} = \overbrace{\frac{C_c}{1+e_0} \cdot U(t) \cdot \log\left(\frac{\sigma_v+\Delta\sigma_v}{\sigma_v}\right)}^{\text{Primary subsidence}} + \overbrace{C_\alpha \cdot \log\left(\frac{t}{d_t}\right)}^{\text{Secondary Subsidence}} \quad \text{(Eq 4)}$$

Here, the -H/H represents a change in thickness, C_c the compressibility index, e_o the initial void ratio, σ_v the grain stress and $\Delta\sigma_v$ the change in grain stress, U the consolidation index, C_a the secondary compressibility index, t the change in years and Δt the reference time (1 year).

The calculated subsidence is split up into two different components. The primary subsidence is caused by an increase in grain stress which is caused by groundwater extraction. The secondary component is caused by the slow deformation of clay soils: creep.

The consolidation index ranges from $0 - 1$ and represents the amount of subsidence at different points in time. Since the reference time is one year, and the increase in grain stress is derived from groundwater extraction data for over 25 years, a consolidation index of 1 represents the amount of subsidence in 25 years.

All the parameters described in previous sections are summarized in a spreadsheet model (Subsidence_MKD). Since groundwater is being extracted out of seven different aquifers, subsidence is calculated for these seven aquifers. Groundwater extraction does not occur in aquitards but creep still occurs. This means land subsidence is calculated for aquitards as well. For each aquifer, the boreholes found in that aquifer are selected and primary subsidence due to groundwater extraction and secondary subsidence due to creep are calculated and summed in the total subsidence for each borehole. For each aquitard, boreholes are selected as well and only secondary subsidence due to creep is calculated and summed in the total subsidence. A more detailed description of the spreadsheet model is given in the supplementary material.

Since the subsidence is calculated in each borehole, kriging is used to create an interpolated, continuous map for the MKD that visualizes the subsidence in 25 years. The kriging is done with the same parameters as described in section 3.2.

The full methodology is summarized in a flowchart in figure 14.

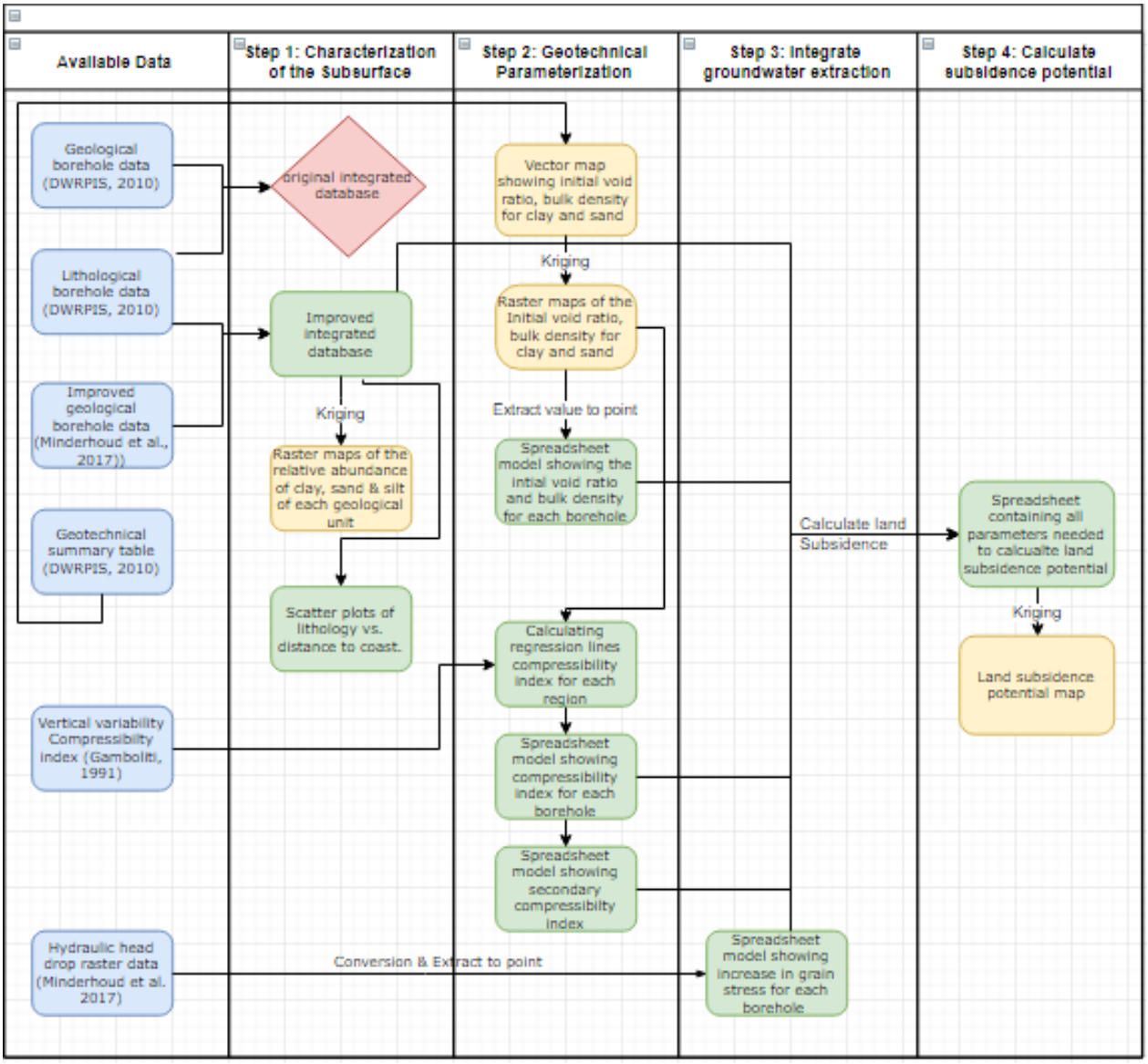

Figure 14: Flowchart describing the complete methodology. Blue = input data, Yellow = result in ArcGIS. Green = result in Excel. Red = rejected integrated database.

4. Results

4.1 Hydrogeology & lithology of the subsurface

The integrated databases describe the distribution of the depth, thickness and lithological composition of the different hydrogeological units in the subsurface of the Mekong Delta. The databases are described in the supplementary material. The lithological composition of each unit is converted to a fraction clay, sand and silt. The lithological fractions of each hydrogeological unit are summarized in table 5 for the original model and the improved model.

Table 5: Summary of the fractions in clay, sand and silt of each aquifer and aquitard for both models. Aquitards are shown in the grey columns and aquifers are shown in white columns.

-	**Original Model (Minderhoud et al. 2017)**			**Improved model (Minderhoud et al. 2017)**		
-	**Clay**	**Sand**	**Silt**	**Clay**	**Sand**	**Silt**
PT (-)	0.82	0.06	0.11	0.78	0.19	0.03
Q2 (aqt)	0.7	0.17	0.13	0.70	0.17	0.13
qh (aqf)	0.53	0.32	0.15	0.53	0.32	0.15
Q13 (aqt)	0.32	0.56	0.12	0.51	0.34	0.15
qp3 (aqf)	0.35	0.52	0.13	0.33	0.55	0.12
Q12-3 (aqt)	0.23	0.66	0.10	0.35	0.52	0.13
qp2-3 (aqf)	0.32	0.54	0.13	0.22	0.68	0.1
Q11 (aqt)	0.24	0.63	0.13	0.3	0.56	0.14
qp1 (aqf)	0.25	0.63	0.12	0.25	0.64	0.11
N22 (aqt)	0.26	0.63	0.11	0.29	0.6	0.11
n22 (aqf)	0.23	0.65	0.12	0.26	0.63	0.11
N21 (aqt)	0.25	0.63	0.12	0.22	0.67	0.11
n21 (aqf)	0.24	0.63	0.13	0.26	0.62	0.11
N13 (aqt)	0.29	0.6	0.11	0.26	0.63	0.11
n13 (aqf)	0.26	0.65	0.08	0.27	0.61	0.12

In general, both models seem better in identifying aquifers compared to aquitards. The fractions sand are in all hydrogeological units (except Q2) higher compared to the fractions clay and silt. Fractions of clay are in general around 0.3 in both aquifers and aquitards. Fractions of silt are in all hydrogeological units relatively low (around 0.1).

However, the improved model seems to identify the lithology in some hydrogeological units better compared to the original model (Minderhoud et al. 2017). The aquitards Q13, Q12-3 and Q11 are containing a higher fraction of clay in the improved model compared to the original model. The same accounts for the aquifers qp3 and qp2-3. These aquifers contain a higher fraction of sand in the improved model compared to the original model.

In the oldest hydrogeological units from the early-Pliocene and late Miocene the original model seems to assign the correct lithology better. In aquitards N21 and N13 and aquifer n13 respectively, the fractions clay and sand are higher compared to the improved model.

Overall, the improved model seems to be the more accurate model of the two models. This model identified a higher fraction of the correct lithology at five hydrogeological units (Q13, qp3, Q12-3, qp2-3 & Q11) compared the original model. The original model only identified a higher fraction of the correct lithology at three hydrogeological units (N21, N13 & n13).

Additionally, the difference of the better estimated fractions in the improved model compared to the original model is larger than the difference of the better estimated fractions in the original model compared to the improved model. The fractions of the correct lithology of the improved model at Q13, qp3, Q12-3, qp2-3 & Q11 are respectively improved by 0.19, 0.03, 0.12, 0.12, & 0.06. This difference is more compared to the improved fractions at the original model where the fractions of the correct lithology at N21, N13 & n13 are respectively improved by 0.03, 0.03 & 0.04.

In conclusion, it seems that the improved model is better at predicting the right lithology in general. More hydrogeological units are connected with the correct lithology and the difference in fractions is higher compared to the difference in fractions of the original model. The improved model is used in the further analysis of the subsurface of the MKD.

4.2 Lithological maps of the subsurface of the Mekong Delta

The fractions of the integrated database are used to create 15 sets of 3 raster maps to visualize the clay, sand and silt abundance of each hydrogeological unit. The raster maps are added as supplementary material.

Spatial trends exist in some of the aquifers and aquitards. Spatial trends in the first aquitard (Q2) and aquifer (qh) are non-existent. The lithology of the second aquitard (Q13) is mainly identified as clay. However, the eastern coast of the MKD contains more sand compared to the rest of the delta. The same applies for the second aquifer (qp3). The lithology of the hydrogeological layer is identified as sand in large parts of the MKD, but the eastern coast is the sandiest area. The southern part of the Delta – Ca Mau – contains more clay compared to the rest of the delta. The third aquitard (Q12-3) and aquifer (qp2-3) show the same spatial trend. The southern area of the delta contains higher fractions of clay while the northern part of the delta is sandier. In the fourth aquitard (Q11) and aquifer (qp1) the spatial trends are less present and only minor differences exist within the lithological characterization of the delta.

Spatial trends in the final six hydrogeological layers (N22, n22, N21, n21, N13 & n13) are more difficult to describe. Spatially, differences exist within the different lithologies of the six hydrogeological layers, but a trend or pattern is not found. However, small areas with an abundance of clay are found in e.g. N21, N13 & n13. The same accounts for small areas with an abundance of sand (n22 & n21) and areas with an abundance of silt (N22, N21).

Overall, the most common trend found is that the soil in the southern parts of the MKD consists of a higher fraction of clay compared to the northern area of the MKD. The opposite trend is observed regarding sand in the MKD. The northern areas contain in general a higher fraction of sand compared to the

southern areas. Spatial trends in silt are difficult to distinguish since fractions of silt are in general relatively low compared to other lithologies and over all different hydrogeological layers the same.

4.3 Apex-to-Coast Trends

The apex-to-coast trend is described for four hydrogeological units in the scatter plots shown in the appendix 2. Trends within the abundance of clay, sand and silt and their distance to the apex are not present. The boreholes selected along the two distributary channels of the Mekong river do not show a correlation between the fraction of one of the lithologies and the distance from the apex.

The linear regression lines in Q2, qp2-3 and Q11 suggest that there is a positive correlation regarding the distance from the coast and the fraction of clay. This should suggest clay deposits become more frequent inland and the river sediment becomes sandier near the coast. Besides this observation is counter-intuitive, the r^2-value of the different regression lines are very low (<0,1) which suggest no correlation exists within the abundance of clay, sand and silt and the distance towards the coast in the selection of boreholes. With exclusion of the spatial patterns described in section 4.2, no correlation exists regarding lithological fraction and distance towards coast.

4.4 Geotechnical parameterization of the subsurface

4.4.1 Compressibility index

The compressibility index of each borehole is summarized in the spreadsheet 'Geo_Tech.xlsx'. The regression lines required to calculate the compressibility index for each different region are shown in Appendix 3.

In the spreadsheet model several trends within the compressibility index can be observed. The first trend is that the index decreases according to the depth. While the compressibility index of the top-most aquifer (qh) ranges from 0,005 – 0,1, the compressibility index of the deepest aquifer (n13) ranges from 0,0003 – 0,03. This means deeper lithological units are far less compressible than shallower lithological units.

Furthermore, the higher the fraction of clay is in an aquifer of a borehole, the more compressible the lithological unit is. This is in line with the observations done by Widado & Ibrahim (2012) and Gambolati (1991). However, this relationship becomes weaker with increasing depth. The differences between the compressibility index of borehole sample that contains sand and a borehole sample that contains clay are e.g. 0,19 in Ha Tien if the samples are both found on one meter of depth. When the same samples are found at 800 meters deep, the difference is only 0,0001.

4.4.2 Initial void ratio

The initial void ratio is measured by the DWRPIS (2010) and varies from 0,71 – 0,76 for sandy soils and from 0,71 – 1,39 for clay soils in the MKD (figure 15). The spatial trend observed for sand soils is that the void ratio increases in a northern direction. For clay soils the opposite is true whereas the void ratio

increases in a southern direction with exceptions for the eastern and western areas of the delta where the void ratio is relatively low. The void ratio for each borehole is shown in spreadsheet Geo_Tech.

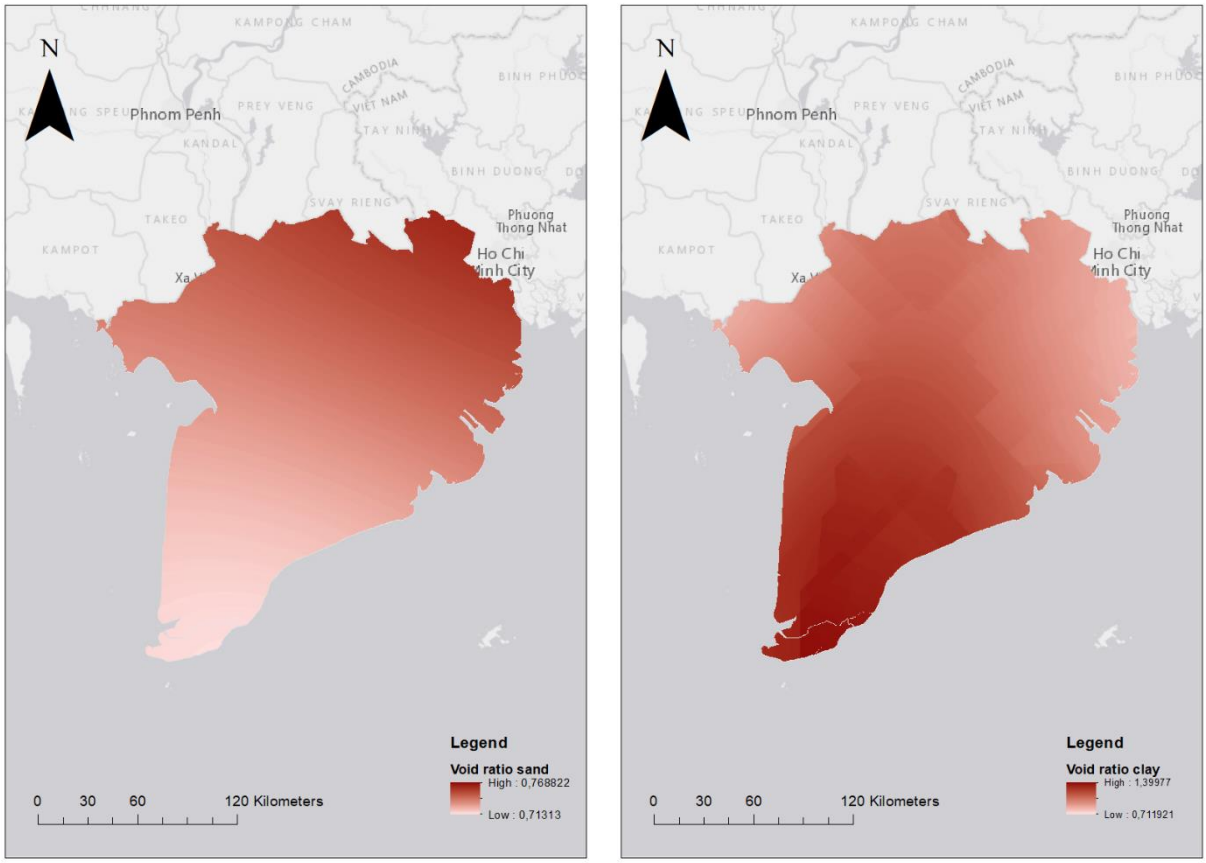

Figure 15: left: the initial void ratio of sandy soils. right: the initial void ratio of clay soils. Results after ordinary kriging based on in field measurements of the DWRPIS (2010)

4.4.3 Bulk density

The bulk density is measured by the DWRPIS (2010) for both sand soils and clay soils. The value for sand soils ranges from 16,8 – 18,1 kN/m^3 and for clay soils the value ranges from 16,9 – 18,6 kN/m^3 (figure 16).

The spatial trend observed should be the inverse of the trend observed of the initial void ratio. Hence, a higher void ratio means more space between the pores for air or water, so the density of the soil becomes less. Vice versa a low void ratio means a higher density of the soil. This trend is observed in the bulk density of the clay soil. Where the void ratio is low in the eastern and western part of the delta, the bulk density is relatively high. The same accounts for the north-south trend. The bulk density is increasing going southwards, while the void ratio is decreasing in this direction. The same trend is not observed in sand

soils of the MKD. Here, an increase in bulk density means an increase in void ratio as well. The bulk density of each borehole is extracted and recorded in the spreadsheet Geo_Tech.

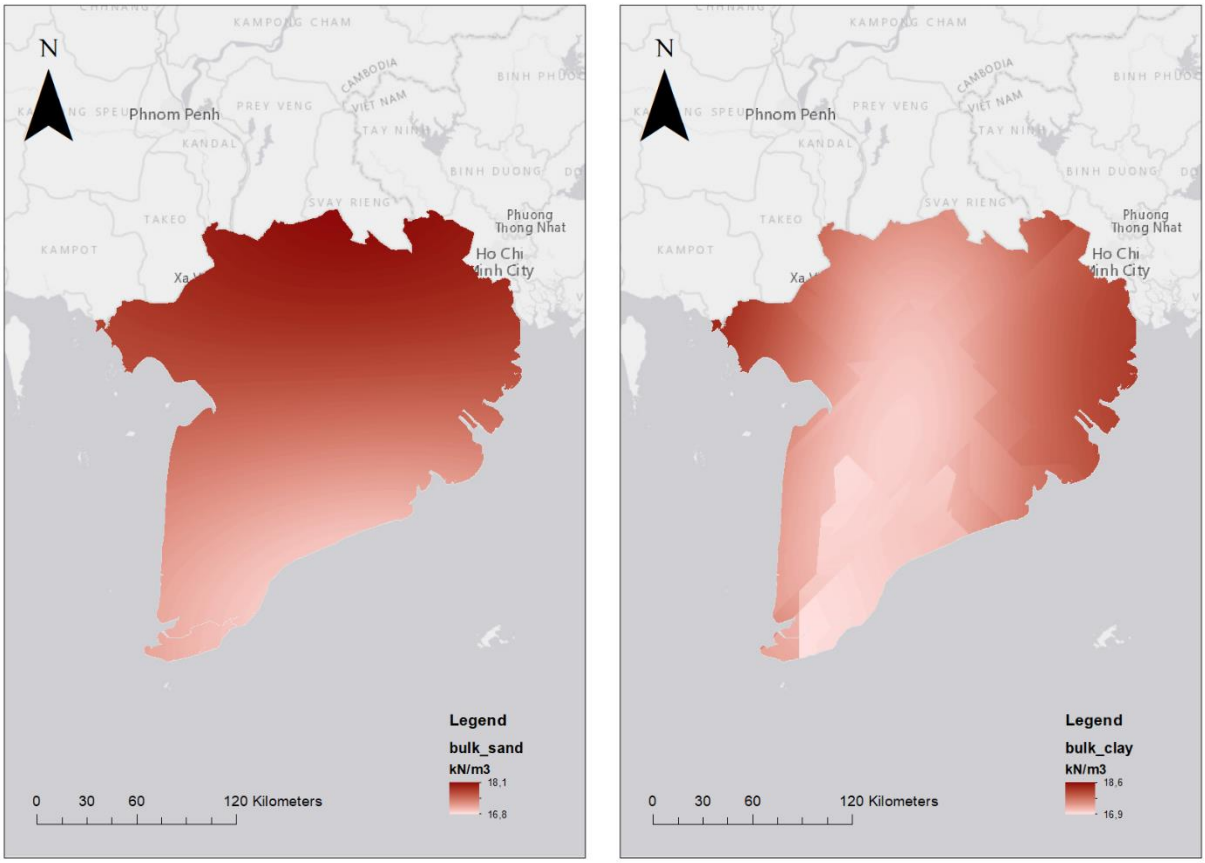

Figure 16: left: the bulk density of sandy soils. right: the bulk density of clay soils. Results after ordinary kriging based on in field measurements of the DWRPIS (2010)

4.4.4 Secondary compressibility index

The secondary compressibility index is calculated for each borehole and shown in the spreadsheet model subsidence_MKD.xlsx. Since the secondary compressibility index is derived from the primary compressibility index the same trend as the primary index exists. This means the secondary compressibility index decreases with depth. An increased depth means a more compressed soil and the creep process already occurred. In the spreadsheet this means that the average secondary compressibility index value of the qh-aquifer (0,002) is higher than the secondary compressibility index of the n13-aquifer (0,0001).

4.5 Groundwater extraction and the effect on grain stress

The average hydraulic head drops per aquifer are included in figure 13. The average increase in grain stress is shown in table 6. This table shows most groundwater is being extracted out of aquifer qp1 followed by the aquifers n22, n21, n13, qp2-3, qp3 and finally the least groundwater is extracted out of aquifer qh. Spatially, groundwater hotspots are located surrounding urban areas like Cau Ma and Ho Chi

Minh City. In the spreadsheet model this is registered as a relatively high increase in grain stress. The highest increases in grain stress in the aquifers are found in boreholes in those areas. The exact values can be found in the spreadsheet model subsidence_MKD.

Table 6: The average geotechnical parameters and average subsidence calculated per aquifer after 25 years. The grey and white rows represent aquitards and aquifers respectively.

-	Thick-ness (m)	Primary compressibility index (-)	Secondary compressibility index (-)	Initial void ratio (-)	Initial Grain stress (kPa)	Increase in grain stress (kPa)	Primary subsidence (cm)	Secondary subsidence (cm)	Total subsidence (cm)
Q2	17.35	0.072	0.0031	1.03	131.16	0	0	7.37	7.37
qh	7.55	0.058	0.0024	0.998	183.92	33.28	0.94	2.29	3.22
Q13	14.27	0.048	0.002	0.964	279.73	34.38	1.12	3.58	4.70
qp3	23.66	0.03	0.0012	0.901	465.78	87.08	2.70	3.78	6.49
Q12-3	14.08	0.024	0.0009	0.88	571.81	86.17	1.36	2.23	3.59
qp2-3	33.08	0.015	0.0005	0.84	819.18	148.51	2.05	2.60	4.66
Q11	16.19	0.014	0.0005	0.84	930.07	141.24	0.82	1.45	2.28
qp1	33.47	0.011	0.0004	0.84	1184.2	222	1.21	1.86	3.07
N22	24.17	0.009	0.0003	0.84	1382.2	223.21	0.64	1.12	1.76
n22	41.02	0.007	0.0002	0.85	1695.1	299.5	1.02	1.27	2.3
N21	21.23	0.005	0.0001	0.83	1908.2	278.7	0.27	0.41	0.68
n21	44.09	0.005	0.0001	0.85	2229.84	349.04	0.55	0.76	1.31
N13	29.59	0.004	0.0001	0.84	2472.34	348.95	0.22	0.27	0.49
n13	51.6	0.003	0.0001	0.85	2832.79	416.88	0.31	0.37	0.68
Total	-	-	-	-	-	-	**13.30**	**30.21**	**43.51**

Table 7: The average depth, fraction clay, sand and silt and total subsidence after 25 years. The grey and white rows represent aquitards and aquifers respectively.

-	Depth (m)	Thickness (m)	Fraction clay (-)	Fraction sand (-)	Fraction silt (-)	Total Subsidence (cm)
Q2	9.46	17.35	0.7	0.16	0.14	7.37
qh	21.29	7.55	0.53	0.32	0.15	3.22
Q13	30.79	14.27	0.51	0.34	0.15	4.70
qp3	50.26	23.66	0.33	0.55	0.12	6.49
Q12-3	69.27	14.08	0.35	0.52	0.13	3.59
qp2-3	92.89	33.08	0.22	0.68	0.1	4.66
Q11	115.90	16.19	0.3	0.56	0.14	2.28
qp1	140.50	33.47	0.25	0.64	0.11	3.07
N22	171.30	24.17	0.29	0.6	0.11	1.76
n22	203.72	41.02	0.26	0.63	0.11	2.3
N21	239.42	21.23	0.22	0.67	0.11	0.68
n21	269.42	44.09	0.26	0.62	0.11	1.31
N13	309.05	29.59	0.26	0.63	0.11	0.49
n13	345.44	51.6	0.27	0.61	0.12	0.68

Table 8: The average total subsidence in centimeters per aquifer for consolidation ratios of 0,2, 0,4, 0,6, 0,8 & 1 representing the average total subsidence after 5, 10, 15, 20, 25 years.

-	Total subsidence (U=0,2; 5 year)	Total subsidence (U=0,4; 10 year)	Total subsidence (U=0,6; 15 year)	Total subsidence (U=0,8; 20 year)	Total subsidence (U=1; 25 year)
Q2	3.68	5.27	6.20	6.86	7.37
qh	1.33	2.01	2.49	2.88	3.22
Q13	2.14	3.21	3.95	4.55	4.70
qp3	2.42	3.77	4.78	5.66	6.49
Q12-3	1.39	2.14	2.69	3.17	3.59
qp2-3	1.71	2.69	3.42	4.07	4.66
Q11	0.89	1.37	1.72	2.01	2.28
qp1	1.17	1.81	2.29	2.70	3.07
N22	0.69	1.06	1.33	1.56	1.76
n22	0.84	1.32	1.68	2.00	2.30
N21	0.26	0.40	0.51	0.60	0.68
n21	0.49	0.76	0.97	1.14	1.31
N13	0.18	0.28	0.36	0.43	0.49
n13	0.25	0.39	0.50	0.60	0.68
Total aquifer	8.21	12.74	16.14	19.05	21.72
Total aquitard	9.12	13.71	16.73	19.09	21.13
Total	17.33	26.45	32.87	38.14	43.3

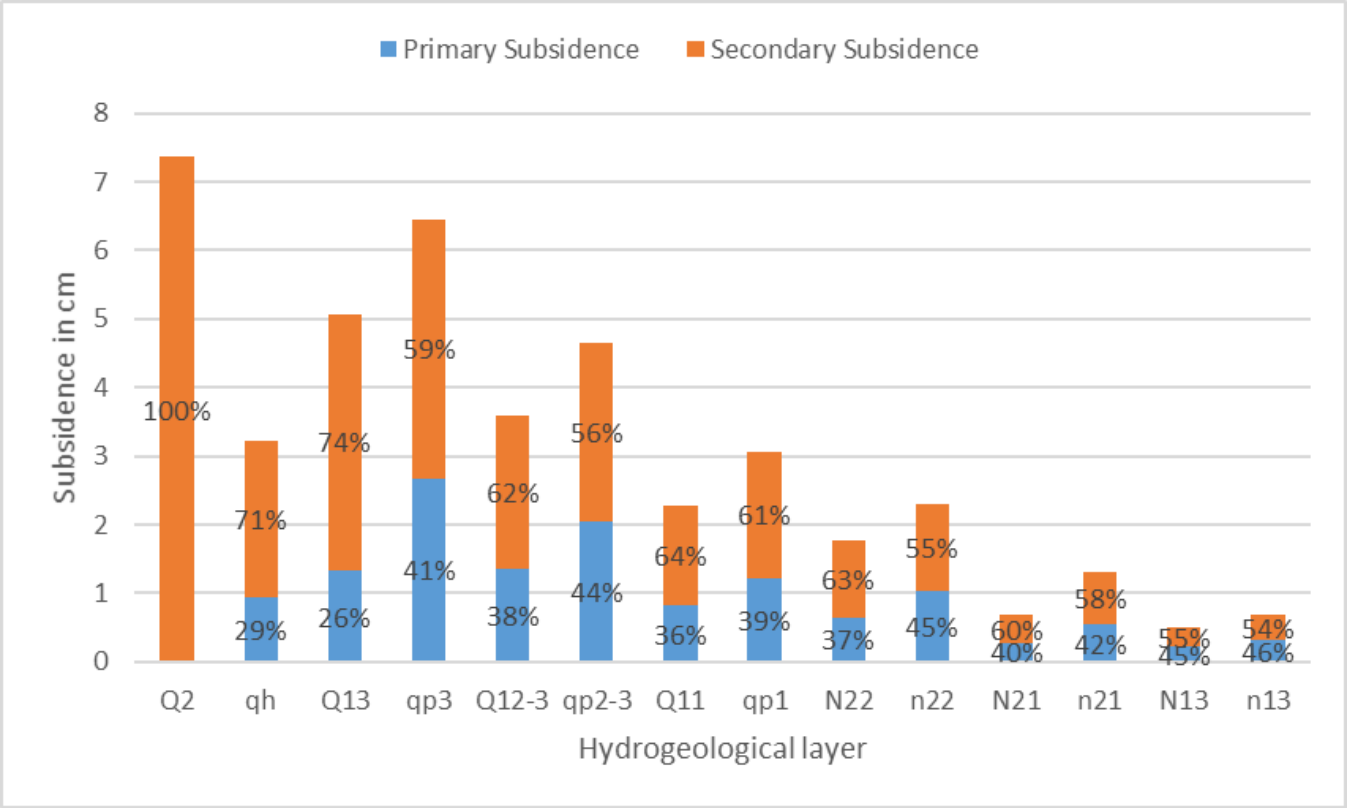

Figure 17: The primary and secondary subsidence of each hydrogeological layer after 25 years.

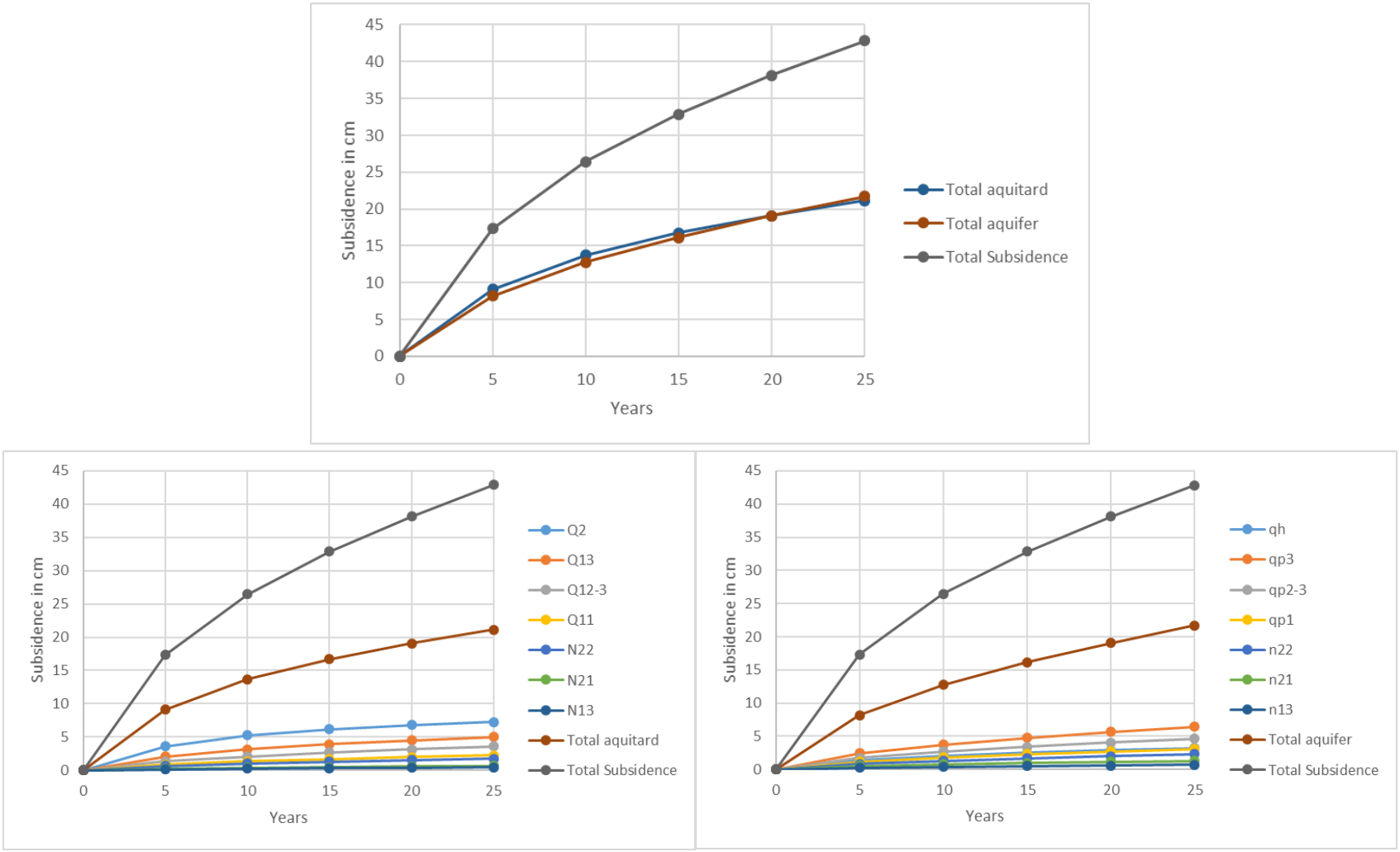

Figure 18: top: the total subsidence for both all the aquifers and all the aquitards for 0 – 25 years. Left: the total subsidence for all the aquitards for 0 – 25 years. Right: the total subsidence for all the aquifers for 0 – 25 years.

4.6 Subsidence potential

The average subsidence potential for the seven different aquifers in 25 years is shown in table 7. According to the presented method, the delta-wide, average subsidence rate is 43.3 cm in 25 years. 13.3 cm (31%) is caused by primary subsidence which is mainly caused by an increase in grain stress and 30.2 cm (69%) is caused by secondary subsidence or creep. Aquitard Q2 is the aquifer where most of the subsidence will happen: 7.37 cm in 25 years. The aquifer with the highest subsidence rate is qp3: 5.66 cm in 25 years. The aquifer qh and aquitard Q13 subside with 3.23 and 4.55 cm in 25 years respectively. The upper-middle Pleistocene hydrogeological layers: Q12-3 and qp2-3 subside 5.24 and 4.66 cm in 25 years respectively. The lower Pleistocene aquitard (Q11) and aquifer (qp1) subside with a rate of 3.37 and 2.70 cm in 25 years respectively. The deeper aquifers and aquitards experience less subsidence. The aquitards N22, N21 and N13 subside 1.56 cm, 0.68 cm and 0.50 cm in 25 years respectively. Aquifers n22, n21 and n13 subside 2.00 cm, 1.31 cm and 0.69 cm in 25 years respectively (table 6).

The total average subsidence for each hydrogeological layer for 25 years, depth, thickness and lithological fractions are shown in table 7. This table partly shows the role of the thickness, depth and the lithology of the hydrogeological layer regarding the amount of subsidence. The aquifers n22 and n21 are subsiding more than the aquitards N22 and N21 on approximately the same depth with the same lithology. This is because the average thickness of the aquifers n22 and n21 is 41 meter and 44 meter respectively, compared to an average thickness of 24 meter and 21 meter for the aquitards N22 and N21. The role of lithology and depth is visible when considering the relatively high amount of subsidence in aquitard Q2 (7.37 cm). The relatively high amount of subsidence is explained by the relatively low depth (9.5 meter) and the relatively high fraction of clay (0.7) in this layer. The low depth and high fraction of clay cause a high compressibility rate which results in a relatively high amount of subsidence.

Next, the results show that land subsidence is slowing down over time (table 8 and figure 18). At a consolidation ratio of 0,2 which represents a timestep of 5 years, the expected average land subsidence of the MKD is 17.33 cm. The pace of the subsidence slowly decreases over time. The expected average land subsidence at a consolidation ratio of 0,4, 0,6, 0,8 and 1 (representing respectively 10, 15, 20 & 25 years) equals 26.45, 32.87 cm, 38.14 cm and 43.3 cm.

Next, figure 17 shows the subsidence rate for each hydrogeological layer, divided in subsidence caused by an increase in grain stress (primary subsidence) and subsidence caused by creep (secondary subsidence). The first aquitard Q2 does not experience an increase in grain stress, thus resulting in a subsidence rate caused completely by secondary subsidence. The subsidence of other geohydrological layers are on average mainly caused by secondary subsidence (54% - 77%) compared to primary subsidence (23-46%). The hydrogeological layer where the relative amount of primary subsidence is the highest is aquifer n13 (46%). The hydrogeological layer where the relative amount of secondary subsidence is the highest, with the exception of aquitard Q2, is Q13 (77%).

Furthermore, figure 18 shows the subsidence rate of the seven aquifers and seven aquitards in the MKD. The total subsidence rate of the seven aquifers over 25 years is 21.72 cm. The total subsidence rate of the seven aquitards over 25 years is 21.13 cm.

The spatial variability of land subsidence is high. This means relatively large differences exist between different areas as can be seen in figure 19. The subsidence rate is the highest near the urban areas of Ca Mau and Soc Trang. In Ca Mau the subsidence rate equals 74 cm in 25 years (2.96 cm year^{-1}) and near Soc Trang the subsidence rate equals 50 cm in 25 years (2 cm year^{-1}). In the central area of the MKD the subsidence rate ranges from 30 cm – 40 cm in 25 years (1.2 cm year^{-1} – 1.6 cm year^{-1}). The eastern areas My Tho and Ben Tre have a subsidence range that ranges from 20 cm – 30 cm in 25 years (0.8 cm year^{-1} – 1.2 cm year^{-1}). The area west of Long Xuyen experiences the lowest subsidence rate ranging from 7 cm – 20 cm in 25 years (0.3 cm year^{-1}– 0.8 cm year^{-1}). On average the land subsidence rate in the MKD equals 1.7 cm year^{-1}.

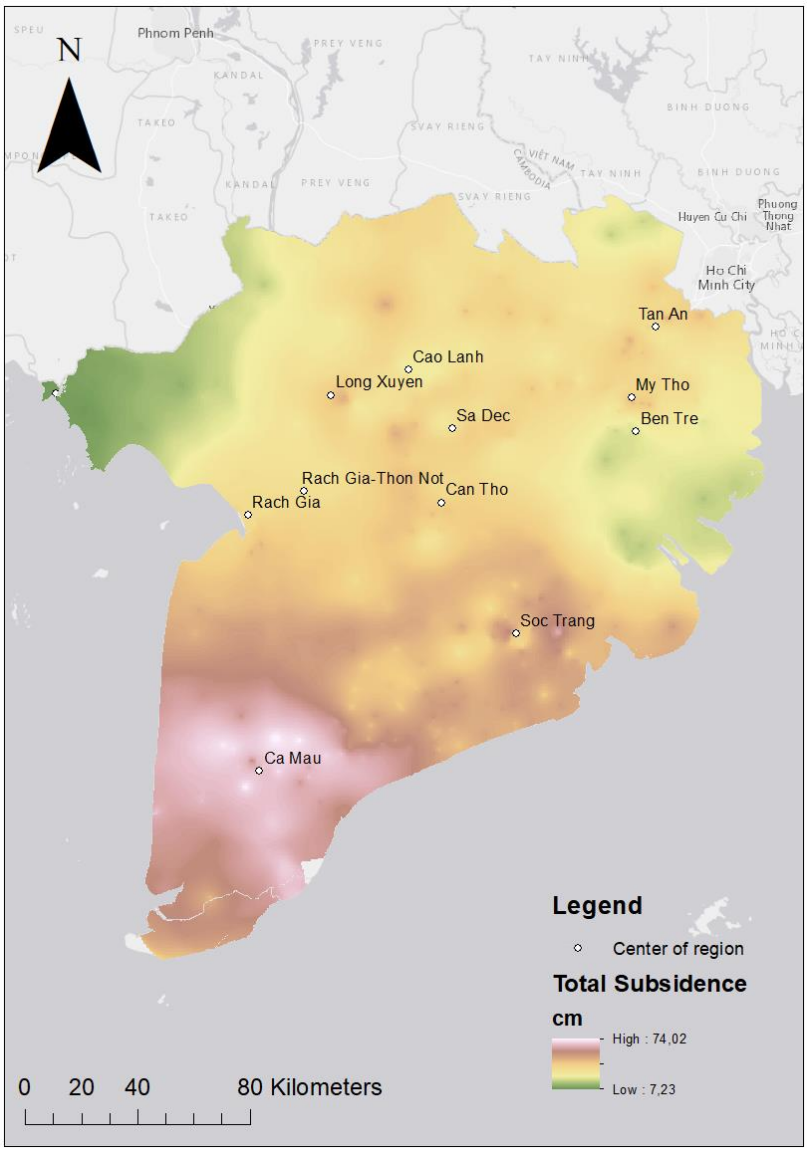

Figure 19: The subsidence rate for the MKD over 25 years.

5. Discussion

5.1 Subsidence in the MKD

The land subsidence rate presented in this paper exceed estimates of earlier land subsidence estimates in the Mekong Delta. Minderhoud et al. (2017) estimated an average land subsidence rate of 18 cm that ranges from 8 cm – 53 cm caused by groundwater extraction in the time-period 1991 – 2016. This study found an average land subsidence rate of 43.3 cm that ranges from 7 cm – 73 cm using groundwater extraction data from the same time period.

Spatially, the hotspot of Ca Mau is both identified in this paper as in Erban et al., (2014) and Minderhoud et al., (2017). The same accounts for the area of Soc Trang region. In terms of absolute land subsidence rate the difference with the average land subsidence rate is less compared to the area of Ca Mau, but the land subsidence rate in the area of Soc Trang is higher than the average land subsidence rate. Northwards from Soc Trang, the land subsidence rate remains around the average rate while the eastern areas (My Tho & Ben Tre) and western area (west of Long Xuyen) have a subsidence rate lower than average. This spatial pattern is in line with the spatial patterns found in Erban et al. (2014) and Minderhoud et al. 2017).

The average land subsidence rate per year found in this study equals 1.7 cm year^{-1}. This rate is in line with the average land subsidence rate per year reported by Erban et al. (2014) (1.6 cm year^{-1}) but slightly higher than the value reported by Minderhoud et al. (2017) (1.1 cm year^{-1}). The average land subsidence rate ranges from 0.3 cm year^{-1} – 2.96 cm year^{-1}. This result is in line with InSAR-measured land subsidence rates. Erban et al. (2014) measured a land subsidence rate of 1 cm year^{-1} – 4 cm year^{-1}. This range includes the area surrounding Ho Chi Minh City, an area not included in this study. When Ho Chi Minh City is excluded the subsidence rate ranges from 0.5 cm year^{-1}– 3 cm year^{-1}. The range is in line with the results by Minderhoud et al. (2017) as well: 0.6 cm year^{-1} – 3.1 cm year^{-1}.

The results of this study suggest that only 30 % of the occurring land subsidence is caused by primary subsidence which is caused by an increase in grains tress. The remaining 70 % is caused by secondary subsidence which is caused by creep. This is contrary to the results presented by Erban et al. (2014) where groundwater-induced land subsidence was estimated to be 50-95% of the total land subsidence. The difference is mainly caused by the characterization of the subsurface of the MKD. Since these results show relatively high fractions of clay – even in the seven aquifers – and clay is the most sensitive lithology regarding creep, this can explain the relative high land subsidence rates caused by creep.

Next, the apex-to-coast analysis did not find any trends within the delta. A possible reason for this is the complex geomorphology of the delta. The alternation of glacial periods and interglacial periods caused the distributary channels of the Mekong Delta to change their position and create a complex sequence of lithologies. Besides the distributary channels, the incised valleys that filled up with marine sediments create a complex geomorphology as well. This could be the cause for the absence of trends in this analysis.

Additionally, the results of this study provide insight in which hydrogeological layers are more susceptible and which aquifers are less susceptible for land subsidence. The analysis showed that aquitard Q2 is most susceptible for land subsidence. A possible explanation is that this layer contains thick clay layers

which experience relatively a high amount of creep. Relatively high compressibility indices caused by the low average depth of the aquitard could cause the high amount of creep.

The aquifer qh and aquitard Q13 have relatively low subsidence rates considering these hydrogeological layers are relatively shallow layers. The reason for this is the relative thinness of these layers. The aquifer qh is on average only 7 meters thick and the aquitard Q13 is only 14 meters thick which is relatively thin compared to other hydrogeological layers.

The land subsidence rates of deeper aquifers and aquitards (N22, n22, N21, n21, N13, n13) are the lowest. Since these are the deepest aquifers these hydrogeological layers have the lowest compressibility indices which result in a low subsidence rate.

Spatially, Ca Mau is identified as an area that is susceptible for land subsidence. This is caused by a combination of groundwater withdrawal and compressibility index. The extraction of groundwater is currently concentrated in the area near Ca Mau (figure 13). In the aquifers qp3, qp2-3, qp1 and n22 the hydraulic head drop is the largest in the area of Ca Mau (excluding Ho Chi Minh City). The compressibility index is the highest in the area of Ca Mau (table 3). The high compressibility index in combination with the relatively large hydraulic head drop causes a relatively high amount of land subsidence in Ca Mau.

Overall, by considering the lithology and land subsidence rate of different aquifers and aquitards new groundwater policies can be developed taking into account the local variety in characteristics of the subsurface. The land subsidence rate of the MKD shown in figure 19 shows a high amount of spatial variety compared to previous result by Minderhoud et al. (2017). Small local hotspots within Ca Mau are visible which represent area where a lot of water is being extracted and the compressibility index is high. Besides these hotspots, the local variety is also visible in other areas in the MKD such as the area between Ca Mau and Soc Trang and the area between Can Tho, Rach Gia and Cao Lanh. Integrating the lithological composition and its geotechnical parameters results in a spatially variable and detailed map of land subsidence in the MKD. By taking into account this spatial variability of land subsidence new policies can avoid the extraction of groundwater in Ca Mau or Soc Trang, areas susceptible to groundwater extraction.

Besides the spatial patterns, the results of this study contribute to providing insight into the subsidence rate per hydrogeological layer. The results show that Q2 is the most compactible aquitard and qp3 is the most compactible aquifer. The deepest aquifer n13 is experiencing the lowest amount of subsidence. The differences in subsidence rate per aquifer can be used in the decision-making process of groundwater policies. To reduce the amount of land subsidence, groundwater extraction should be concentrated in aquifers n22, n21 and n13 due to their relatively low compressibility index and low subsidence rate.

5.2 Limitations of the study

The methodology of this study contains certain limitations or assumptions which influence the results. A few of these limitations are found in the determination of different geotechnical parameters. First, the approach of calculating the void ratio for sand soils contains inaccuracies. The kriging process to create a delta-wide map is based on only three measurement points which is unrepresentative for the full delta of 40.000 km^2. Furthermore, the assumption that the initial void ratio has no vertical variability is false. This

causes the void ratio in deeper aquifers to be an overestimation which results in an underestimation of land subsidence.

Second, the calculation of the bulk density includes questionable assumptions. Again, the vertical variability is neglected. This means the bulk density in lower aquifers is underestimated. This means the grain stress in deeper aquifers is an underestimation and thus, the land subsidence is underestimated as well. However, this does not mean depth is totally neglected in the equation since the depth of the aquifer is still included to calculate grain stress.

Third, geotechnical parameters do not change over time. This means when the consolidation ratio is adjusted the geotechnical parameters remain the same. When the consolidation ratio is adjusted from 0.2 to 0.4 which represent a timestep of 5 years, subsidence has occurred which affect the bulk density, initial void ratio and the compressibility index. Since these parameters do not change over time, primary subsidence is slightly overestimated.

Next, the lithological simplification has implications as well. By simplifying the ten lithologies determined by the DWRPIS to three main lithologies variety is neglected. The main issue with the simplification is the determination of geotechnical parameters of silty soils. The bulk density for silty soils in the delta is unknown and the assumption here is made on a limited number of sources. Overall, the simplification of the lithological classes results in less detailed land subsidence estimations.

Furthermore, the lithological fractions in each hydrogeological layer is determined based on heterogeneity of borehole samples. This affects the lithological fractions in a way that aquifers are relatively clay-rich which is counter-intuitive. The relatively high clay rates in aquifers are the cause of an overestimation of land subsidence and the relatively high subsidence rate caused by creep.

Additionally, the spatial location of aquifers is questionable. The size and location of the seven aquifers is determined based on the boreholes. If an aquifer was not found in the records of a borehole, the boundary of an aquifer is drawn by hand based on data of surrounding boreholes. This results in questionable aquifer boundaries which affect groundwater extraction rates and thus land subsidence.

Finally, aquifer drawdown data is not related to time. The hydraulic head drop data in the spreadsheet model does not change over time. This means the 25 years of groundwater extraction are extracted instantly. This results in the relatively large subsidence rate in the first 5 years.

5.3 Improvements & Recommendations

The results in this study are summarized in a spreadsheet subsidence_MKD. The initial grain stress parameter in this spreadsheet model is based on groundwater extraction data. This groundwater extraction data originates from Minderhoud et al. (2017) and is from the years 1991-2016. Since groundwater extractions tend to increase in the future, this data can be considered outdated. Extrapolating current groundwater extraction rates in the Mekong Delta to the future is helpful to calculate a more specific hydraulic head drop which again contributes to a more accurate increase in grain stress.

Next, the geotechnical parameterization could be improved in several ways. First, an increase of measurement points of initial void ratio and bulk density is required to include local variety of geotechnical parameters in the analysis. Ideally, a database is created similar to the compressibility index measurements.

This means measurements of bulk density and initial void ratio for both clay and sand are done in all of the twelve regions. Second, the consolidation ratio should affect the geotechnical parameters in the spreadsheet model. The increased subsidence by an increase in consolidation ratio causes an increase in bulk density and a decrease in initial void ratio which affect the subsidence rate. If these parameters are dependent on consolidation ratio the subsidence rate estimates improve.

Furthermore, the analysis can be extended by removing the simplification of the different lithological classes. Geotechnical parameters are available for six different lithologies (DWPRIS, 2010). Since this data is available, the simplification becomes unnecessary. The same analysis can be carried out for six lithologies instead of three which will result in a more detailed estimation of land subsidence of the Mekong Delta and the land subsidence sensitivity of different lithologies. This causes the overestimation and relatively high creep rate to decrease due to the distinction of different clay types which are less susceptible for land subsidence.

Finally, aquifer drawdown data should be time-dependent. When the hydraulic head drop per aquifer is calculated for 5, 10, 15 and 20 years, the groundwater extraction in these years can be estimated more precisely. This will result in better primary land subsidence estimations.

6. Conclusion

Overall, the results of this study are contributing to a better understanding of land subsidence in the Mekong Delta. The amount and pace of land subsidence is in line with previous estimations, but the characterization of the subsurface provided new insights into the main causes of the subsidence. The analysis in this study showed that creep in clay soils based on the secondary compressibility index is causing the most land subsidence.

The analysis in this study provided answers to all the sub-questions. The characterization of the subsurface precisely identified fractions clay, sand and silt for each aquifer. Furthermore, the spreadsheet model showing the characterization of the subsurface (Integrated_Database) offers a complete overview of each borehole including the lithology per meter depth and the aquifer this meter depth is located in. Additionally, 15x3 raster maps are created to give an overview of the delta-wide lithological fractions of the MKD.

Furthermore, the apex-to-coast trend analysis did not result in a meaningful trend. Several reasons that can explain the absence of a clear trend in this analysis relate to the complexity of the geomorphology of the delta. The change in river-course and deep-incised river valleys that are filled up with marine sediment are examples of this.

The determination of geotechnical parameters is done based on the combination of measurements carried out in the delta and literature. The primary and secondary compressibility index, initial void ratio, bulk density and grain stress are determined. These parameters are combined with the integrated database to assign each borehole with unique parameters which allow for a precise land subsidence estimate.

Additionally, the modelled hydraulic head drop is used to calculate the increase in grain stress per aquifer per borehole location. By adding this data to the land subsidence equation, the increase in grain stress and thus primary subsidence can be calculated for each hydrogeological layer.

By combining the integrated database, geotechnical parameters & groundwater extraction data land subsidence could be estimated for the full MKD per hydrogeological layer. This analysis resulted in an average land subsidence rate of 43,3 cm in 25 years for the delta with hotspots up to 73 cm near the urban areas of Ca Mau and Soc Trang.

Overall, the analysis contributes to a better understanding of land subsidence in the MKD and provided a quantification of the different parameters affecting land subsidence. Due to this better understanding of the different parameters and their effect on land subsidence, more deliberated groundwater policies can be developed (e.g. the relative high subsidence potential of the qp3 aquifer or the hotspots near the urban areas of Ca Mau or Soc Trang).

In the future, the spreadsheet model can be updated with more recent groundwater extraction data or a more extended lithological analysis to improve the parametrization of geotechnical properties and thus land subsidence estimates.

V. Acknowledgements

I would like to thank Dr. Esther Stouthamer for her supervision during the period of this research. The meetings on a regular basis were very helpful and greatly appreciated. The difficulties and questions I encountered were always solved due to insightful comments and problem-solving feedback. Also, I would like to thank Philip Minderhoud MSc for his open communication, providing me with the right data and sending my thesis into the right direction at the start. Furthermore, I would like to thank Simon van Laarhoven for his clarifying comments on the geotechnical parameterization of the subsurface. Finally, I would like to Hung Van Pham for his explanation on the lithological and geological datasets.

Appendices

Appendix 1: The table used to convert the lithology assigned by the DWRPIS to three lithological classes: clay, silt & sand.

Class	Lithology	Abbreviation	Lithological Class
1	Sét = clay (c)	S	Clay
2	Sét bột, bột sét = silty clay (sc)	SB,BS	Clay
3	bột/bột cát = sandy silt (ss)	B, BC	Silt
4	Cát bột, cát sạn sỏi= silty sand, gravel and sand(ss, gs)	CB , CS	Sand
5	Cát = sand	C	Sand
6	Bùn, bùn sét = mud, muddy clay	M, MS	Clay
7	Sét kết, bột kết, cát kết= Claystone, Sandstone, Siltstone	SK, BK, CK	Clay/Sand/Silt

Appendix 2: Distance-to-apex trend analysis for the Holocene Aquitard (Q2), the upper-Pleistocene aquifer (qp3), the Upper-middle Pleistocene aquifer (qp2-3) and the Lower Pleistocene aquitard (Q11)

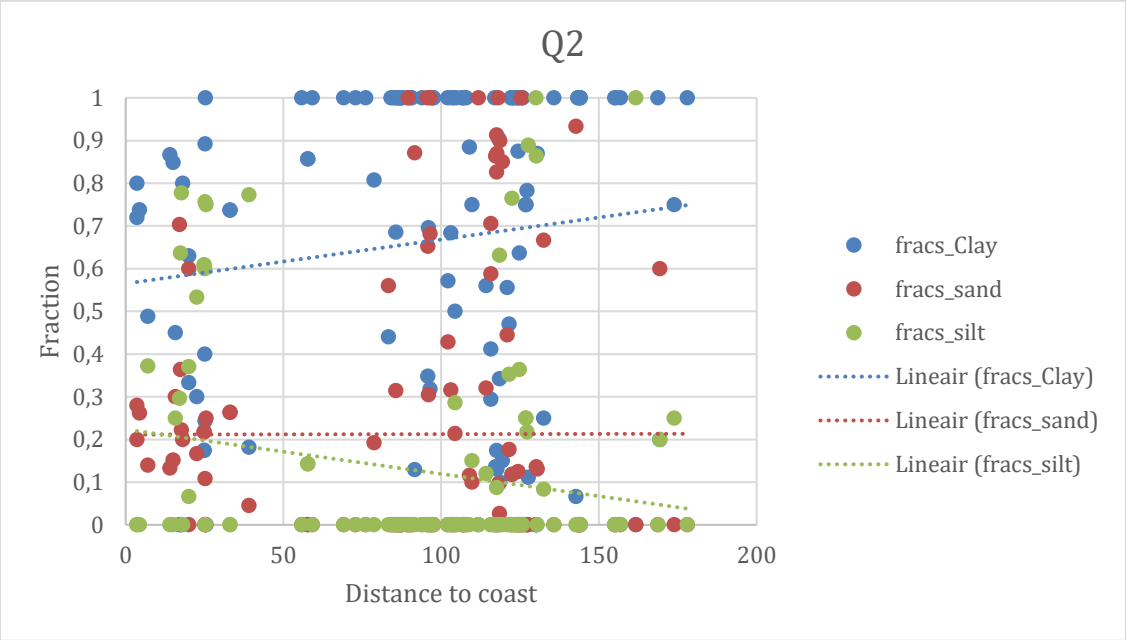

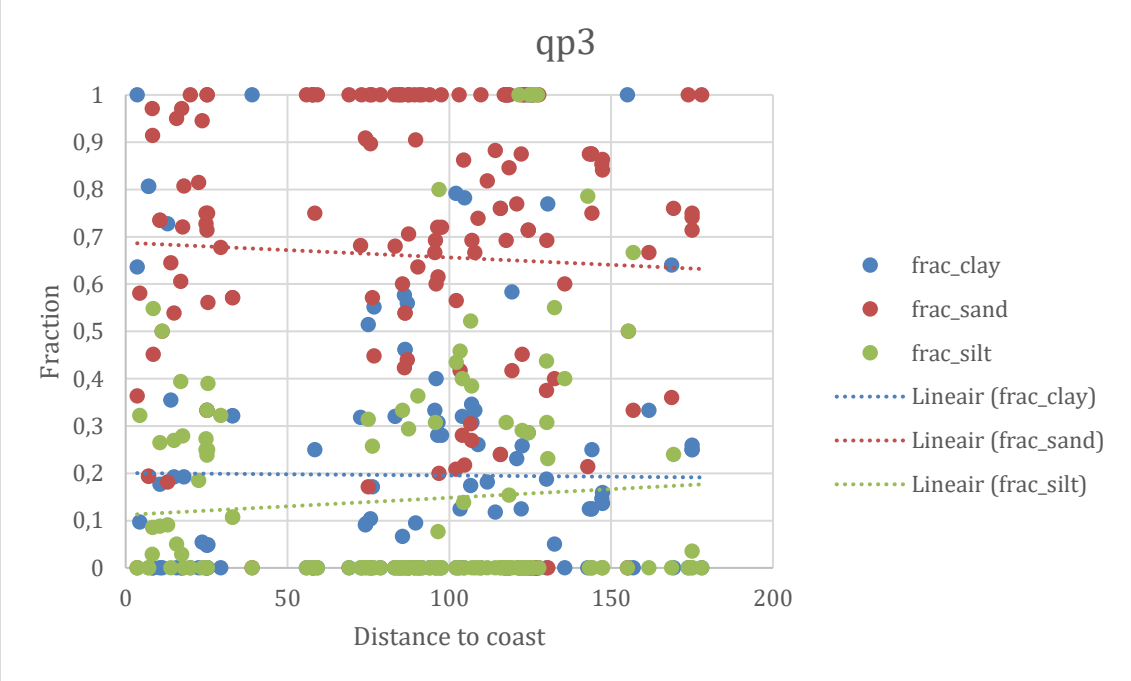

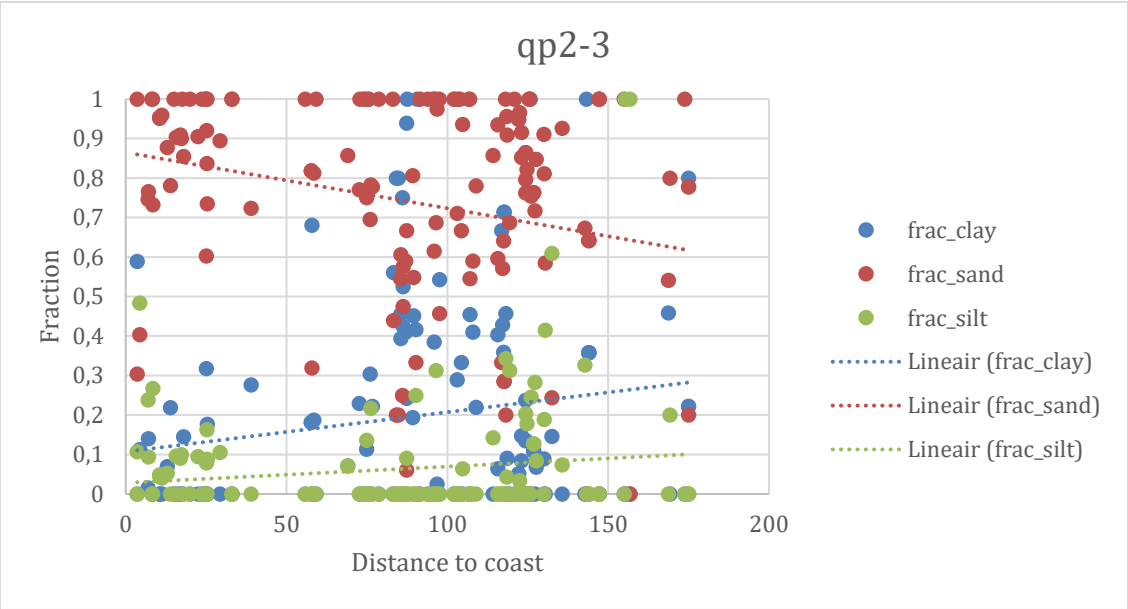
qp2-3
Fraction
Distance to coast
0
0,1
0,2
0,3
0,4
0,5
0,6
0,7
0,8
0,9
1
0
50
100
150
200
frac_clay
frac_sand
frac_silt
Lineair (frac_clay)
Lineair (frac_sand)
Lineair (frac_silt)

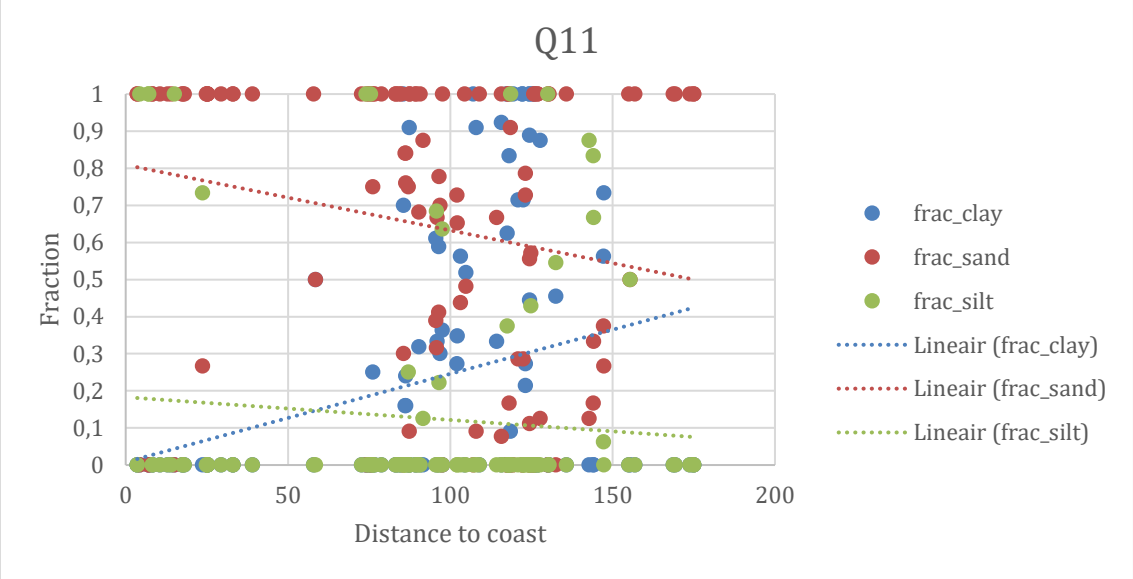
Q11
Fraction
Distance to coast
0
0,1
0,2
0,3
0,4
0,5
0,6
0,7
0,8
0,9
1
0
50
100
150
200
frac_clay
frac_sand
frac_silt
Lineair (frac_clay)
Lineair (frac_sand)
Lineair (frac_silt)

Appendix 3: The regression lines showing the correlation between depth and compressibility index of clay soils for the 12 different regions in the Mekong Delta.

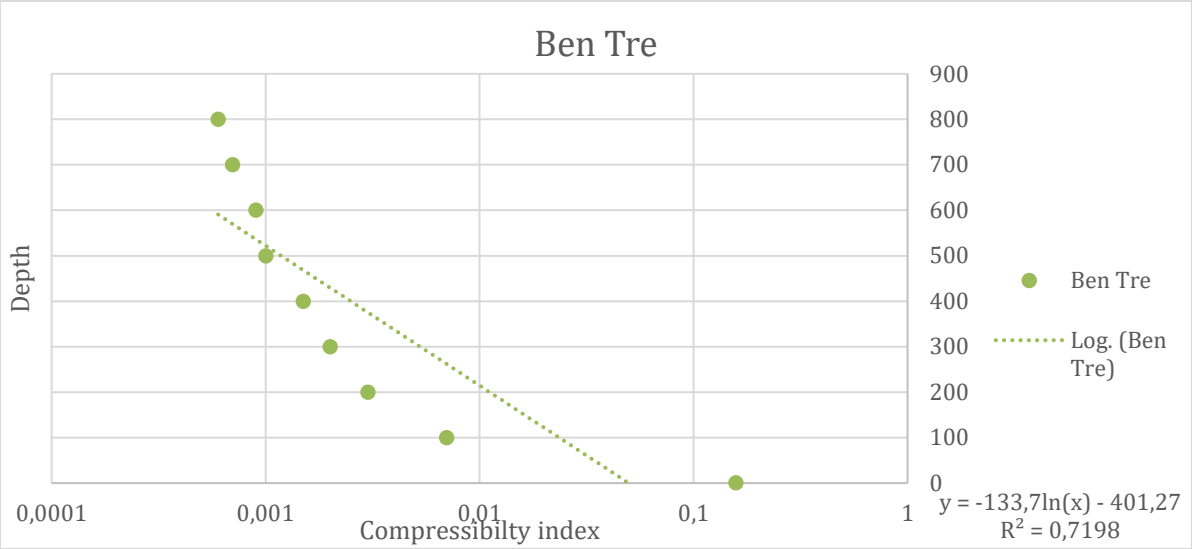

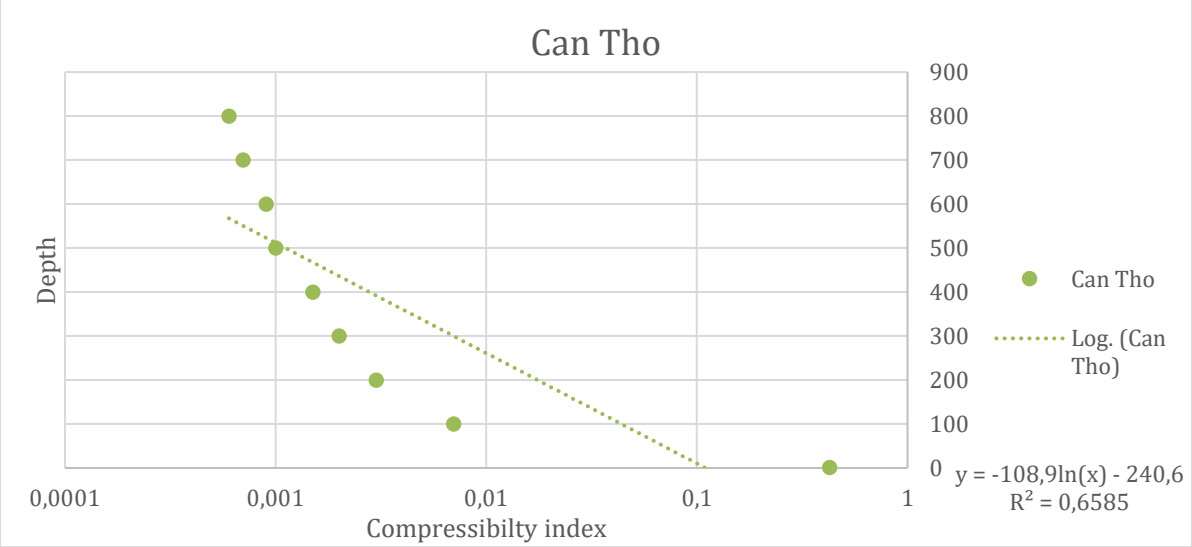

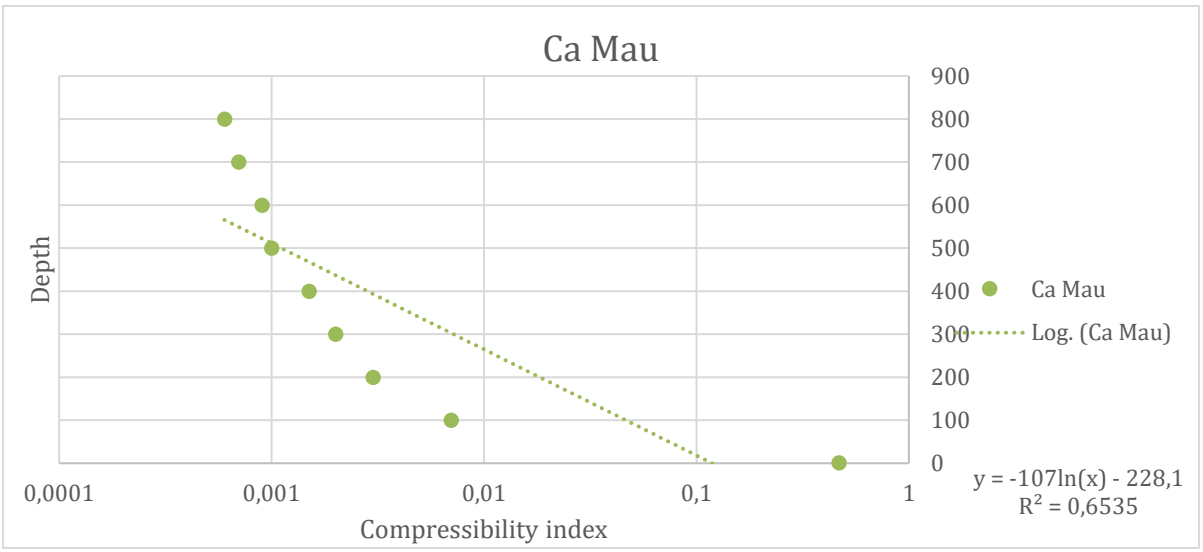
Ca Mau
Depth
900
800
700
600
500
400
300
200
100
0
0,0001
0,001
0,01
0,1
1
Compressibility index
Ca Mau
Log. (Ca Mau)
y = -107ln(x) - 228,1
R² = 0,6535

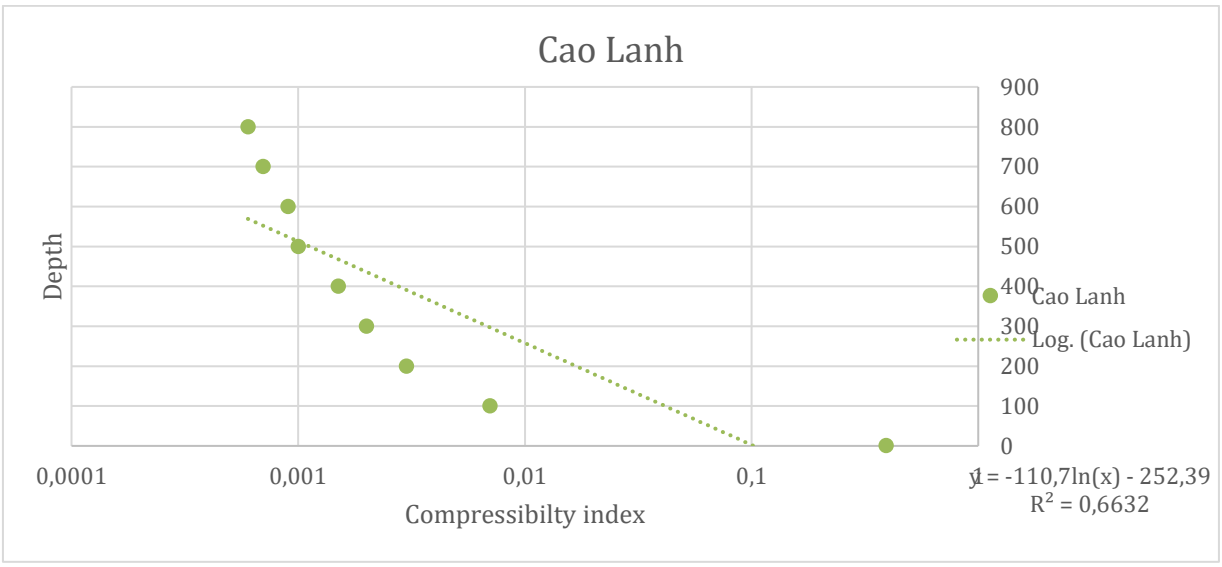
Cao Lanh
Depth
900
800
700
600
500
400
300
200
100
0
0,0001
0,001
0,01
0,1
1
Compressibilty index
Cao Lanh
Log. (Cao Lanh)
y = -110,7ln(x) - 252,39
R² = 0,6632

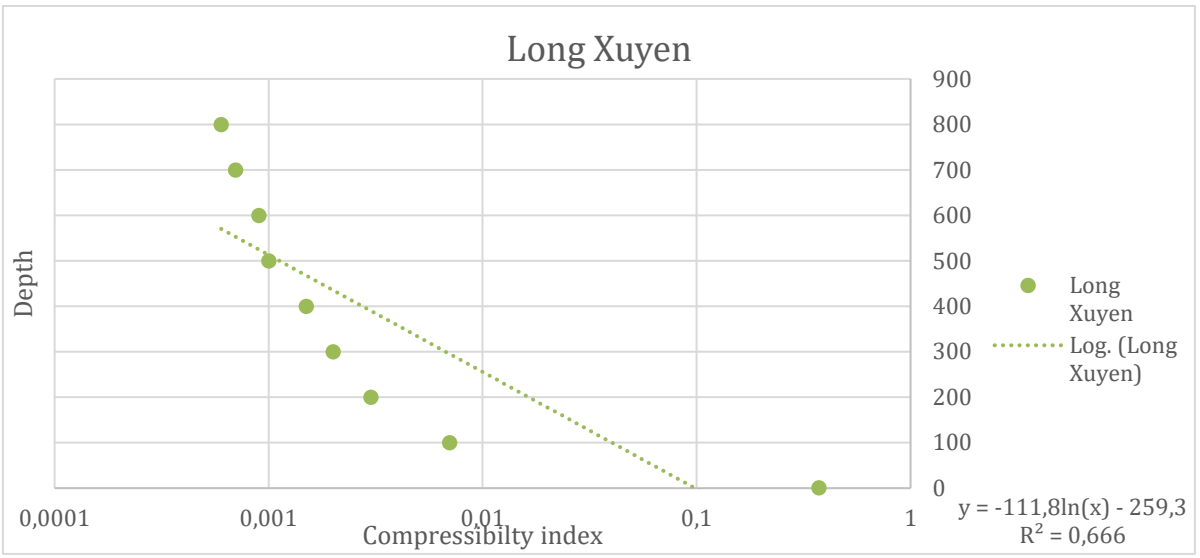
Long Xuyen
Depth
900
800
700
600
500
400
300
200
100
0
0,0001
0,001
0,01
0,1
1
Compressibilty index
Long Xuyen
Log. (Long Xuyen)
y = -111,8ln(x) - 259,3
R² = 0,666

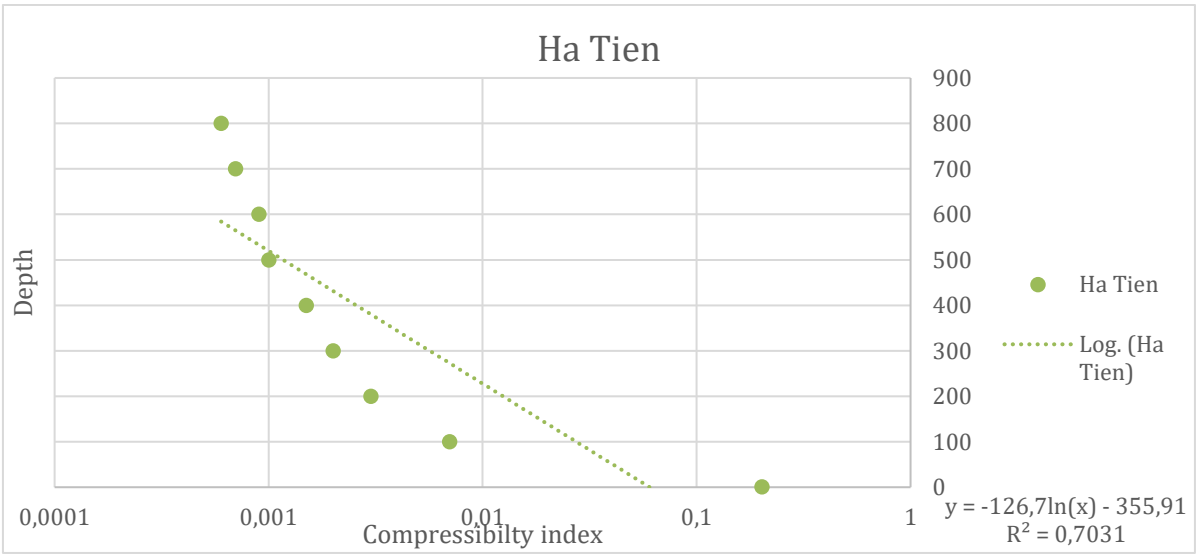
Ha Tien
Depth
900
800
700
600
500
400
300
200
100
0
0,0001
0,001
0,01
0,1
1
Compressibilty index
Ha Tien
Log. (Ha Tien)
y = -126,7ln(x) - 355,91
R² = 0,7031


My Tho
Depth
900
800
700
600
500
400
300
200
100
0
0,0001
0,001
0,01
0,1
1
Compressibilty index
My Tho
Log. (My Tho)
y = -113,5ln(x) - 270,02
R² = 0,6702

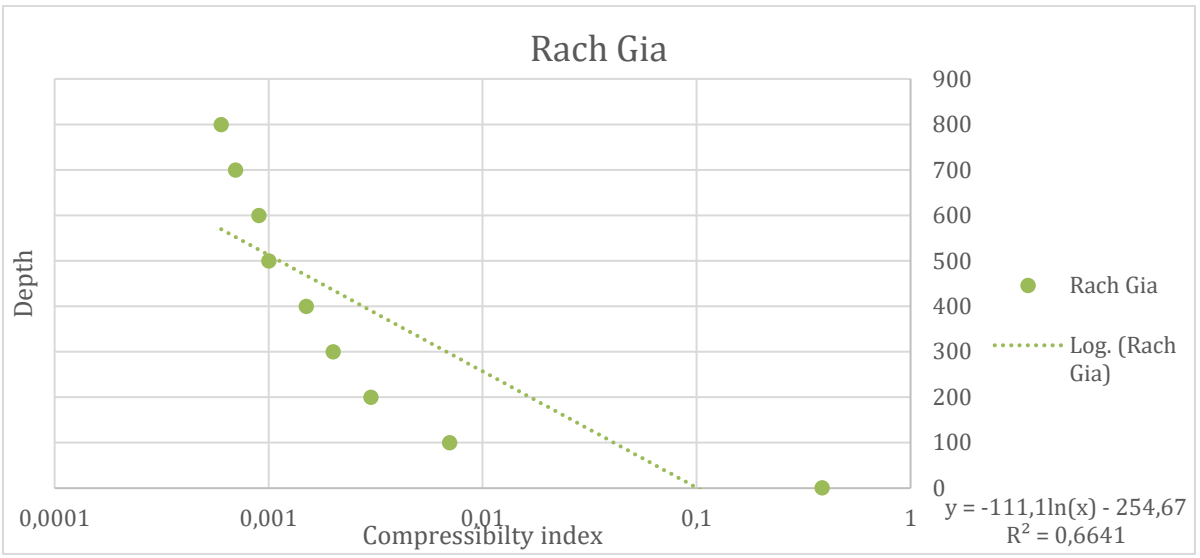
Rach Gia
Depth
900
800
700
600
500
400
300
200
100
0
0,0001
0,001
0,01
0,1
1
Compressibilty index
Rach Gia
Log. (Rach Gia)
y = -111,1ln(x) - 254,67
R² = 0,6641

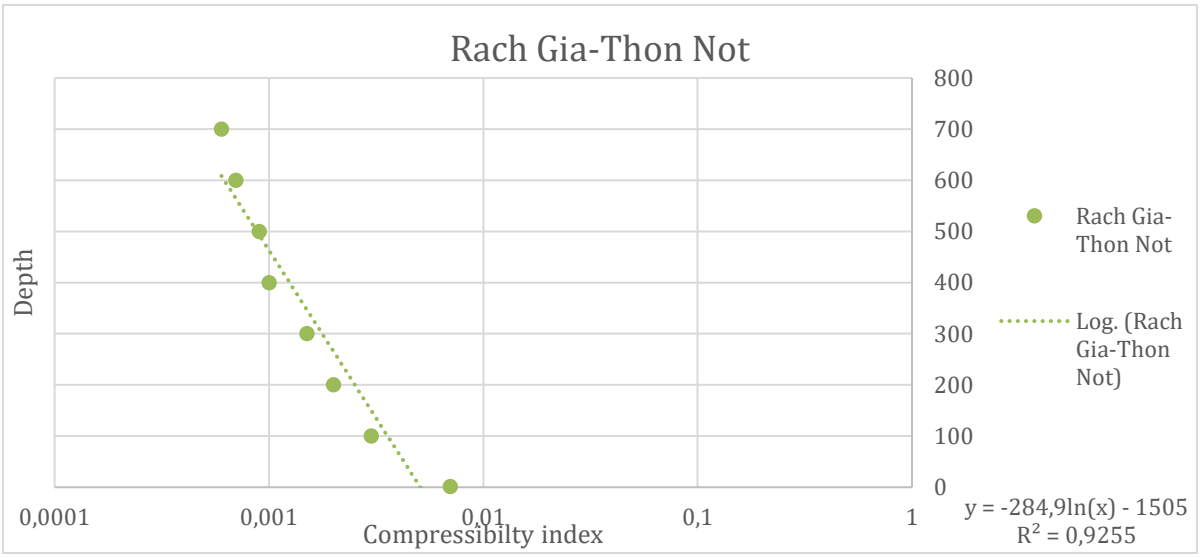
Rach Gia-Thon Not
Depth
800
700
600
500
400
300
200
100
0
0,0001
0,001
0,01
0,1
1
Compressibilty index
Rach Gia-Thon Not
Log. (Rach Gia-Thon Not)
y = -284,9ln(x) - 1505
R² = 0,9255

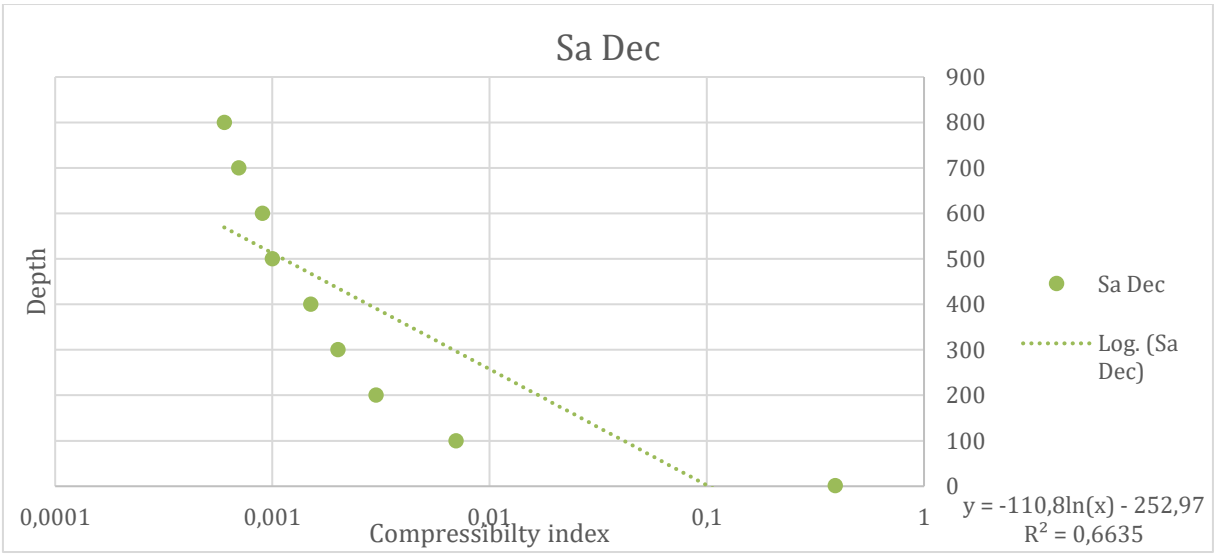
Sa Dec
Depth
900
800
700
600
500
400
300
200
100
0
0,0001
0,001
0,01
0,1
1
Compressibilty index
Sa Dec
Log. (Sa Dec)
y = -110,8ln(x) - 252,97
R² = 0,6635

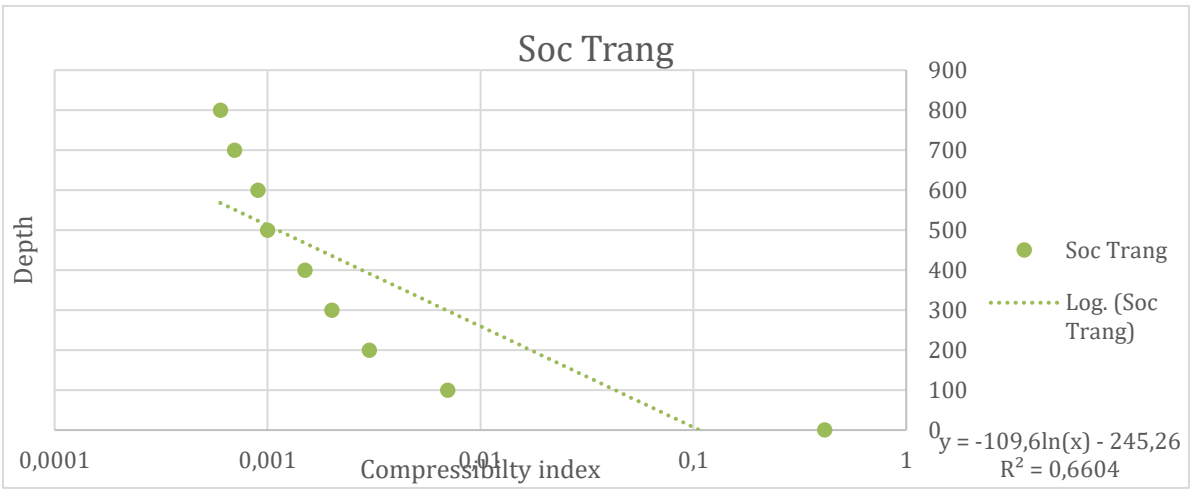
Soc Trang
Depth
900
800
700
600
500
400
300
200
100
0
0,0001
0,001
0,01
0,1
1
Compressibilty index
Soc Trang
Log. (Soc Trang)
y = -109,6ln(x) - 245,26
R² = 0,6604

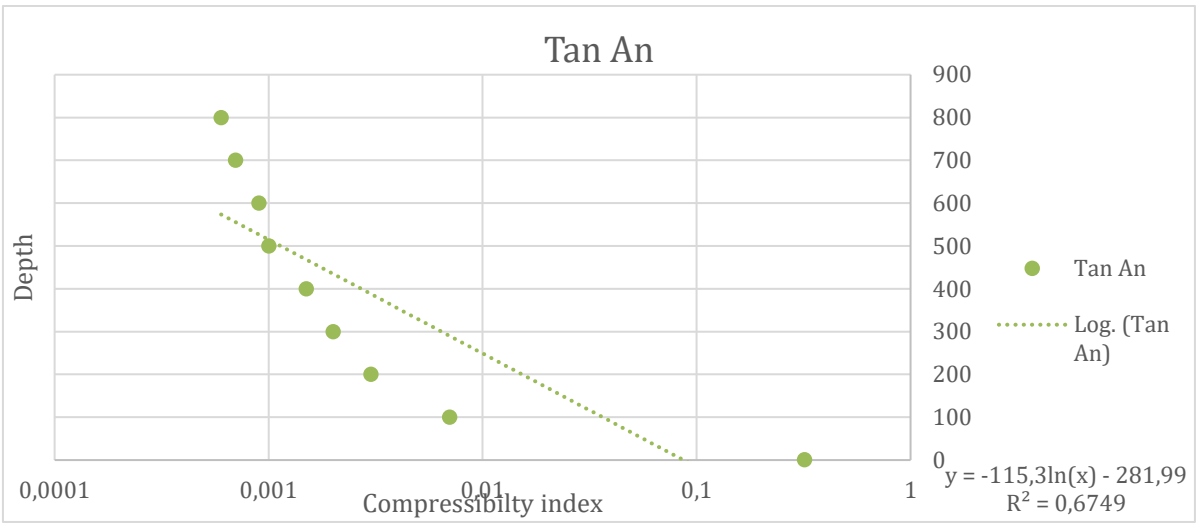
Tan An
Depth
900
800
700
600
500
400
300
200
100
0
0,0001
0,001
0,01
0,1
1
Compressibilty index
Tan An
Log. (Tan An)
y = -115,3ln(x) - 281,99
R² = 0,6749

Appendix 4: The regression line showing the correlation between depth and compressibility index of sand soils for the Mekong Delta.

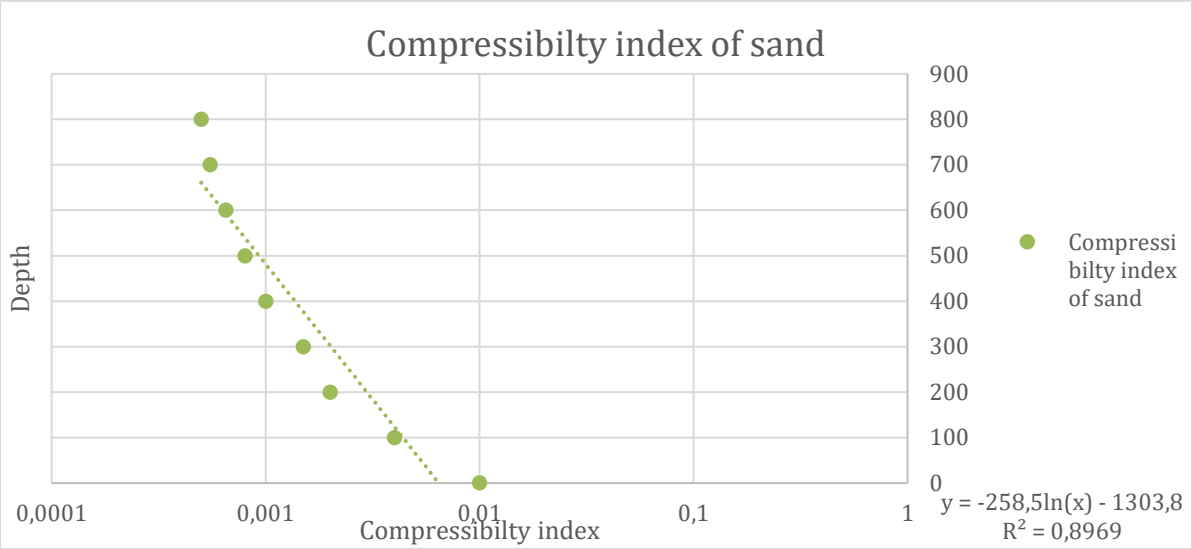

Appendix 5: Mean geotechnical values for each lithological class per region studied in the urban DWRPIS (2010) dataset. S = Clay, SP = Silty clay, C = Sand, CP = Silty sand, BS = Very soft clay & BSP = Soft silty clay.

X	Y	Region		Liquid limit, Cc (%)						Initial void ratio, e0 (-)						Bulk density, ρ_b (kN/m^3)					
				S	SP	C	CP	BS	BSP	S	SP	C	CP	BS	BSP	S	SP	C	CP	BS	BSP
650572	1135108	Ben Tre	Value	0.16	0.17	0.01	0.23	0.52	0.38	0.62	0.65	0.72	0.87	1.70	1.25	19.42	19.62	18.34	19.13	15.99	16.97
			Samples	*36*	*22*		*4*	*48*	*19*	*36*	*22*	*29*	*4*	*48*	*19*	*37*	*22*	*24*	*9*	*48*	*19*
516452	1013930	Ca Mau	Value	0.45		0.01		0.57	0.47	1.41				1.89	1.60	16.78				15.30	15.89
			Samples							*20*				*133*	*3*	*19*				*148*	*3*
581128	1109637	Can Tho	Value	0.43	0.30	0.01	0.26	0.58	0.40	1.21	0.98		0.93	1.96	1.32	16.81	17.66	17.85	18.44	15.16	16.78
			Samples	*17*	*7*		*4*	*146*	*12*	*17*	*7*		*4*	*146*	*12*	*18*	*7*	*1*	*4*	*146*	*90*
569435	1156940	Cao Lanh	Value	0.39	0.26	0.01		0.53	0.34	1.16	0.90			1.65	1.13	17.08	17.87			15.70	17.40
			Samples	*33*	*30*			*7*	*34*	*33*	*30*			*7*	*34*	*61*	*30*			*7*	*31*
443809	1148459	Ha Tien	Value	0.20	0.12	0.01		0.68		0.74	0.54			2.32		19.33	20.11			14.42	12.75
			Samples	*4*	*2*			*9*		*4*	*2*			*9*		*4*	*2*			*9*	*1*
541838	1147935	Long Xuyen	Value	0.37		0.01		0.56	0.43	1.09				1.76	1.33	16.75				17.02	15.60
			Samples	*35*				*102*	*64*	*35*				*102*	*64*	*79*				*28*	*94*
649249	1146948	My Tho	Value	0.34	0.11	0.01	0.17	0.52	0.32	1.04	0.52	0.83	0.69	1.71	1.10	17.07	16.58	17.46	19.13	13.05	17.46
			Samples							*57*	*40*	*3*	*3*	*24*	*18*	*55*	*44*	*5*	*3*	*34*	*15*
512276	1105228	Rach Gia	Value	0.37	0.27	0.01	0.18	0.57	0.46	1.13	0.85		0.69	1.88	1.43	17.46	18.25		19.03	15.45	16.58
			Samples	*18*	*2*		*5*	*50*	*4*	*18*	*2*		*5*	*50*	*4*	*18*	*2*		*5*	*52*	*4*
532252	1113827	Rach Gia-Thon Not	Value	0.43	0.27	0.01		0.60	0.40	1.24	0.85			1.99	1.30	16.78	18.25			15.25	16.97
			Samples	*113*	*2*			*195*	*2*	*113*	*2*			*195*	*2*	*113*	*2*			*194*	*2*
585181	1136175	Sa Dec	Value	0.39	0.33	0.01	0.24	0.52	0.39	1.18	1.12		0.90	1.72	1.24	16.84	17.95	17.95	18.15	15.65	16.78
			Samples	*63*	*22*		*1*	*13*	*53*	*63*	*22*		*1*	*13*	*53*	*53*	*25*	*5*	*1*	*13*	*53*
607874	1062985	Soc Trang	Value	0.31	0.35	0.01	0.28	0.47	0.40	1.17	0.95	0.68	0.67	1.73	1.20	17.67	17.13	16.78	16.28	17.33	17.68
			Samples	*77*	*41*		*56*	*27*	*22*	*77*	*41*	*16*	*56*	*27*	*22*	*77*	*40*	*17*	*51*	*27*	*22*
657714	1172166	Tan An	Value	0.48	0.18	0.01		0.40	0.46	0.95	0.64			1.96	1.23	18.20	19.62			15.16	16.97
			Samples	*52*	*184*			*50*	*4*	*52*	*184*			*50*	*4*	*60*	*184*			*50*	*4*

Appendix 6: subsidence rate for all 14 hydrogeological layers in the Mekong Delta in cm.

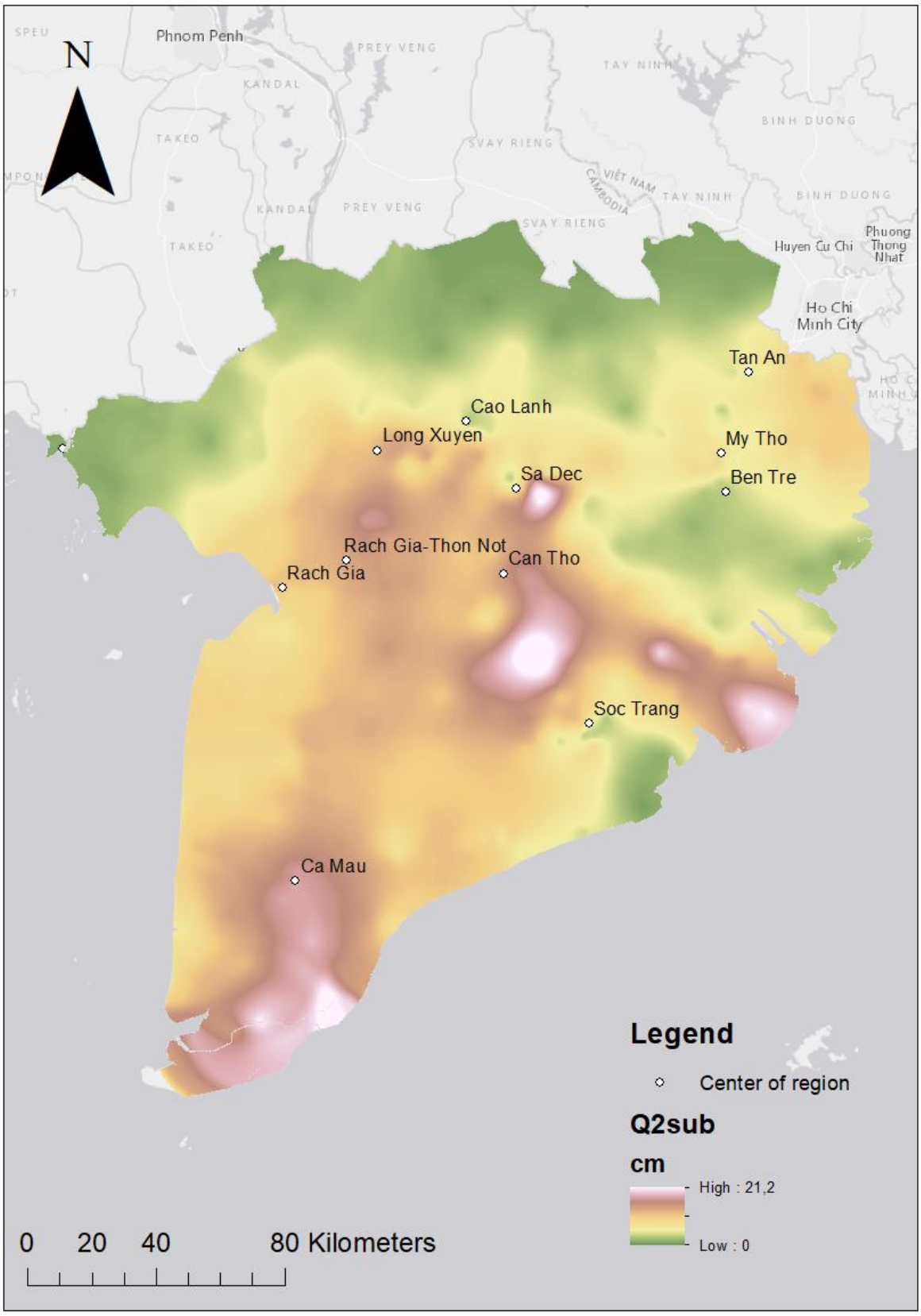

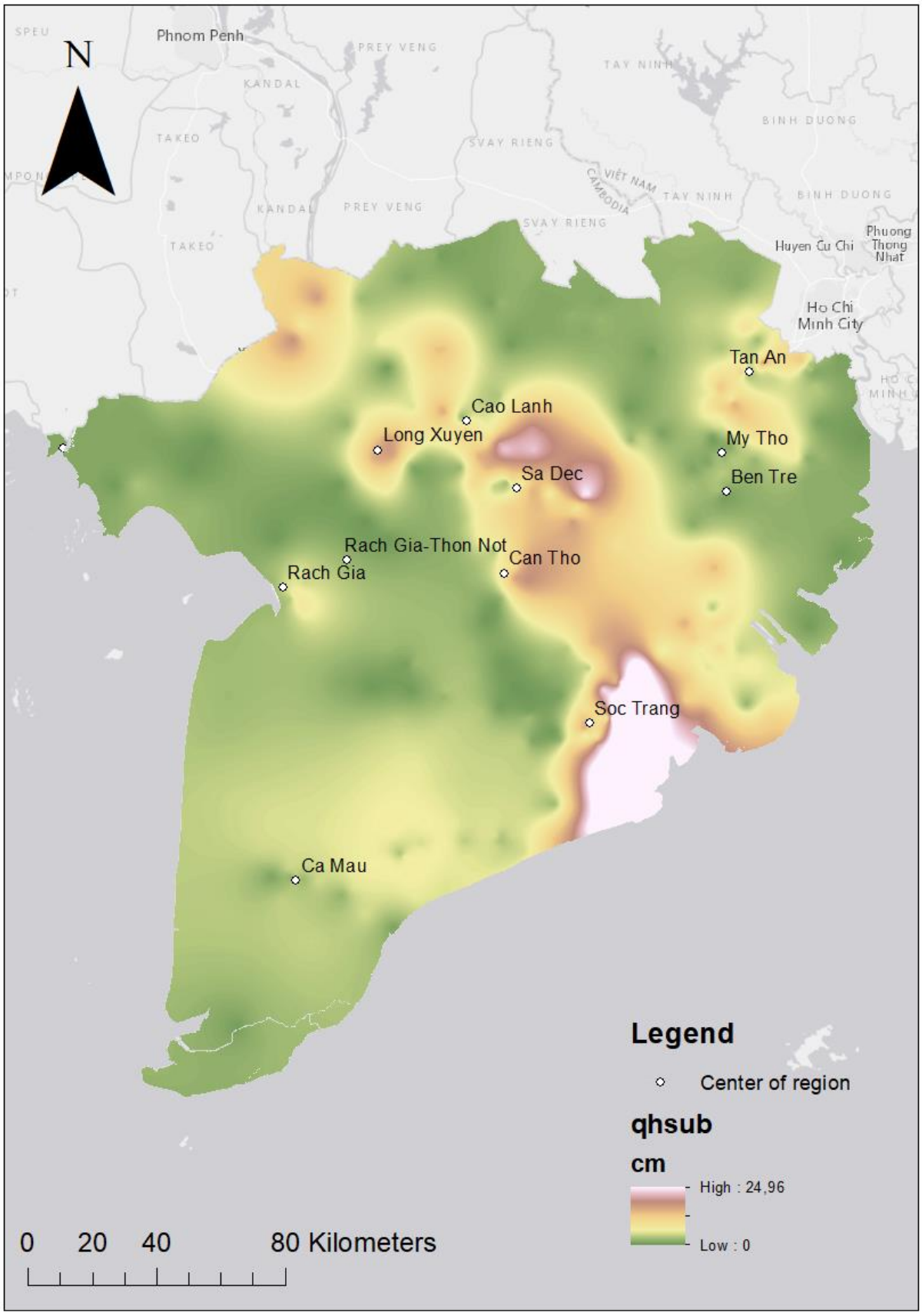
N
Phnom Penh
PREY VENG
KANDAL
TAKEO
SVAY RIENG
VIỆT NAM
CAMBODIA
TAY NINH
BINH DUONG
Huyen Cu Chi
Phuong Thong Nhat
Ho Chi Minh City
Tan An
Cao Lanh
Long Xuyen
My Tho
Sa Dec
Ben Tre
Rach Gia-Thon Not
Rach Gia
Can Tho
Soc Trang
Ca Mau
Legend
Center of region
qhsub
cm
High : 24,96
Low : 0
0 20 40 80 Kilometers

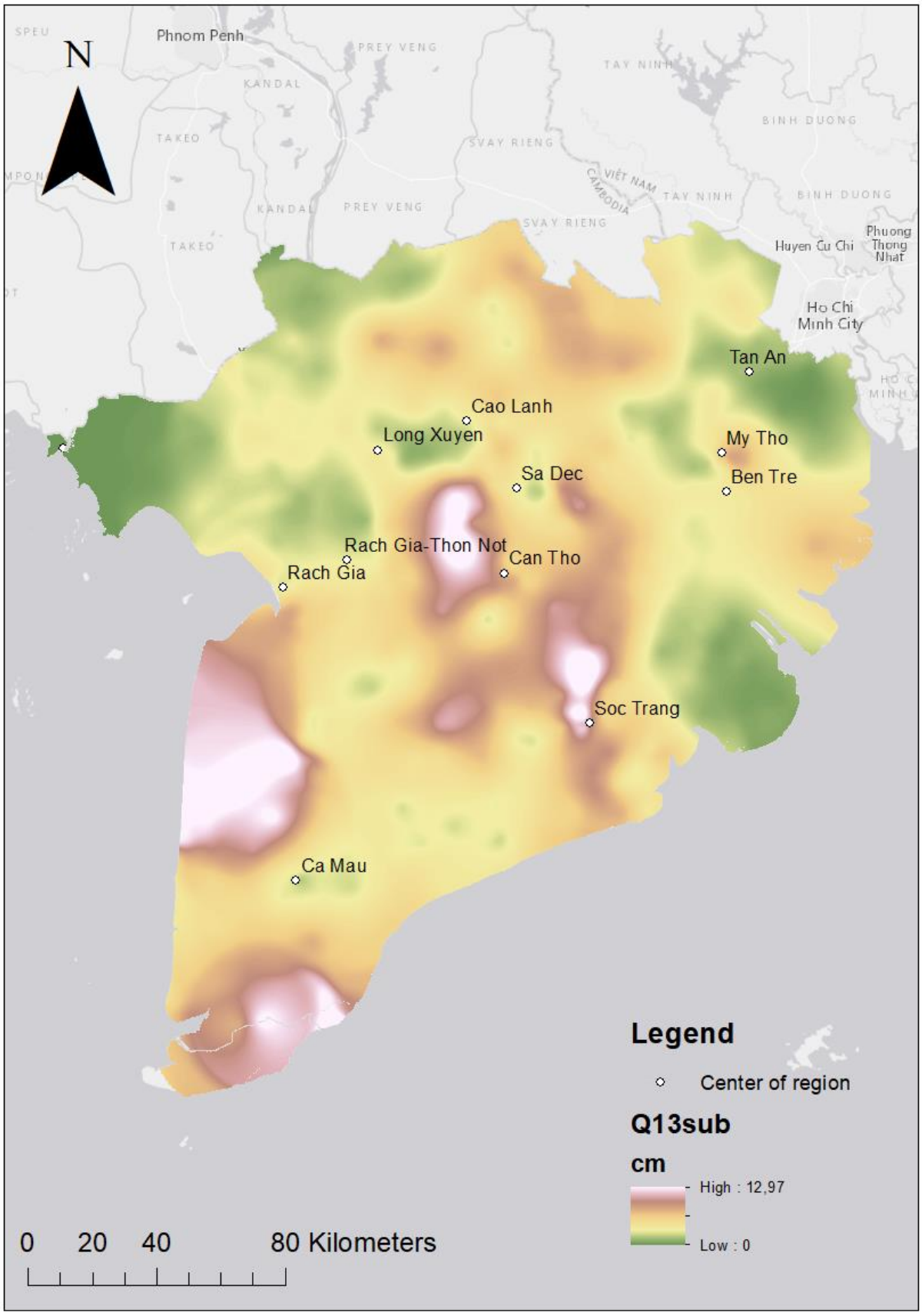
N
Phnom Penh
PREY VENG
KANDAL
TAKEO
SVAY RIENG
TAY NINH
BINH DUONG
VIỆT NAM
CAMBODIA
Huyen Cu Chi
Phuong Thong Nhat
Ho Chi Minh City
Tan An
Cao Lanh
Long Xuyen
My Tho
Sa Dec
Ben Tre
Rach Gia-Thon Not
Rach Gia
Can Tho
Soc Trang
Ca Mau
Legend
Center of region
Q13sub
cm
High : 12,97
Low : 0
0 20 40 80 Kilometers

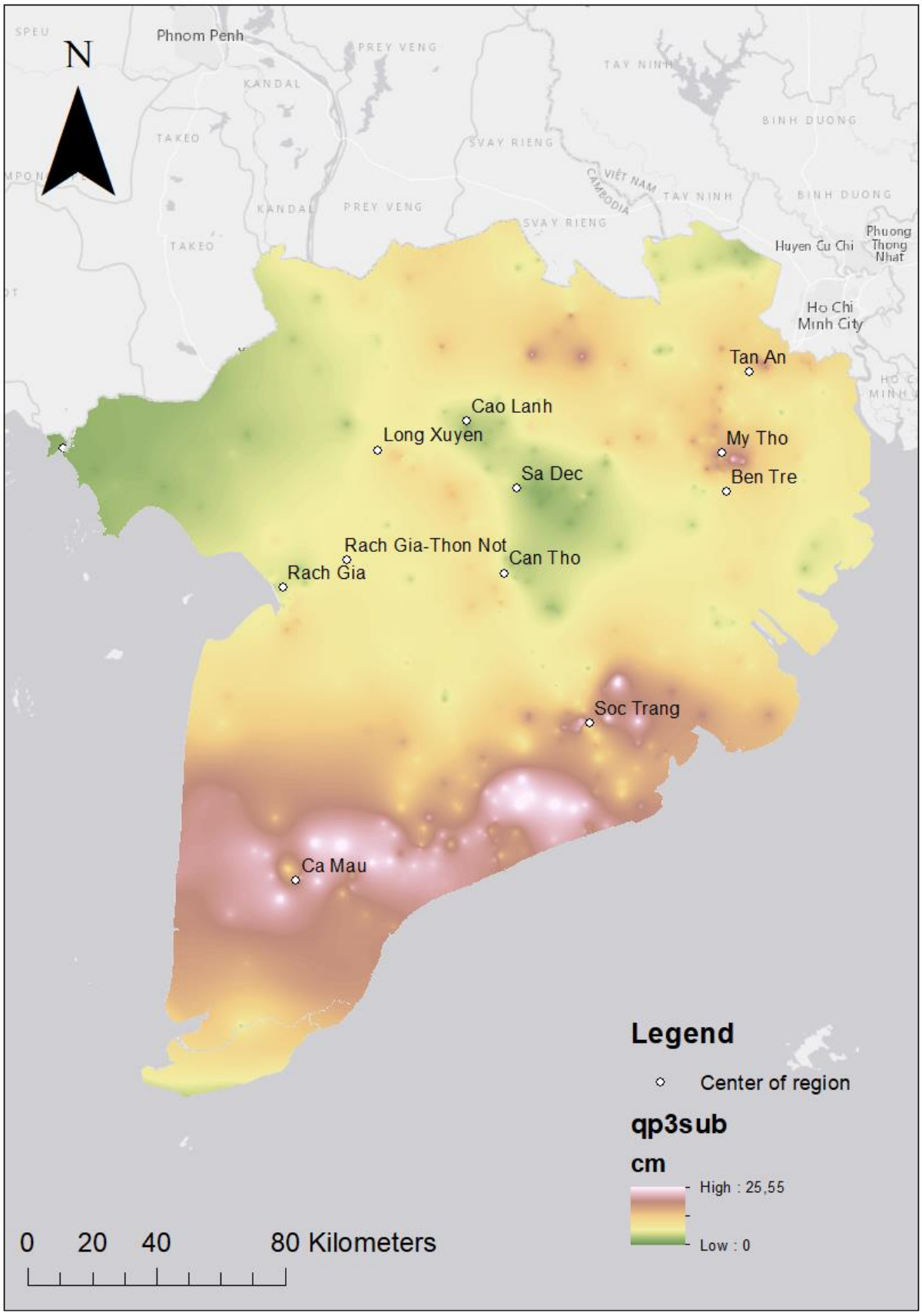
N
Phnom Penh
PREY VENG
KANDAL
TAKEO
SVAY RIENG
TAY NINH
BINH DUONG
VIỆT NAM
CAMBODIA
Huyen Cu Chi
Phuong Thong Nhat
Ho Chi Minh City
Tan An
Cao Lanh
Long Xuyen
My Tho
Ben Tre
Sa Dec
Rach Gia-Thon Not
Rach Gia
Can Tho
Soc Trang
Ca Mau
Legend
Center of region
qp3sub
cm
High : 25,55
Low : 0
0 20 40 80 Kilometers

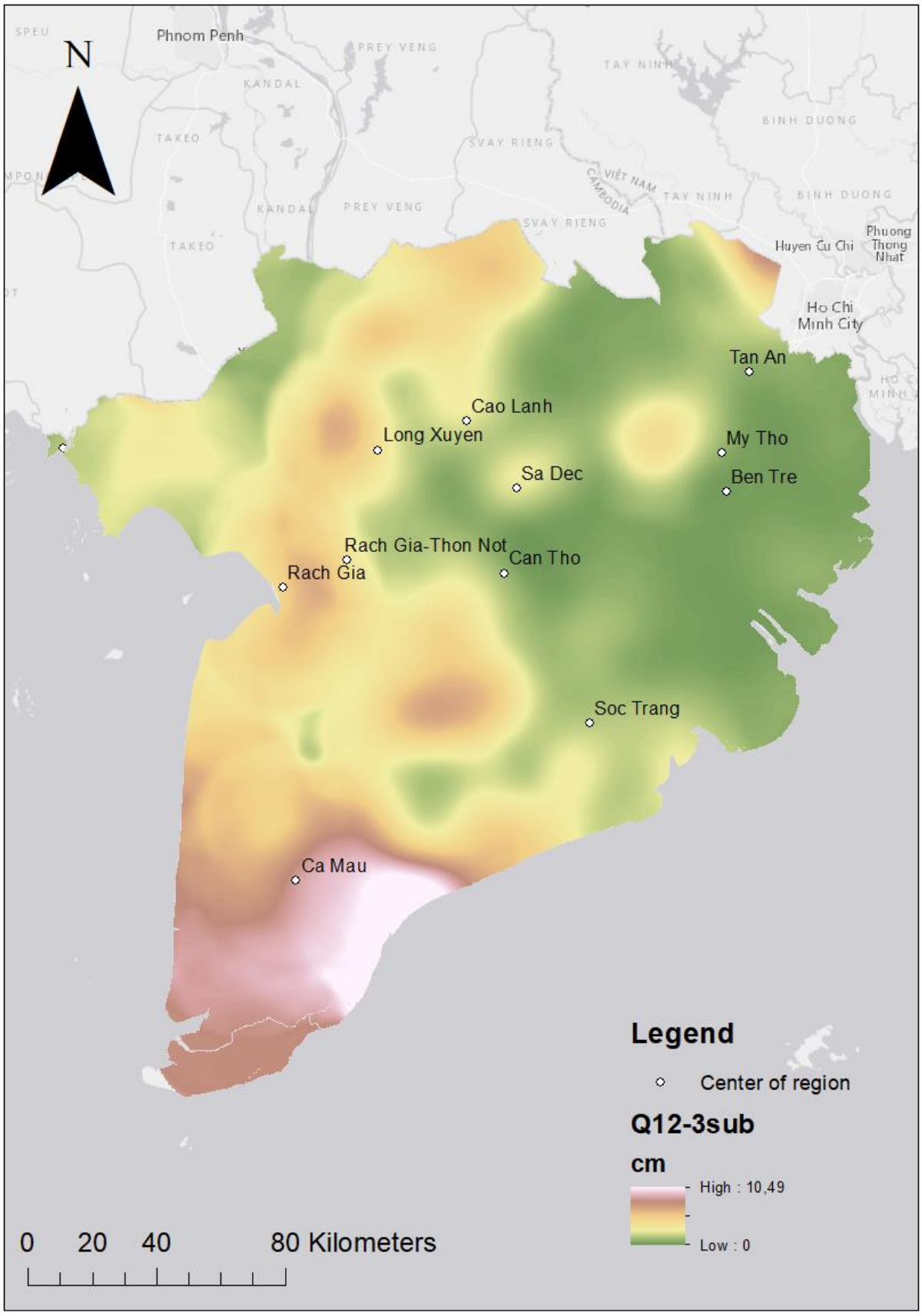
N
Phnom Penh
PREY VENG
KANDAL
TAKEO
SVAY RIENG
TAY NINH
BINH DUONG
VIỆT NAM
CAMBODIA
Huyen Cu Chi
Phuong Thong Nhat
Ho Chi Minh City
Tan An
Cao Lanh
Long Xuyen
My Tho
Sa Dec
Ben Tre
Rach Gia-Thon Not
Rach Gia
Can Tho
Soc Trang
Ca Mau
Legend
Center of region
Q12-3sub
cm
High : 10,49
Low : 0
0 20 40 80 Kilometers

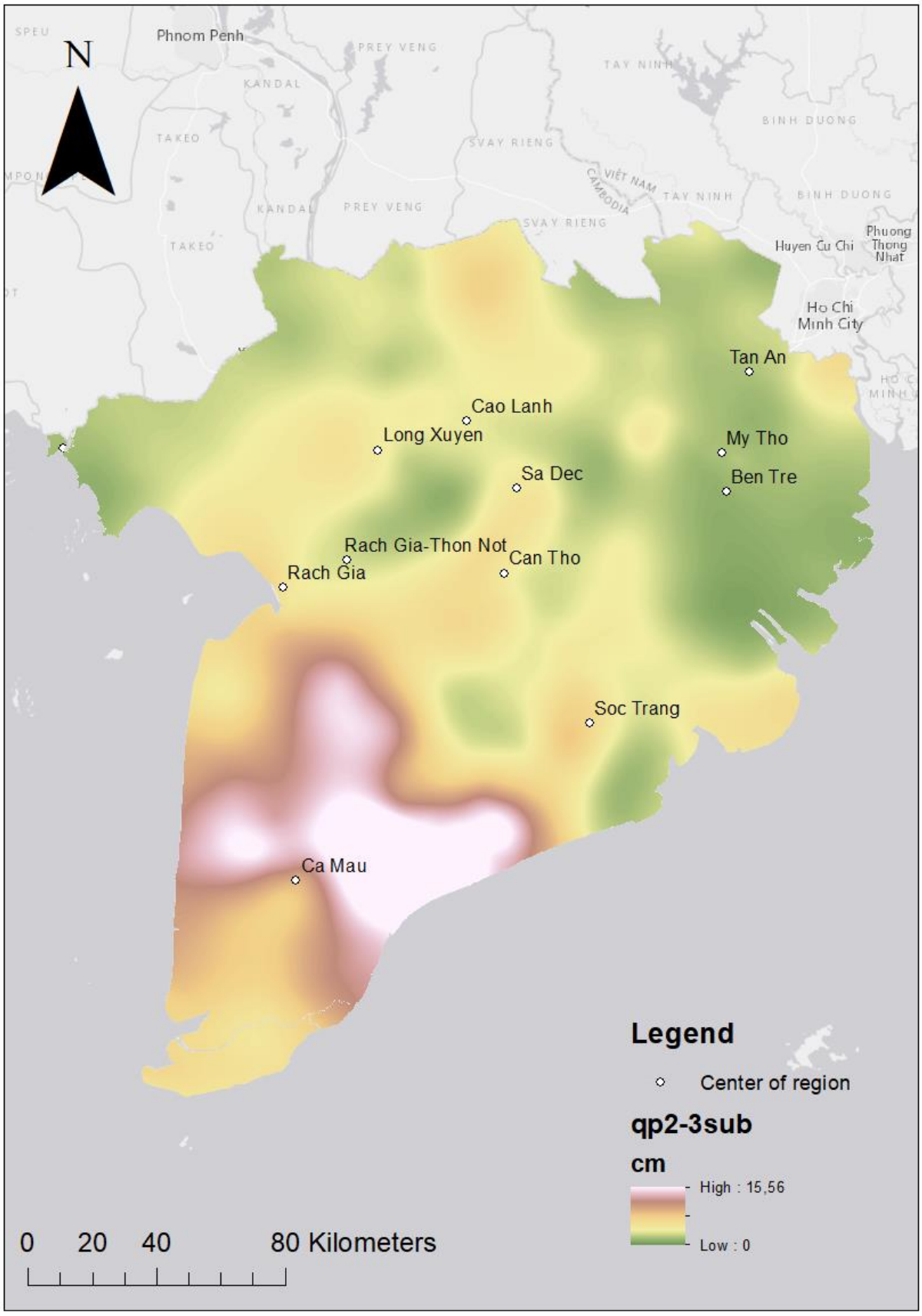
N
Phnom Penh
PREY VENG
KANDAL
TAKEO
SVAY RIENG
TAY NINH
BINH DUONG
VIỆT NAM
CAMBODIA
Huyen Cu Chi
Phuong Thong Nhat
Ho Chi Minh City
Tan An
Cao Lanh
Long Xuyen
My Tho
Sa Dec
Ben Tre
Rach Gia-Thon Not
Rach Gia
Can Tho
Soc Trang
Ca Mau
Legend
Center of region
qp2-3sub
cm
High : 15,56
Low : 0
0 20 40 80 Kilometers

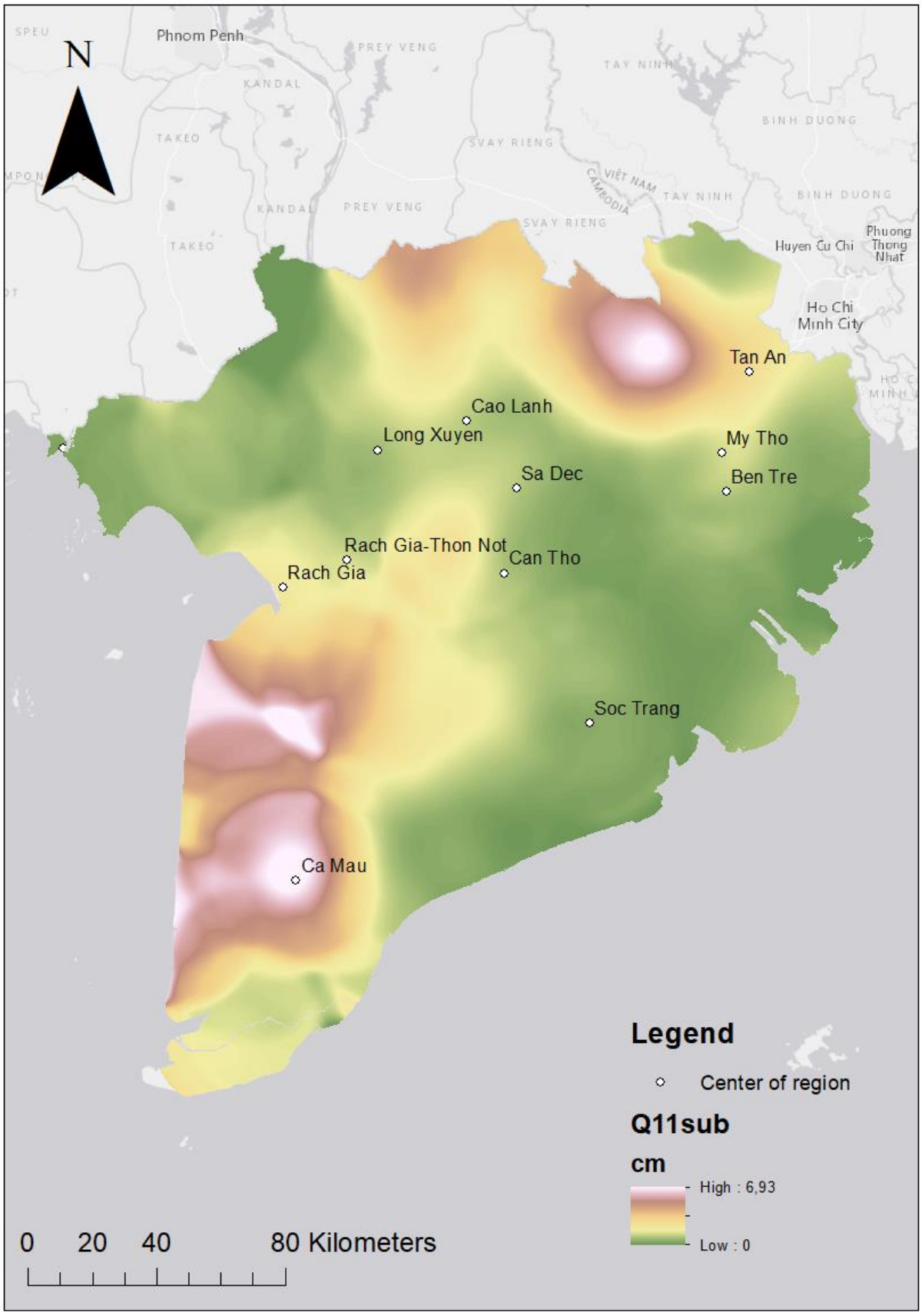
N
Phnom Penh
PREY VENG
KANDAL
TAKEO
SVAY RIENG
TAY NINH
BINH DUONG
VIỆT NAM
CAMBODIA
Huyen Cu Chi
Phuong Thong Nhat
Ho Chi Minh City
Tan An
Cao Lanh
Long Xuyen
My Tho
Sa Dec
Ben Tre
Rach Gia-Thon Not
Rach Gia
Can Tho
Soc Trang
Ca Mau
Legend
Center of region
Q11sub
cm
High : 6,93
Low : 0
0 20 40 80 Kilometers

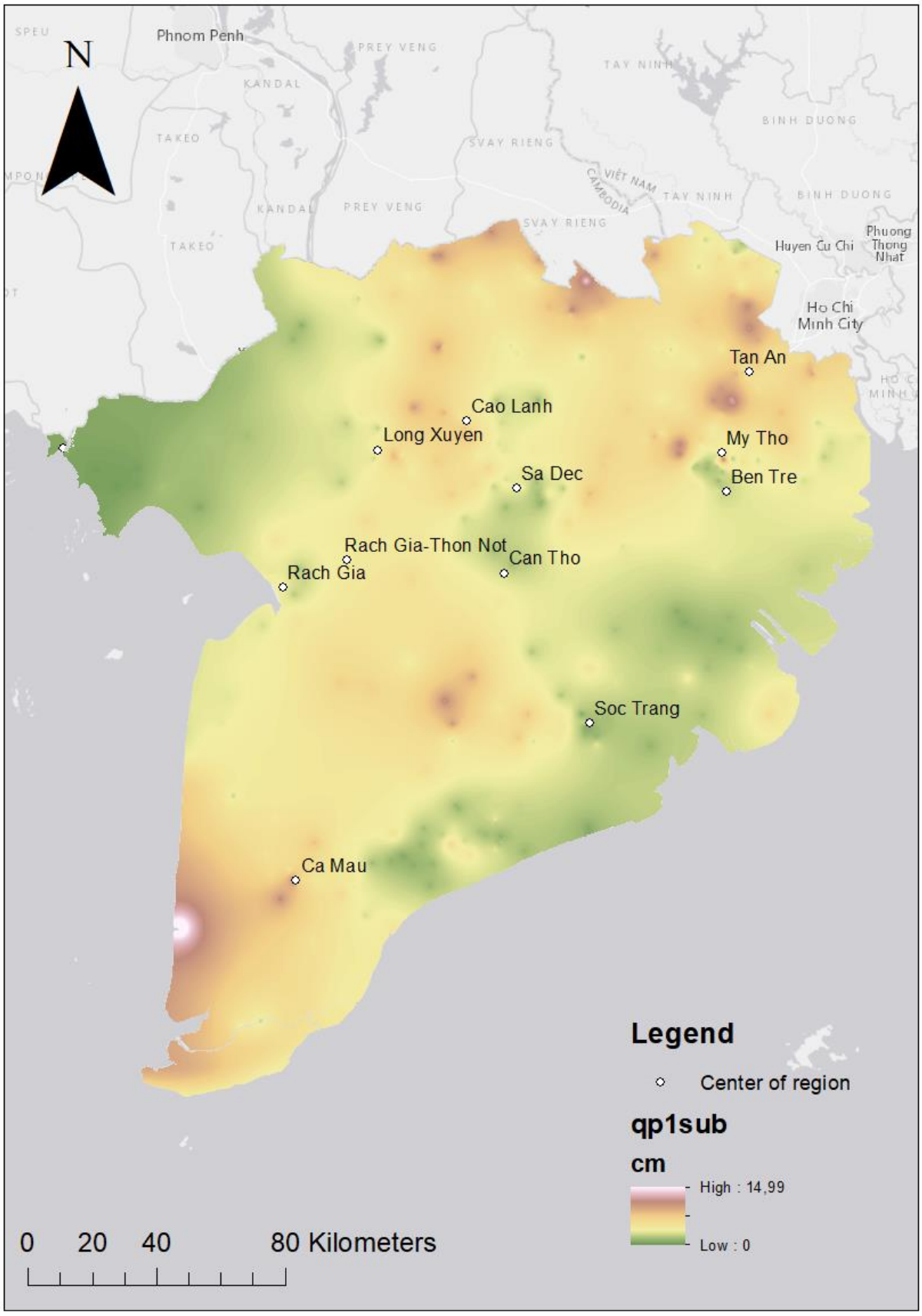
N
Phnom Penh
PREY VENG
KANDAL
TAKEO
SVAY RIENG
TAY NINH
BINH DUONG
VIỆT NAM
CAMBODIA
Huyen Cu Chi
Phuong Thong Nhat
Ho Chi Minh City
Tan An
Cao Lanh
Long Xuyen
My Tho
Sa Dec
Ben Tre
Rach Gia-Thon Not
Rach Gia
Can Tho
Soc Trang
Ca Mau
Legend
Center of region
qp1sub
cm
High : 14,99
Low : 0
0 20 40 80 Kilometers

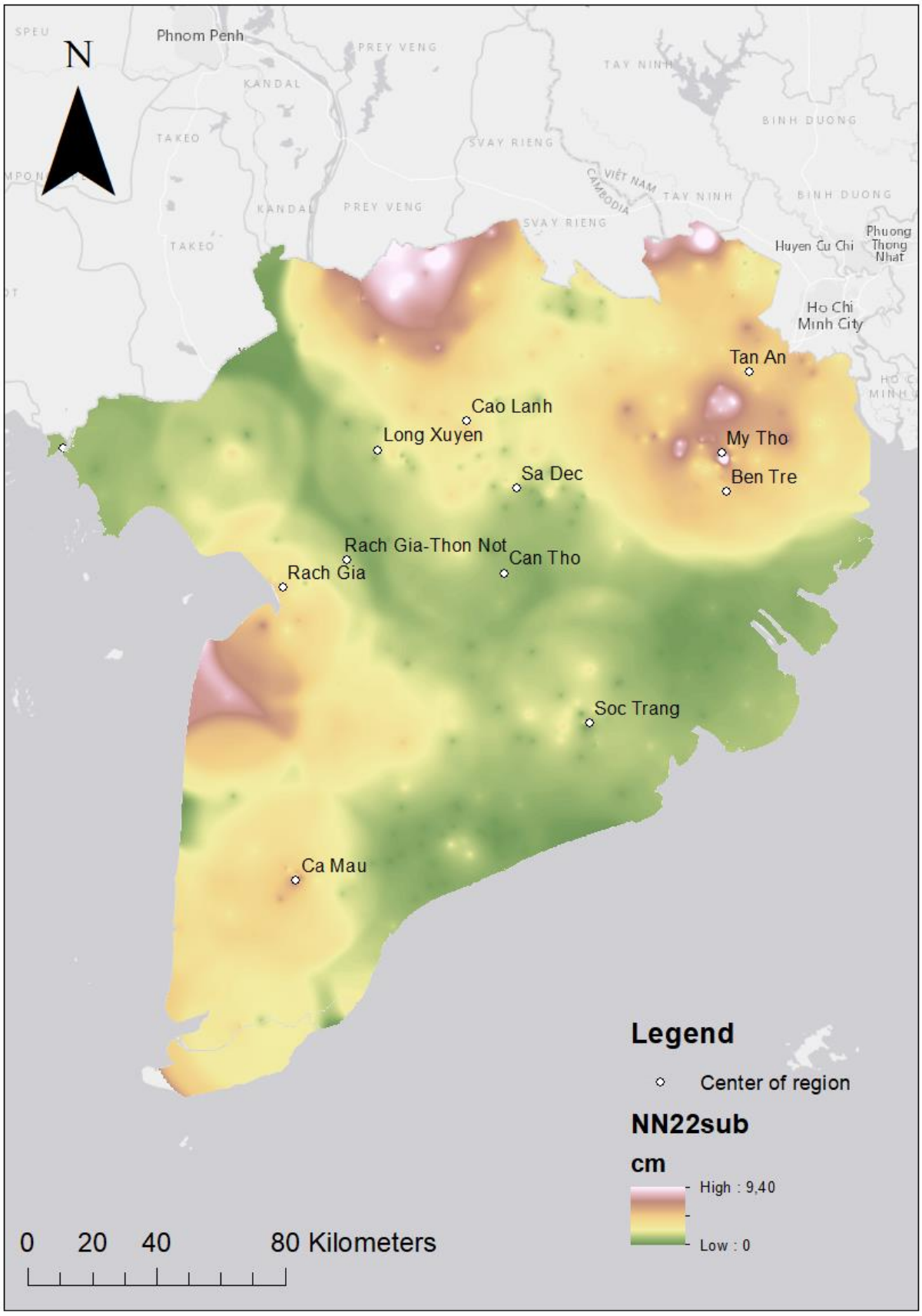
N
Phnom Penh
PREY VENG
KANDAL
TAKEO
SVAY RIENG
VIỆT NAM
CAMBODIA
TAY NINH
BINH DUONG
Huyen Cu Chi
Phuong Thong Nhat
Ho Chi Minh City
Tan An
Cao Lanh
Long Xuyen
My Tho
Ben Tre
Sa Dec
Rach Gia-Thon Not
Rach Gia
Can Tho
Soc Trang
Ca Mau
Legend
Center of region
NN22sub
cm
High : 9,40
Low : 0
0 20 40 80 Kilometers

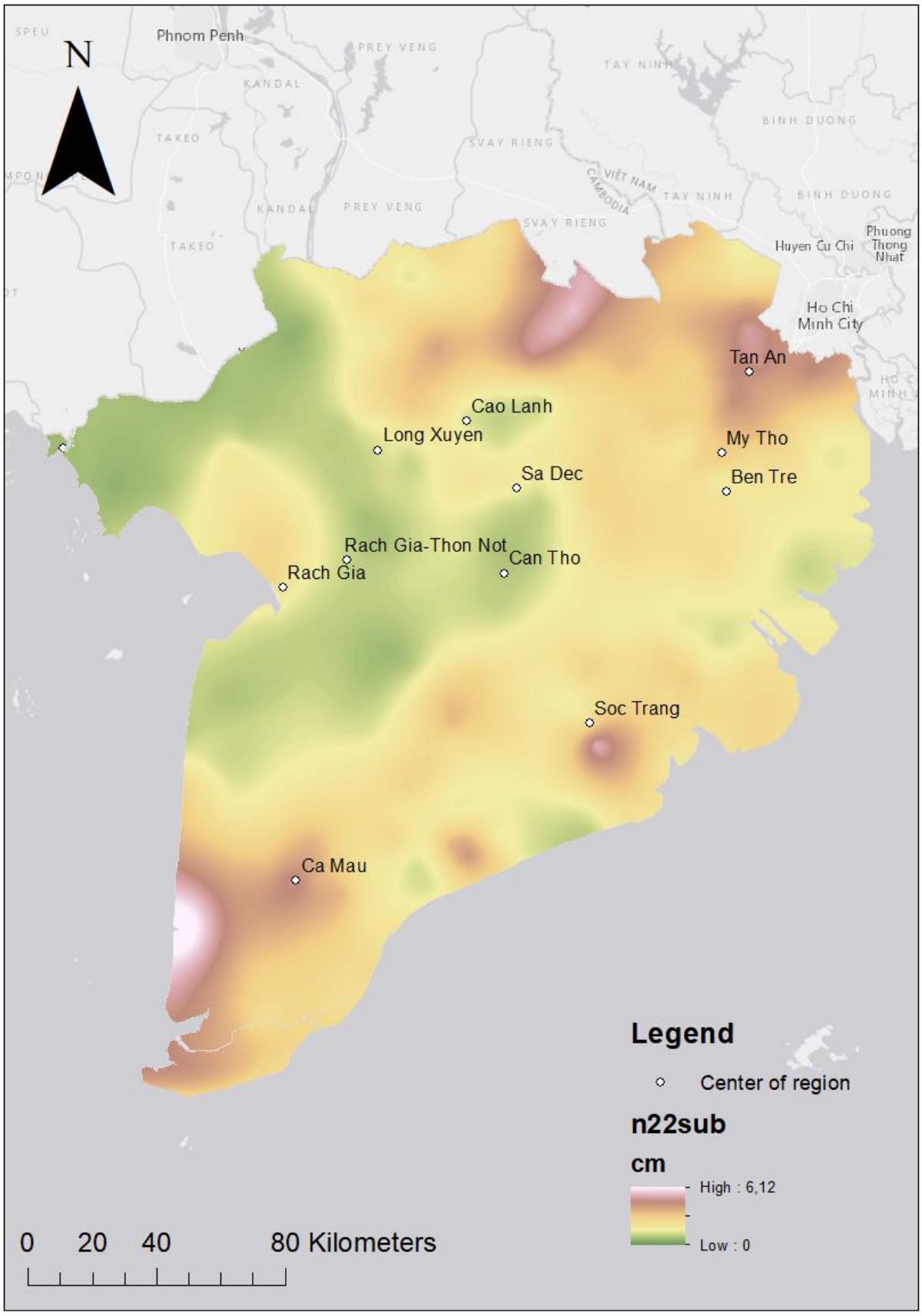
N
Phnom Penh
PREY VENG
KANDAL
TAKEO
SVAY RIENG
VIỆT NAM
CAMBODIA
TAY NINH
BINH DUONG
Huyen Cu Chi
Phuong Thong Nhat
Ho Chi Minh City
Tan An
Cao Lanh
Long Xuyen
My Tho
Sa Dec
Ben Tre
Rach Gia-Thon Not
Rach Gia
Can Tho
Soc Trang
Ca Mau
Legend
Center of region
n22sub
cm
High : 6,12
Low : 0
0 20 40 80 Kilometers

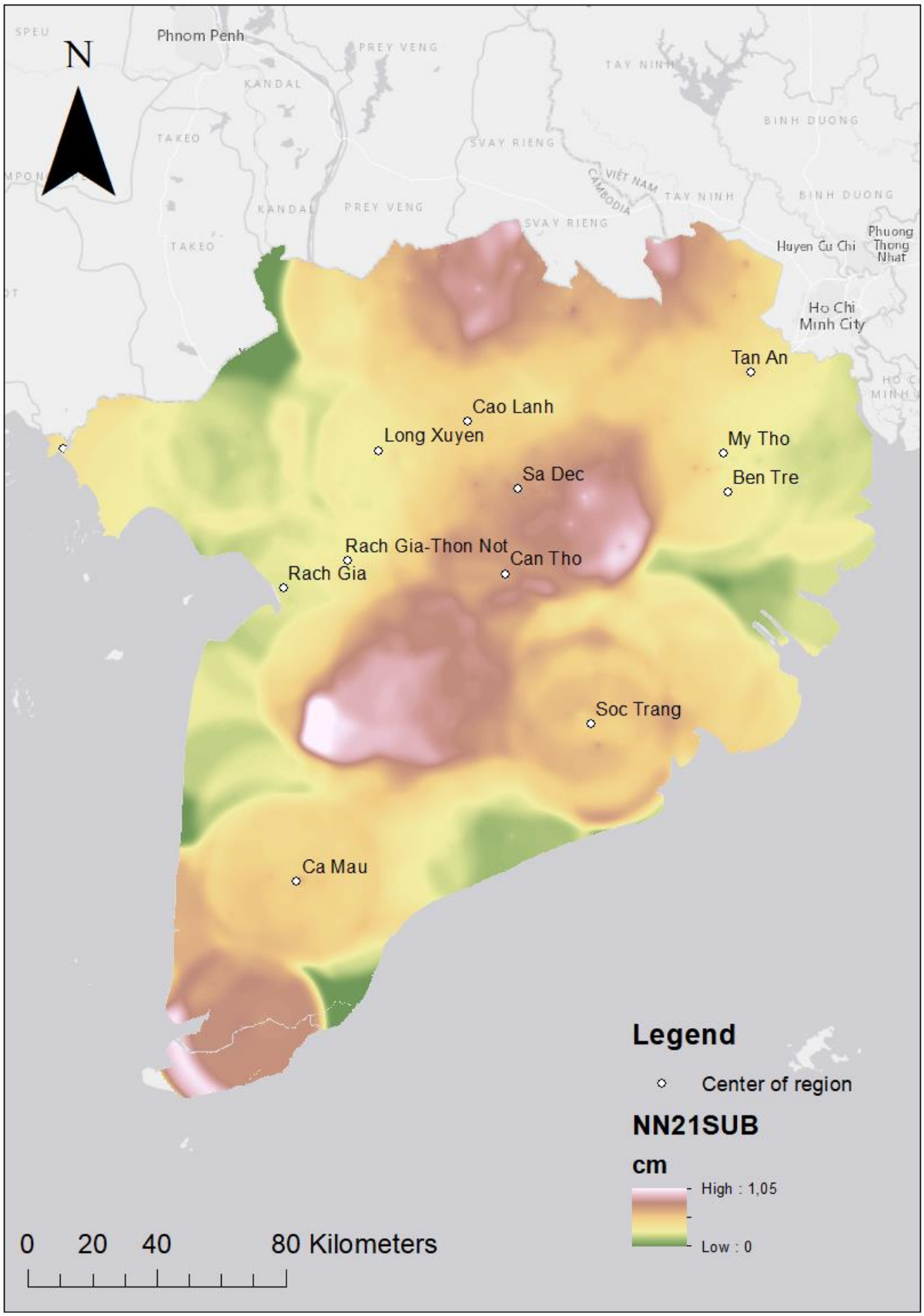
N
Phnom Penh
PREY VENG
KANDAL
TAKEO
SVAY RIENG
VIỆT NAM
CAMBODIA
TAY NINH
BINH DUONG
Huyen Cu Chi
Phuong Thong Nhat
Ho Chi Minh City
Tan An
Cao Lanh
Long Xuyen
My Tho
Sa Dec
Ben Tre
Rach Gia-Thon Not
Rach Gia
Can Tho
Soc Trang
Ca Mau
Legend
Center of region
NN21SUB
cm
High : 1,05
Low : 0
0 20 40 80 Kilometers

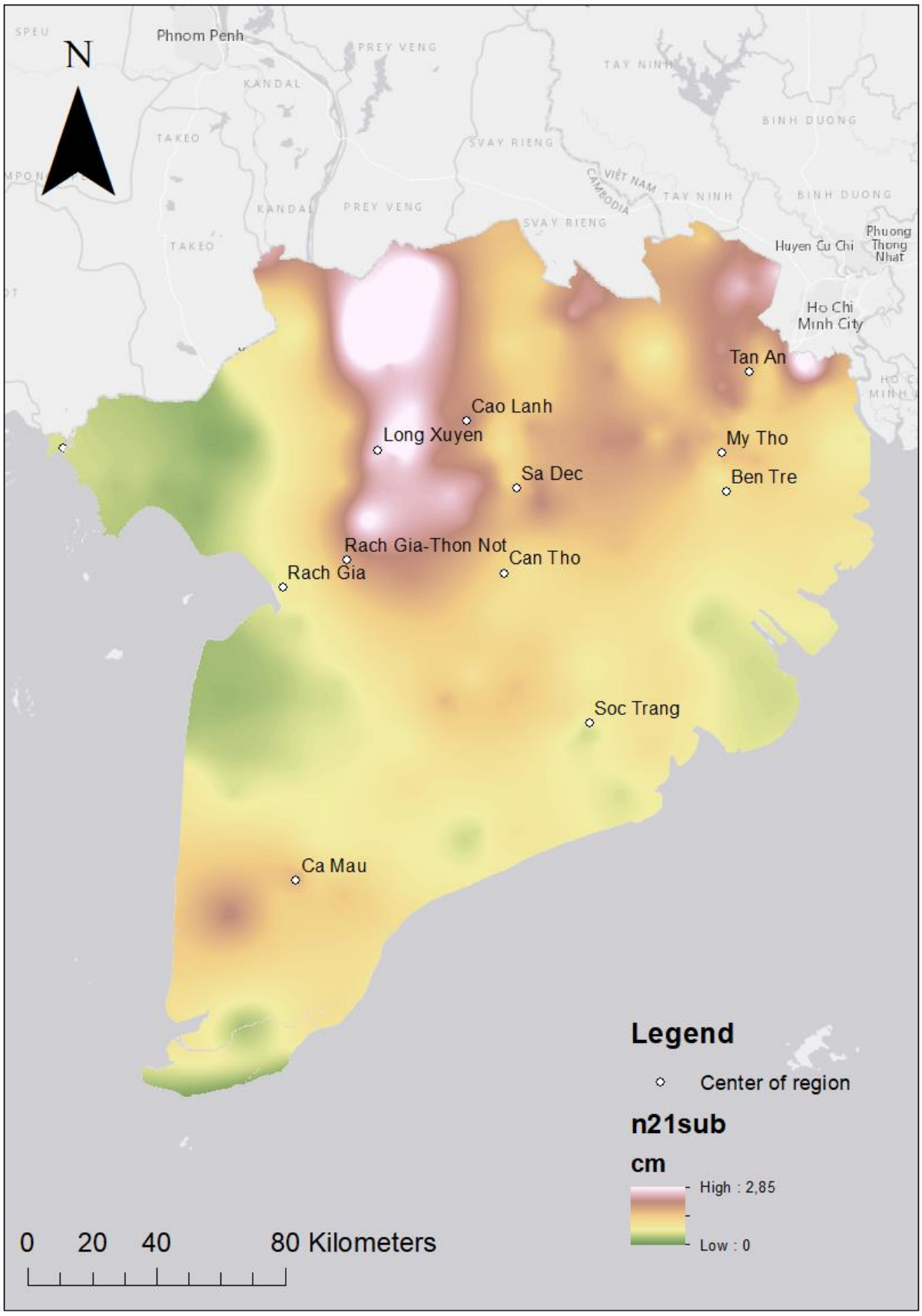
N
Phnom Penh
PREY VENG
KANDAL
TAKEO
SVAY RIENG
VIỆT NAM
CAMBODIA
TAY NINH
BINH DUONG
Huyen Cu Chi
Phuong Thong Nhat
Ho Chi Minh City
Tan An
Cao Lanh
Long Xuyen
My Tho
Sa Dec
Ben Tre
Rach Gia-Thon Not
Rach Gia
Can Tho
Soc Trang
Ca Mau
Legend
Center of region
n21sub
cm
High : 2,85
Low : 0
0 20 40 80 Kilometers

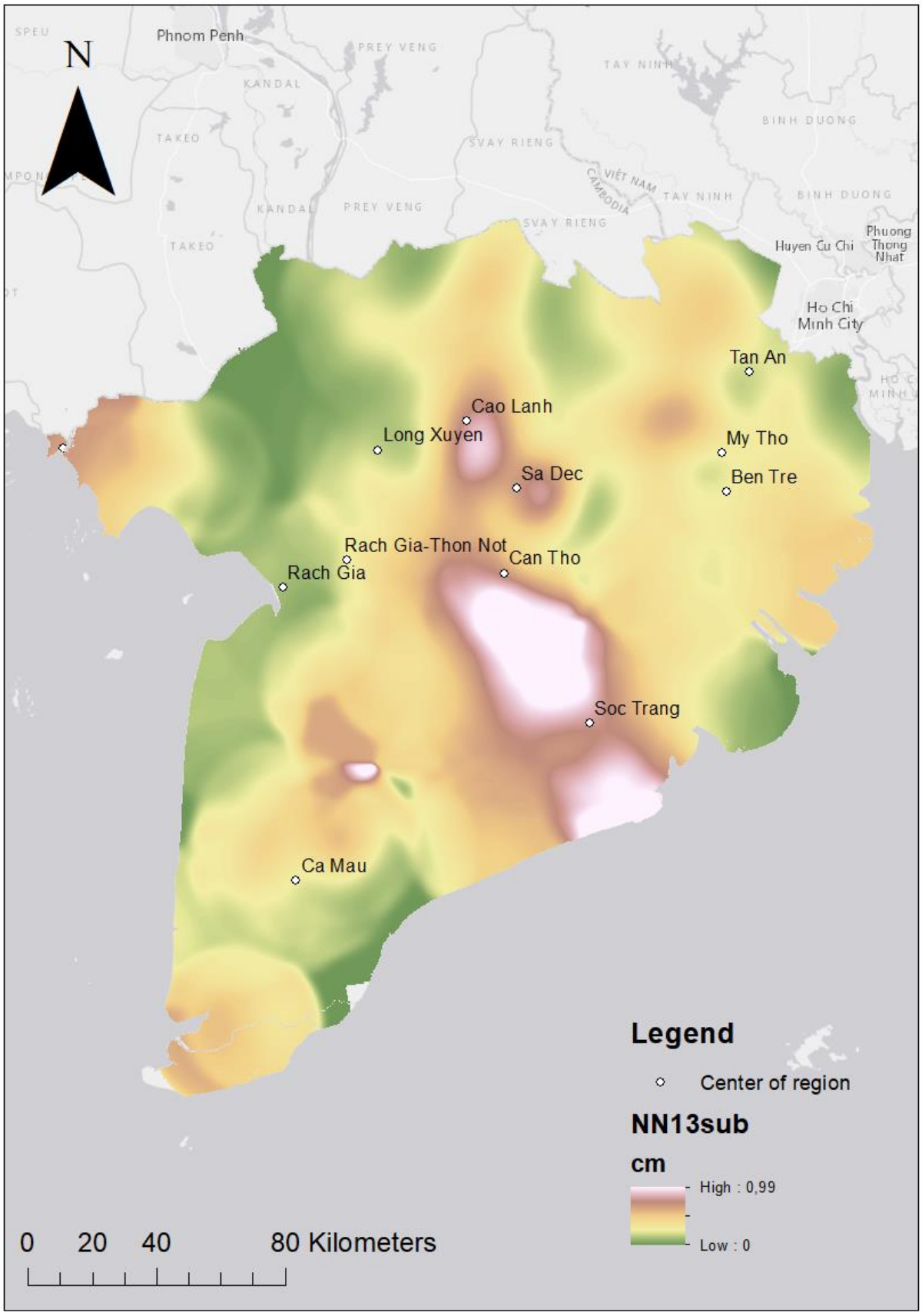
N
Phnom Penh
PREY VENG
KANDAL
TAKEO
SVAY RIENG
TAY NINH
BINH DUONG
VIỆT NAM
CAMBODIA
Huyen Cu Chi
Phuong Thong Nhat
Ho Chi Minh City
Tan An
Cao Lanh
Long Xuyen
My Tho
Sa Dec
Ben Tre
Rach Gia-Thon Not
Can Tho
Rach Gia
Soc Trang
Ca Mau
Legend
Center of region
NN13sub
cm
High : 0,99
Low : 0
0 20 40 80 Kilometers

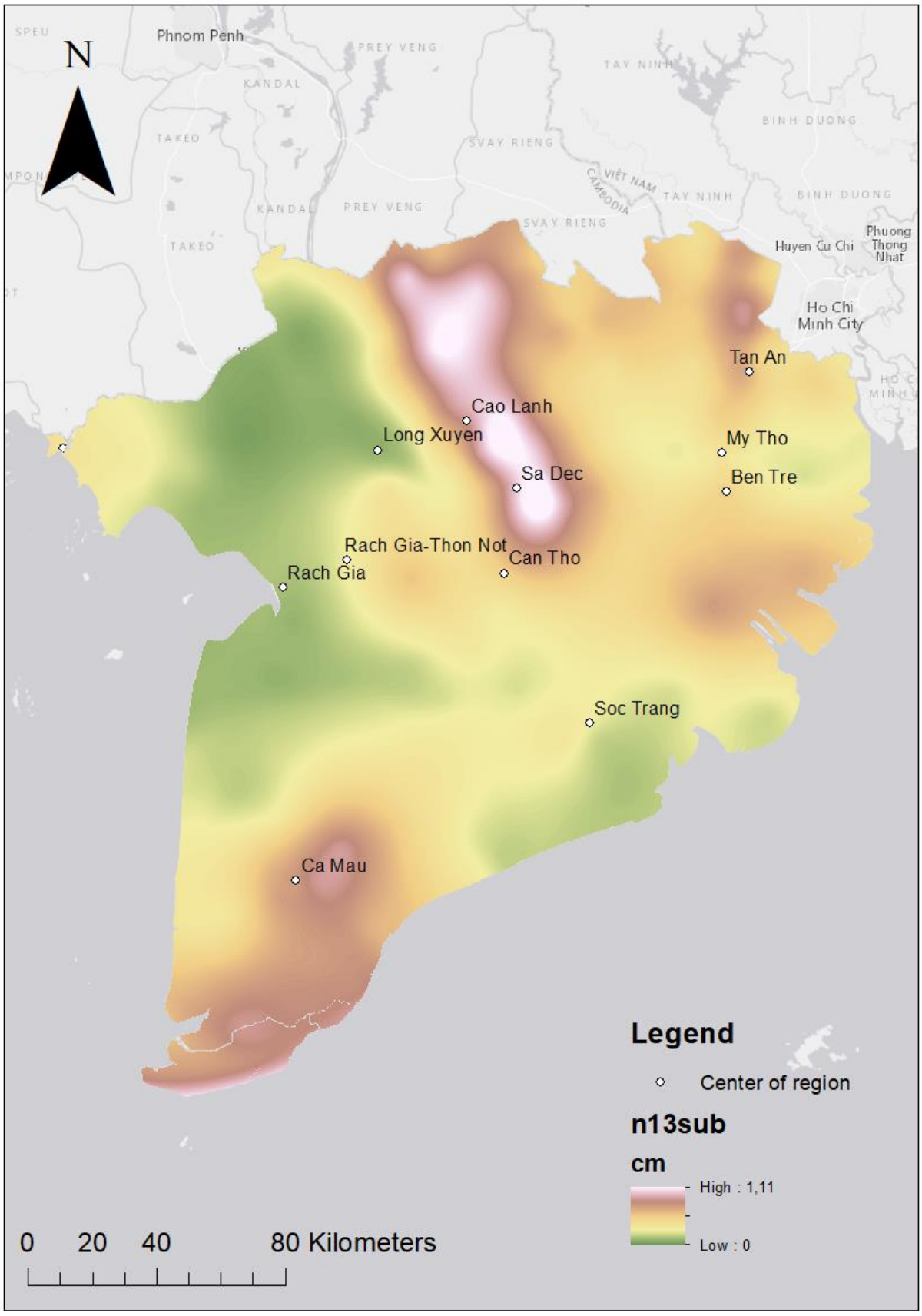
N
Phnom Penh
PREY VENG
KANDAL
TAKEO
SVAY RIENG
TAY NINH
BINH DUONG
VIỆT NAM
CAMBODIA
Huyen Cu Chi
Phuong Thong Nhat
Ho Chi Minh City
Tan An
Cao Lanh
Long Xuyen
My Tho
Sa Dec
Ben Tre
Rach Gia-Thon Not
Can Tho
Rach Gia
Soc Trang
Ca Mau
Legend
Center of region
n13sub
cm
High : 1,11
Low : 0
0 20 40 80 Kilometers

References

Adger, W. N., Hughes, T. P., Folke, C., Carpenter, S. R., & Rockström, J. (2005). Social ecological resilience to coastal disasters. *Science*, *309*(5737), 1036-1039.

Akayuli, C. F. A., & Ofosu, B. (2013). Empirical model for estimating compression index from physical properties of weathered birimian phyllites. *Electron J Geotech Eng*, *18*, 6135-6144.

Ammerlaan P.R.M. (2011). Proefterpen project bloemendalerpolder te weesp (Dutch). Fugro geoservices B.V.

Van Asselen, S., Stouthamer, E., & Van Asch, T. W. (2009). Effects of peat compaction on delta evolution: a review on processes, responses, measuring and modeling. *Earth-Science Reviews*, *92*(1-2), 35-51.

Blum, M. D., & Roberts, H. H. (2009). Drowning of the Mississippi Delta due to insufficient sediment supply and global sea-level rise. *Nature Geoscience*, *2*(7), 488-491.

Chan, F. K. S., Mitchell, G., Adekola, O., & McDonald, A. (2012). Flood risk in Asia's urban mega-deltas: drivers, impacts and response. *Environment and Urbanization Asia*, *3*(1), 41-61.

Dettinger, M., & Cayan, D. R. (2014). Drought and the California delta—A matter of extremes. *San Francisco Estuary and Watershed Science*, *12*(2).

DGMS 2004 Research of geological structure and classification of N-Q sediments in Mekong Delta H D Nguyen (Ho Chi Minh City: Division of Geology and Minerals of the South of Viet Nam (DGMS)) (unpublished)

Dinh, Q., Balica, S., Popescu, I., & Jonoski, A. (2012). Climate change impact on flood hazard, vulnerability and risk of the Long Xuyen Quadrangle in the Mekong Delta. *International journal of river basin management*, *10*(1), 103-120.

Division of Water Resources Planning and Investigation for the South of Vietnam (DWRPIS) (2010) National groundwater monitoring network for Nam Bo Plain report

Division of Water Resources Planning and Investigation for the South of Vietnam (DWPRIS)(2018) Lithological and geological dataset. Unpublished

Erban, L. E., Gorelick, S. M., & Zebker, H. A. (2014). Groundwater extraction, land subsidence, and sea-level rise in the Mekong Delta, Vietnam. *Environmental Research Letters*, *9*(8), 084010.

Ericson, J. P., Vörösmarty, C. J., Dingman, S. L., Ward, L. G., & Meybeck, M. (2006). Effective sea-level rise and deltas: causes of change and human dimension implications. *Global and Planetary Change*, *50*(1), 63-82.

Environmental Systems Research Institute (ESRI), (2017). ArcGIS Desktop Help 10.5 Geostatistical Analyst.

Elbasiouny, H., Abowaly, M., Abu_Alkheir, A., & Gad, A. (2014). Spatial variation of soil carbon and nitrogen pools by using ordinary Kriging method in an area of north Nile Delta, Egypt. Catena, 113, 70-78.

Gambolati, G., Ricceri, G., Bertoni, W., Brighenti, G., & Vuillermin, E. (1991). Mathematical simulation of the subsidence of Ravenna. *Water Resources Research*, *27*(11), 2899-2918.

Gambolati, G., & Teatini, P. (2015). Geomechanics of subsurface water withdrawal and injection. *Water Resources Research*, *51*(6), 3922-3955.

Gkiougkis, I., Kallioras, A., Pliakas, F., Pechtelidis, A., Diamantis, V., Diamantis, I., ... & Dafnis, I. (2015). Assessment of soil salinization at the eastern Nestos River Delta, NE Greece. *Catena*, *128*, 238-251.

Hanebuth, T., Stattegger, K., & Grootes, P. M. (2000). Rapid flooding of the Sunda Shelf: a late-glacial sea-level record. Science, 288(5468), 1033-1035.

Heege, H. J. (2013). Heterogeneity in Fields: Basics of Analyses. In *Precision in Crop Farming* (pp. 3-13). Springer Netherlands.

Higgins, S. A., Overeem, I., Steckler, M. S., Syvitski, J. P., Seeber, L., & Akhter, S. H. (2014). InSAR measurements of compaction and subsidence in the Ganges-Brahmaputra Delta, Bangladesh. *Journal of Geophysical Research: Earth Surface*, *119*(8), 1768-1781.

Karim, M. F., & Mimura, N. (2008). Impacts of climate change and sea-level rise on cyclonic storm surge floods in Bangladesh. *Global Environmental Change*, *18*(3), 490-500.

Koster, K., Erkens, G., & Zwanenburg, C. (2016). A new soil mechanics approach to quantify and predict land subsidence by peat compression. *Geophysical Research Letters*, *43*(20).

Laarhoven, van, S. (2017) Subsidence potential of Holocene deposits of the Mekong Delta. Unpublished.

Ladd, C., (1977) Stress - deformation and strength characteristics: state of the art report Proc. 9th ICSMFE 4 421–94

Liu, S., Lu, P., Liu, D., Jin, P., & Wang, W. (2009). Pinpointing the sources and measuring the lengths of the principal rivers of the world. *International Journal of Digital Earth*, *2*(1), 80-87.

McGranahan, G., Balk, D., & Anderson, B. (2007). The rising tide: assessing the risks of climate change and human settlements in low elevation coastal zones. *Environment and urbanization*, *19*(1), 17-37.

Mekong River Commision (2005), Overview of the Hydrology of the Mekong Basin

Mesri, G. and Godlewski P. M. (1977) Time-and stress-compressibility interrelationship J. Geotech. Geoenvironmental Eng. 103

Milliman, J. D., Broadus, J. M., & Gable, F. (1989). Environmental and economic implications of rising sea level and subsiding deltas: the Nile and Bengal examples. *Ambio*, 340-345.

Minderhoud, P. S. J., Erkens, G., Pham, V. H., Bui, V. T., Erban, L., Kooi, H., & Stouthamer, E. (2017). Impacts of 25 years of groundwater extraction on subsidence in the Mekong delta, Vietnam. *Environmental Research Letters*, *12*(6), 064006.

Moayed, R. Z., Kordnaeij, A., & Mola-Abasi, H. (2017). Compressibility indices of saturated clays by group method of data handling and genetic algorithms. *Neural Computing and Applications*, *28*(1), 551-564.

Neumann, J. E., Emanuel, K. A., Ravela, S., Ludwig, L. C., & Verly, C. (2015). Risks of coastal storm surge and the effect of sea level rise in the Red River Delta, Vietnam. *Sustainability*, *7*(6), 6553-6572.

Nguyen, V. L., Ta, T. K. O., & Tateishi, M. (2000). Late Holocene depositional environments and coastal evolution of the Mekong River Delta, Southern Vietnam. *Journal of Asian Earth Sciences*, *18*(4), 427-439.

Nguyen, H. N., Vu, K. T., & Nguyen, X. N. (2007). Flooding in Mekong River Delta, Viet Nam. *Human development report*, *2008*, 23.

Nicholls, R. J. (1995). Coastal megacities and climate change. *GeoJournal*, *37*(3), 369-379.

Nicholls, R. J. (2004). Coastal flooding and wetland loss in the 21st century: changes under the SRES climate and socio-economic scenarios. *Global Environmental Change*, *14*(1), 69-86.

Nicholls, R. J., & Cazenave, A. (2010). Sea-level rise and its impact on coastal zones. *science*, *328*(5985), 1517-1520.

Park, H. I., & Lee, S. R. (2011). Evaluation of the compression index of soils using an artificial neural network. *Computers and Geotechnics*, *38*(4), 472-481.

Poland, J. F., & Davis, G. H. (1969). Land subsidence due to withdrawal of fluids.

Sekovski, I., Newton, A., & Dennison, W. C. (2012). Megacities in the coastal zone: Using a driver-pressure-state-impact-response framework to address complex environmental problems. *Estuarine, Coastal and Shelf Science*, *96*, 48-59.

Syvitski, J. P., Kettner, A. J., Overeem, I., Hutton, E. W., Hannon, M. T., Brakenridge, G. R., & Nicholls, R. J. (2009). Sinking deltas due to human activities. *Nature Geoscience*, *2*(10), 681-686.

Ta, T. K. O., Nguyen, V. L., Tateishi, M., Kobayashi, I., & Saito, Y. (2001). Sedimentary facies, diatom and foraminifer assemblages in a late Pleistocene–Holocene incised-valley sequence from the Mekong River Delta, Bentre Province, Southern Vietnam: the BT2 core. Journal of Asian Earth Sciences, 20(1), 83-94.

Ta, T. K. O., Nguyen, V. L., Tateishi, M., Kobayashi, I., Tanabe, S., & Saito, Y. (2002). Holocene delta evolution and sediment discharge of the Mekong River, southern Vietnam. Quaternary Science Reviews, 21(16-17), 1807-1819.

Tanabe, S., Ta, T. K. O., Nguyen, V. L., Tateishi, M., Kobayashi, I., & Saito, Y. (2003). Delta evolution model inferred from the Holocene Mekong Delta, southern Vietnam.

Tiwari, B., & Ajmera, B. (2011). New correlation equations for compression index of remolded clays. *Journal of Geotechnical and Geoenvironmental Engineering*, *138*(6), 757-762.

Törnqvist, T. E., Wallace, D. J., Storms, J. E., Wallinga, J., Van Dam, R. L., Blaauw, M., & Snijders, E. M. (2008). Mississippi Delta subsidence primarily caused by compaction of Holocene strata. *Nature Geoscience*, *1*(3), 173.

Tran, K. T. (1986). Sedimentary map of the Mekong Plain, 1/250,000. *Project of Investigating and Developing the Mekong Plain. Ho Chi Minh City Univ.*

Verruijt, A., & Van Baars, S. (2007). Soil mechanics VSSD Delft, the Netherlands.

Wagner, F., Tran, V. B., & Renaud, F. G. (2012). Groundwater resources in the Mekong Delta: availability, utilization and risks. In *The Mekong Delta System* (pp. 201-220). Springer Netherlands.

Widodo, S., & Ibrahim, A. (2012). Estimation of primary compression index (CC) using physical properties of Pontianak soft clay. *International Journal of Engineering Research and Applications (IJERA) Vol*, *2*, 2232-2236.

Xue Z, Liua JP, DeMastera D, Nguyen LV, Ta TKO (2010) Late Holocene evolution of the Mekong Subaqueous Delta, Southern Vietnam. Mar Geol 269:46–60.

Zhang, H., Ma, W. C., & Wang, X. R. (2008). Rapid urbanization and implications for flood risk management in hinterland of the Pearl River Delta, China: The Foshan study. *Sensors*, *8*(4), 2223-2239.